ARL-TR-90-44

Copy No. 40

Flutter and Its Effect upon Replica Correlation Sonar

Technical Report under Contract N00039-88-C-0043,
TD No. 03A007, Special Acoustic Signals, and
TD No. 03A011, Special Acoustic Signals - Phase II

Terry L. Henderson

Applied Research Laboratories
The University of Texas at Austin
P. O. Box 8029 Austin, TX 78713-8029

5 December 1990

Technical Report

Prepared for:
Naval Coastal Systems Center
Panama City, FL 32407

Monitored by:
Space and Naval Warfare Systems Command
Department of the Navy
Washington, D.C. 20363-5100

REPORT DOCUMENTATION PAGE

Form Approved
OMB No. 0704-0188

1. AGENCY USE ONLY (Leave blank)	2. REPORT DATE	3. REPORT TYPE AND DATES COVERED
	5 Dec 90	technical

4. TITLE AND SUBTITLE
Flutter and Its Effect upon Replica Correlation Sonar, Technical Report under Contract N00039-88-C-0043, TD No. 03A007, Special Acoustic Signals, and TD No. 03A011, Special Acoustic Signals - Phase II

5. FUNDING NUMBERS
N00039-88-C-0043
TD No. 03A007 and
TD No. 03A011

6. AUTHOR(S)
Henderson, Terry L.

7. PERFORMING ORGANIZATION NAMES(S) AND ADDRESS(ES)
Applied Research Laboratories
The University of Texas at Austin
P.O. Box 8029
Austin, Texas 78713-8029

8. PERFORMING ORGANIZATION REPORT NUMBER
ARL-TR-90-44

9. SPONSORING/MONITORING AGENCY NAME(S) AND ADDRESS(ES)
Naval Coastal Systems Center
Panama City, Florida 32407

Space and Naval Warfare
Systems Command
Department of the Navy
Washington, D.C. 20363-5100

10. SPONSORING/MONITORING AGENCY REPORT NUMBER

11. SUPPLEMENTARY NOTES

12a. DISTRIBUTION/AVAILABILITY STATEMENT
Approved for public release; distribution is unlimited.

12b. DISTRIBUTION CODE

13. ABSTRACT (Maximum 200 words)

The effect of flutter, i.e., of rapidly fluctuating phase variations, is studied in detail, insofar as it affects the performance of a high resolution active sonar that uses replica correlation to achieve pulse compression. Flutter is defined in terms of a time varying, random displacement of the time variable, at the point of reception. Several causes of flutter are investigated, including target motions, turbulence in the propagating medium, and motions of the sonar platform at the times of pulse transmission and echo reception. Results are extracted from the literature regarding effects of the medium. Detailed theoretical analyses are presented for the cases where the transmitted pulse is a linear-FM waveform or a stepped-FM "hopcode" signal. Results of computer simulations are also presented. It is demonstrated that there is a law of diminishing returns in regards to increases in time-bandwidth product.

14. SUBJECT TERMS

sonar	pulse compression	spread Doppler	frequency hopped
flutter	matched filter	linear FM	time-bandwidth product
phase fluctuations	replica correlation	hopcode	

15. NUMBER OF PAGES
204

16. PRICE CODE

17. SECURITY CLASSIFICATION OF REPORT	18. SECURITY CLASSIFICATION OF THIS PAGE	19. SECURITY CLASSIFICATION OF ABSTRACT	20. LIMITATION OF ABSTRACT
UNCLASSIFIED	UNCLASSIFIED	UNCLASSIFIED	SAR

TABLE OF CONTENTS

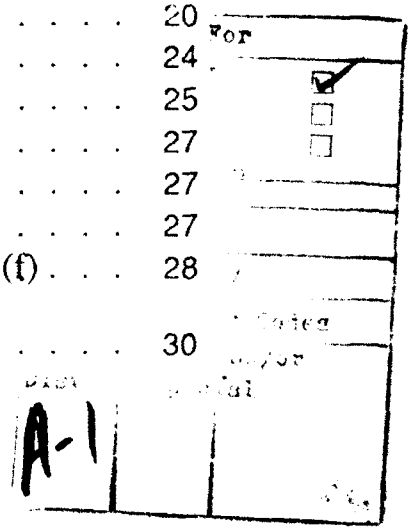

Page

Page

LIST OF FIGURES

LIST OF TABLES

1. INTRODUCTION

Large time-bandwidth product waveforms are sometimes used in active sonars to improve range resolution or target detection performance in the presence of noise or reverberation. Waveforms with *very* large time-bandwidth products may be attractive when one wishes to avoid detection. Such waveforms cannot be effective unless the target's echoes are compressed to pulses of short duration by a replica correlation receiver. Ideally, an exact replica of the waveform should be used for this purpose, including compensation for distortions attributed to the operating environment, such as Doppler and frequency dependent absorption. However, in the presence of random oscillatory motions of the sonar platform and target, or ocean turbulence, it may be impossible to compensate the replica for all such distortions. The echo will then fail to match the replica, reducing the effectiveness of the pulse compression. Because of this fundamental limitation, very large values of time-bandwidth product may not yield as much performance as expected.

1.1 SCOPE

This report examines the effects of random, uncompensated distortions that can be categorized under the general heading of "flutter", for certain classes of large time-bandwidth waveforms, including linear FM sweeps, and pseudo-random noise. Of primary interest is operation within the frequency limits of 25-500 kHz, at ranges of 10-1000 m, covering the operational regime of what might be categorized as *high resolution sonars*.

The effects of flutter can be considered as phase fluctuations. No attempt is made to account for any associated amplitude fluctuations. The report does not address beamforming, nor does it discuss the effects of noise, imperfections, and approximations that are often made in practical sonar signal processing systems.

1.2 TECHNICAL CONTEXT AND USAGE

Mathematical analysis forms the core of this report, and some sections consist almost entirely of formulas and equations. Approximations are heavily used . Many of them are supported by error bounds, but others are more reliant upon heuristic reasoning and experiential inferences.

The terminologies of signal processing theory and linear systems analysis are used throughout the report. For example, the rectangle function $\Pi(\cdot)$, the triangle function $\Lambda(\cdot)$, and the function $\mathrm{sinc}(\cdot)$ are heavily used. (They are defined in Section 2.1.) It is assumed that the reader is familiar with the Fourier transform techniques that are used in systems analysis and communications theory, with power spectral densities of stationary random process, with matched filtering theory, and with the manipulation of convolution and correlation integrals.

In keeping with modern practice in acoustical analysis, complex signals are used throughout; e.g., $\exp(j2\pi f_0 t)$ is used instead of $\cos(2\pi f_0 t)$. A brief discussion of the impact of that usage in practical sonar terms is provided in Section 2.8.

Mathematical developments will often be aided by a change of variables. In this regard, the notation $\tau \rightarrow \lambda - t$ is to be read as "τ becomes $\lambda - t$", or "substitute $\lambda - t$ in place of τ". It is important not to confuse this with the usage that is sometimes encountered in computer programming context, where $a \leftarrow b$ means "replace the contents of register a by the contents of register b".

Many references to prior work are contained in the report. Direct quotations of phrases and sentences are denoted by quotation marks, with editorial insertions indicated by square brackets.

1.3 GUIDE TO THE SECTIONS

Section 2 reviews time-bandwidth product theory and the method of pulse compression filtering by means of replica correlation. Formulas for computing bandwidth and pulse duration are given, and mathematical and notational conventions are established.

Section 3 defines flutter and gives several ways to characterize it. Elementary properties of flutter are discussed, and particular attention is given to spectral broadening of a pure tone due to flutter. Sources of flutter (other than the propagation medium itself) are described. Formulas are given for flutter induced by sonar platform motion. Asymptotic behavior of the flutter spectrum is discussed, for high and low frequencies.

Section 4 extracts pertinent information from published experimental studies of a number of different investigators, with a view toward ascertaining the nature of flutter induced by the propagation medium. Wherever possible, data are taken from the published curves and used to determine flutter strengths and spectra. A general flutter model is developed and compared with reported data.

Section 5 contains an exhaustive theoretical analysis of the effect of flutter upon replica correlation filtering when the sonar waveform is a linear FM wave burst. After a very tedious mathematical development containing many approximations, it is determined that the fluttered and compressed pulse has the form of an estimated spectrum of the phase deviation induced by the flutter, using a simple linear transformation between the time and frequency axes. Based upon this representation, formulas are derived for the duration of the pulse, as elongated by the flutter. Subsequently, a formula for processing gain (of the pulse compression filter) is derived. It is shown that increases in time-bandwidth product, made by extending the duration of a fixed bandwidth waveform, do not increase the processing gain without limit. A formula for maximum processing gain is given. The maximum gain depends upon the sonar "Q" and the strength of the flutter.

Section 6 is a theoretical analysis of the effect of flutter upon replica correlation filtering when the sonar waveform is a frequency-hopped waveform of a particular standard form. The mathematical developments are more difficult and obscure than those of Section 5, with more approximations, and the results are not as illuminating. Nevertheless, the basic nature of the fluttered and compressed pulse is determined. Formulas for pulse duration and processing gain are given. It is confirmed that the frequency-hopped waveform behaves (approximately) like a linear FM wave burst when the frequency sequence is ordered rather than random. When the sequence is random, the performance is still analogous to the linear FM case except that the flutter is "time scrambled" by the hopcode sequence, with the result that the flutter spectrum is effectively whitened. As a result, flutter causes the energy of the fluttered and compressed pulse to be bled away and redistributed as "self-noise" over a large time interval, instead of merely being spread over a slightly larger interval, as is the case for the linear FM wave burst.

Section 7 is a computer simulation study of the effects of flutter upon pulse-compression filtering. The frequency-hopped waveform is used for this purpose, since it includes the linear FM-wave burst as a special case (at least as an approximation). Results are plotted in tandem for the linear FM and random hopcode waveforms. Instead of a random flutter, a deterministic flutter waveform is selected, whose spectral properties are in keeping with those described in Section 4. The theoretical results of Sections 5 and 6 are confirmed. In particular, the fluttered and compressed pulse duration formula of Section 5 is found to be very reliable. The combined studies of Sections 5, 6, and 7 lead to the conclusion that the linear FM waveform probably cannot be improved upon, insofar as its flutter tolerance is concerned. In particular, the random frequency-hopped waveform becomes progressively inferior as the flutter strength is increased.

Section 8 contains a "short story" review of the entire report, and also provides some simplified formulas. It also contains some suggested techniques for measuring flutter experimentally, as well as final remarks and conclusions of a general nature.

2. TIME-BANDWIDTH PRODUCTS AND REPLICA CORRELATION

The analysis relies heavily upon the theory of signals and replica correlation (i.e., matched filtering). The following tutorial review is provided to lay the theoretical groundwork and to introduce notational conventions.

2.1 TIME-BANDWIDTH PRODUCT THEORY

Time-bandwidth product theory is widely discussed in the signal processing and radar/sonar literature (Bracewell, 1978; Rihaczek, 1969; de Coulon, 1986; Papoulis, 1977; McGillem and Cooper, 1974). The time-bandwidth product "theorem", also known as the uncertainty principle, has been stated succinctly by Bracewell (1978):

> *"It is well known that the bandwidth-duration product of a signal cannot be less than a certain minimum value."*

That minimum value depends upon the exact definitions of bandwidth and duration, but is on the order of unity. This "theorem" is easy to demonstrate in practice, but the theoretical underpinnings are somewhat obscure. Explicit mathematical inequalities have been derived (several are given in the references just cited), but they use clumsy definitions of bandwidth and duration that are inappropriate for many waveforms of interest.

Regardless of the limitations of formal theory, the following approximate inequality is an undisputed fact:

$$BT \gtrsim 1, \tag{2.1}$$

where B represents the bandwidth (in hertz) and T is the duration (in seconds).

2.1.1 Definition of Bandwidth B_e

Our definition of bandwidth is

$$B_e = \frac{\left[\int_{-\infty}^{+\infty} |X(f)|^2 \, df\right]^2}{\int_{-\infty}^{+\infty} |X(f)|^4 \, df}, \qquad (2.2)$$

where $X(f)$ denotes the Fourier transform of the signal $x(t)$,

$$X(f) = \int_{-\infty}^{+\infty} x(t)\, e^{-j2\pi ft} \, dt. \qquad (2.3)$$

The number B_e computed by Eq. (2.2) has been variously called *effective* bandwidth (Peebles, 1976; Burdic, 1984), *efficient* bandwidth (de Coulon, 1986), *occupied* bandwidth (Rihaczek, 1969) and *information* bandwidth (Deutsch, 1969). As defined in Eq. (2.2), it is intended to be applied to complex-valued signals whose spectral energy is distributed around some positive frequency f_0. It can also be applied to the complex baseband signal that is obtained when such a signal is demodulated, in which case it represents a "two-sided" bandwidth.

The value of B_e is independent of time and frequency translations, and is independent of the phase structure of the signal (since it is computed from the energy spectrum $|X(f)|^2$). A reassuring feature of B_e is that if a signal's energy spectrum $|X(f)|^2$ is flat over the range $f_1 \le f \le f_2$ and zero elsewhere, then Eq. (2.2) gives $B_e = f_2 - f_1$.

2.1.2 Bandwidths of Generic Sonar Waveforms

If $x(t)$ is a complex tone burst of duration T, namely,

$$x(t) = e^{j2\pi f_0 t}\,\Pi\left(\frac{t}{T}\right), \qquad \left\{\text{where} \quad \begin{array}{l}\Pi(t) = 1 \text{ for } |t| \le \frac{1}{2} \\ \Pi(t) = 0 \text{ for } |t| > \frac{1}{2}\end{array}\right. \tag{2.4}$$

then

$$X(f) = T\,\mathrm{sinc}(Tf) \qquad \left\{\text{where} \quad \mathrm{sinc}(f) = \frac{\sin(\pi f)}{\pi f}\right. \tag{2.5}$$

with the result that

$$B_e = \frac{1.5}{T} \ . \tag{2.6}$$

This gives a time-bandwidth product ($B_e T$) equal to 1.5.

Another very important waveform for sonar applications is the linear FM wave burst of duration T, starting at instantaneous frequency $f_0 - \frac{1}{2}\Delta f$ and ending at frequency $f_0 + \frac{1}{2}\Delta f$, namely,

$$x(t) = \Pi\left(\frac{t}{T}\right) e^{j2\pi f_0 t} \exp\left(j2\pi \frac{\Delta f}{2T} t^2\right). \tag{2.7}$$

It does not admit a simple formula for its exact bandwidth B_e or time-bandwidth product $B_e T$. However, numerical computations show that $B_e T$ is very close to $\Delta f T$ when its value exceeds 3, but close to 1.5 when the product $\Delta f T$ has less than unit value. Certainly as $\Delta f \to 0$ the FM wave burst becomes a simple tone burst, so that its time-bandwidth product $B_e T$ must converge exactly to the minimum value of 1.5. Figure 2.1 illustrates this behavior.

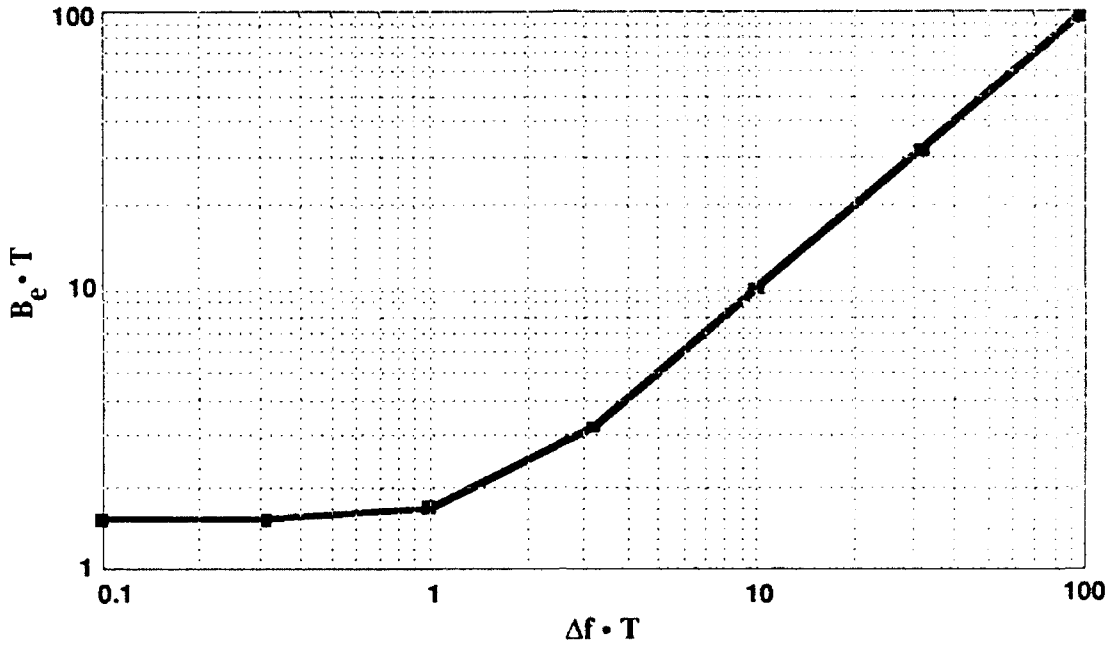

FIGURE 2.1
TIME-BANDWIDTH PRODUCT OF A LINEAR FM WAVE BURST

2.1.3 Definition of Duration T_e

In all of the examples discussed above the signals had constant amplitude during an interval of length T, so their durations were unequivocally equal to T. In general, however, a waveform could have negligible amplitude over some portion of the interval, or it could continue forever, albeit with decaying amplitude. A more general definition of duration is needed for such a waveform. By analogy with the definition of B_e one can define the duration T_c:

$$T_c = \frac{\left[\int_{-\infty}^{+\infty} |x(t)|^2 \, dt\right]^2}{\int_{-\infty}^{+\infty} |x(t)|^4 \, dt} \qquad (2.8)$$

If a signal has constant magnitude over an interval of length T and is zero outside it, this definition gives $T_e = T$, as desired. On the other hand, if the magnitude of the signal forms a triangular pulse whose base spans an interval of length $2T$, i.e.,

$$|x(t)| = \Lambda\left(\frac{t}{T}\right), \qquad \left\{\text{where} \quad \begin{array}{l} \Lambda(t) = 1 - |t| \ \text{ for } |t| \le 1 \\ \Lambda(t) = 0 \ \text{ for } |t| > 1 \end{array}\right. \tag{2.9}$$

then straightforward integration gives $T_e = \frac{10}{9} T$. Another important waveform is the "sinc burst"

$$x(t) = B\,\mathrm{sinc}(Bt)\, e^{j2\pi f_0 t}, \tag{2.10}$$

whose bandwidth is $B = B_e$, since $X(f) = \Pi((f - f_0)/B)$. By direct analogy with Eqs. (2.5) and (2.6), its duration is

$$T_e = 1.5/B. \tag{2.11}$$

2.2 REPLICA CORRELATION (MATCHED FILTERING) THEORY

2.2.1 The Replica $x_{rep}(t)$

Let $x_{rep}(t)$ denote the theoretical sonar echo from an ideal point target of unit strength at some specified nominal range, including compensation for known Doppler effects. The Doppler compensation might be based upon micro-navigational data from inertial sensors, Kalman filters, and auxiliary instruments (such as a high frequency Doppler velocimeter). Alternatively, if the sonar receiver incorporates a bank of Doppler channels then $x_{rep}(t)$ is the ideal, Doppler-compensated echo for one of those channels. In either case, $x_{rep}(t)$ is called the *replica*.

For convenience, we assume that the time axis is centered at the time-of-arrival of that ideal echo.

2.2.2 The Replica Correlation Filter (Matched Filter)

If $x(t)$ denotes the acoustic signal that is actually received in a complex target environment, then the replica correlating module of the sonar receiver can be regarded as a matched filter whose impulse response $h_{rep}(t)$ is specified to be

$$h_{rep}(t) = x^*_{rep}(-t)\,, \tag{2.12}$$

where * denotes the complex conjugate. The output of this matched filter is

$$z(t) = \int_{-\infty}^{+\infty} h_{rep}(\tau)\, x(t-\tau)\, d\tau \tag{2.13}$$

$$= h_{rep}(t) \otimes x(t)\,, \tag{2.14}$$

where $\otimes$ denotes convolution. With substitution of Eq. (2.12) and the change of variables $\tau \rightarrow -\lambda$, Eq. (2.13) becomes

$$z(t) = \int_{-\infty}^{+\infty} x^*_{rep}(\lambda)\, x(\lambda+t)\, d\lambda\,. \tag{2.15}$$

Equation (2.15) makes the replica correlation self-evident, but the mathematically equivalent form of Eq. (2.14) makes it more obvious that $z(t)$ is the output of a linear time-invariant filter.

2.2.3 The Pulse Compression Effect of the Filter

If the received signal $x(t)$ consists entirely of an echo from an ideal target of strength A, that has a range that exceeds the nominally specified range by a small displacement ζ, then the echo will be scaled by A and delayed, the delay being equal to the increase in the round trip sound path divided by the speed of sound c, i.e.,

$$x(t) = A\, x_{rep}\left(t - 2c^{-1}\zeta\right), \tag{2.16}$$

(assuming that the target has the same Doppler for which $x_{rep}(t)$ was defined). When this is substituted into Eq. (2.15), the following result is obtained:

$$z(t) = A\int_{-\infty}^{+\infty} x^{*}_{rep}(\lambda)\, x_{rep}\left(t - 2c^{-1}\zeta + \lambda\right) d\lambda \tag{2.17}$$

$$= A\, p\left(t - 2c^{-1}\zeta\right), \tag{2.18}$$

where $p(t)$ is the autocorrelation function of the replica,

$$p(t) = x^{*}_{rep}(-t) \otimes x_{rep}(t) = \int_{-\infty}^{+\infty} x^{*}_{rep}(\lambda)\, x_{rep}(\lambda + t)\, d\lambda\,. \tag{2.19}$$

If one takes the Fourier transform of the left-hand equality of Eq. (2.19), the result is

$$P(f) = X^{*}_{rep}(f) \cdot X_{rep}(f) = \left|X_{rep}(f)\right|^2, \tag{2.20}$$

which implies the well-known result that the replica's autocorrelation function is the inverse transform of its energy spectral density:

$$p(t) = \mathcal{F}.\mathcal{T}.^{-1}\left\{\left|X_{rep}(f)\right|^2\right\}. \tag{2.21}$$

If the received signal $x(t)$ consists of echoes from an aggregation of targets of strength $\{A_n\}$ whose range displacements are $\{\zeta_n\}$, i.e.,

$$x(t) = \sum_{n} A_n x_{rep}\left(t - 2c^{-1}\zeta_n\right), \tag{2.22}$$

then by linear superposition Eq. (2.18) becomes

$$z(t) = \sum_n A_n p\left(t - 2c^{-1}\zeta_n\right). \tag{2.23}$$

The benefit of the replica correlation filtering lies in the fact the $p(t)$ pulses summed in Eq. (2.23) are always narrower and taller than the $x_{rcp}(t)$ "pulses" being summed in Eq. (2.22), so that the individual targets can be more easily detected and isolated. This is true because the following rules apply for most plausible signals.

(1) Although the time-bandwidth product of the sonar replica $x_{rcp}(t)$ is very large (by design), the time-bandwidth product of $p(t)$ is always on the order of unity.

(2) The bandwidth of $p(t)$ is comparable to that of $x_{rep}(t)$.

As a consequence, the duration of $p(t)$ must be shorter than that of $x_{rep}(t)$ by a factor that is approximately equal to the time-bandwidth product of $x_{rep}(t)$. However, the difficulty of *proving* (1) and (2) is dependent upon the definition of "plausible". The proof becomes very easy if the sonar designer has ensured that $x_{rep}(t)$ belongs to the following class of signals.

2.3 CONSTANT AMPLITUDE, FLAT SPECTRUM (CAFS) WAVEFORMS

If the amplitude $|x(t)|$ of a complex waveform $x(t)$ is approximately constant over its duration T (which we assume to be centered at the origin, for convenience), and its energy spectrum $|X(f)|^2$ is approximately constant over its bandwidth B, then $x(t)$ is said to be a *constant amplitude, flat spectrum* (CAFS) waveform. In mathematical terms, a CAFS waveform obeys

$$|x(t)| \cong K\,\Pi\left(\frac{t}{T}\right), \tag{2.24}$$

and

$$|X(f)| \cong K\cdot\sqrt{\frac{T}{B}}\cdot\Pi\left[\frac{f - f_c}{B}\right], \qquad (2.25)$$

where f_c is the frequency around which the bandwidth is centered. The amplitude scaling factor K is arbitrary, but the factor $K\sqrt{T/B}$ in Eq. (2.25) is then a consequence of Parseval's theorem, which demands that

$$\int_{-\infty}^{+\infty} |x(t)|^2\, dt = \int_{-\infty}^{+\infty} |X(f)|^2\, df\ . \qquad (2.26)$$

2.3.1 Normalized CAFS Waveforms

The class of CAFS waveforms includes FM wave bursts, bandlimited white noise bursts, and a variety of other waveforms that are of interest as sonar transmissions. For purposes of analysis, and with little loss in generality, it will be assumed in the remainder of this report that the sonar engineer has designed his transmission so that $x_{rep}(t)$ is a CAFS waveform. Furthermore, since the received waveform can be arbitrarily scaled for analysis purposes, it will be assumed for convenience that K is selected to make the factor $K\sqrt{T/B}$ in Eq. (2.25) equal to unity. Thus, for such a *normalized* CAFS waveform, the conditions

$$|x_{rep}(t)| \cong \sqrt{\frac{B_e}{T_e}}\ \Pi\left(\frac{t}{T_e}\right) \qquad (2.27)$$

and

$$|X_{rep}(f)| \cong \Pi\left[\frac{f - f_c}{B_e}\right] \qquad (2.28)$$

will apply.

For the sake of generality, the time-bandwidth parameters B and T have been replaced by B_e and T_e in Eqs. (2.27) - (2.28). For a CAFS sonar

transmission it is likely that the time boundaries will be sharply defined and the amplitude quite constant, so that the defining formula of Eq. (2.8) will give $T_e = T$ anyway. On the other hand, sonar transmissions never have perfectly sharp frequency boundaries, so Eq. (2.25) is just an approximation that holds for some reasonable calculation of bandwidth B, for which B_e is an acceptable choice.

Even a tone burst can be loosely regarded as a CAFS waveform, although it compromises the flat spectrum assumption a bit, since its spectrum actually has the shape of a sinc function (see Eq. (2.5)).

Strictly speaking, no waveform can meet the normalizing conditions of Eqs. (2.27) - (2.28) exactly. However, the larger the time-bandwidth product, the easier it is for a waveform to be made to fit the CAFS assumptions. For example, with a time-bandwidth product of 20 or more an FM wave burst has a very flat, bandlimited spectra (Rihaczek, 1969).

2.3.2 The Nature of the Ideal Compressed Pulse $p(t)$ and the Filter Response $H_{rep}(f)$ for a CAFS Waveform

Since by Eq. (2.21) the autocorrelation pulse $p(t)$ is the inverse transform of $|X(f)|^2$, it follows from Eq. (2.28) that

$$p(t) \cong B_e \, \mathrm{sinc}(B_e t) \, e^{j2\pi f_c t} . \tag{2.29}$$

The action of the replica correlation filter can be described in terms of its system function, $H_{rep}(f)$ which, by taking Fourier transforms in Eq. (2.12), is seen to be

$$H_{rep}(f) = X^*_{rep}(f) . \tag{2.30}$$

The amplitude gain of this filter is, by Eq. (2.28),

$$|H_{rep}(f)| \cong \Pi\left[\frac{f - f_c}{B_e}\right] , \tag{2.31}$$

i.e., the filter is just a unity-gain bandpass filter of bandwidth B_e, with a nontrivial phase response that readjusts the phases of the spectral components so as to make them destructively interfere everywhere except near the time-origin, leaving a short duration pulse. Figure 2.2 depicts this filter.

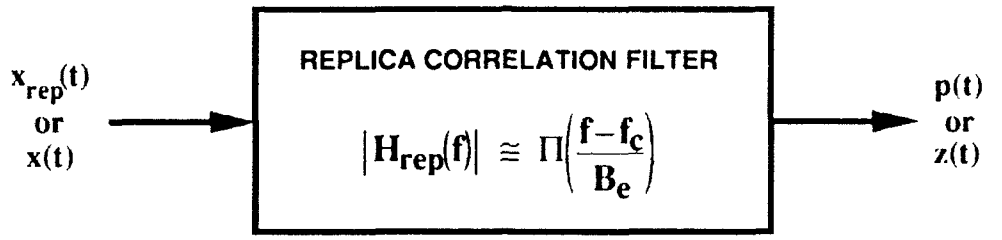

FIGURE 2.2
REPLICA CORRELATION FILTER FOR A CAFS WAVEFORM

2.3.3 Replica Correlation Performance for a CAFS Waveform

Since the filter passes the full bandwidth of the signal, the bandwidth at its output is still B_e. Following the example of Eq. (2.11), one can determine that the duration of $p(t)$ is $1.5/B_e$. Thus, the time-bandwidth product of $p(t)$ is 1.5. The overall input-output performance of the replica correlation filter is summarized in the following table.

TABLE 2.1
REPLICA CORRELATION FILTER FOR A CAFS WAVEFORM: FACTORS OF PERFORMANCE

	IN	OUT	FACTOR
PEAK AMPLITUDE	$\sqrt{B_e/T_e}$	B_e	$\sqrt{B_e T_e}$
DURATION	T_e	$1.5/B_e$	$1.5\cdot(B_e T_e)^{-1}$
TIME-BANDWIDTH PROD.	$B_e T_e$	1.5	$1.5\cdot(B_e T_e)^{-1}$
BANDWIDTH	B_e	B_e	1
TOTAL PULSE ENERGY	B_e	B_e	1
IN-BAND NOISE LEVEL	N_0	N_0	1

Most of the entries in the table have been discussed above. Since the filter has unity gain, it preserves the in-band noise level (due to "sea-state" noise, diffuse reverberation, or preamplifier noise), as the bottom row indicates. The pulse energy at the input is the squared-amplitude multiplied by the duration. (The energies of both quadrature components of the complex signal are included.) The pulse energy is unchanged by the unity gain filter.

2.3.4 Processing Gain

The $\sqrt{B_e T_e}$ amplitude factor is the crucial parameter for improving target detection performance. The signal amplitude gain, in dB, is

$$20 \log_{10}\sqrt{B_e T_e} \;=\; 10 \log_{10}(B_e T_e)\,. \qquad (2.32)$$

However, the detection time constant has to be reduced by the factor $1.5\cdot(B_e T_e)^{-1}$ to fit the shorter duration pulse, and that increases the false alarm rate of the detector.

To maintain the same false alarm rate one must raise the detection threshold, and that reduces the effectiveness of the increased amplitude. The result is that the "processing gain" factor of 10 drops to something between 2.5 and 7.5, depending upon the desired tradeoff between detection probability and

false alarm rate. The value of 5 is often used in sonar designers' calculations (Urick, 1983):

$$\text{True Processing Gain (dB)} \cong 5 \log_{10}\left(B_e \cdot T_e\right). \tag{2.33}$$

It should be remembered that this formula represents only the effect of inserting a replica correlation filter and adjusting the detection time constant in accordance with it, *at the receiver*, under the assumption that the waveform having the specified values of B_e and T_e is already in use. It does not include the effect of having increased the transmitted waveform's time-bandwidth product in the first place.

The implications can be better explained by means of an example. Suppose that a sonar is initially designed to use a transmitted waveform that gives a CAFS waveform at the receiver whose time bandwidth product is $B_e \cdot T_e = 1.5$, so that the received pulse is of duration $T_e = 1.5/B_e$. Then suppose that the sonar is modified to transmit a waveform having the *same power level and bandwidth*, but whose duration is larger by a factor G. (This implies that the transmitted energy is also increased by the factor G.) Suppose, further, that a replica correlation filter is used in the receiver, and that it performs in full accordance with Table 2.1. Then, according to Table 2.1, at the output of the pulse correlation filter the pulse duration is $T_e = 1.5/B_e$ as before. Thus, the detection time constant does not have to be changed. As compared with the sonar's performance before the modification, the ability to resolve targets and discriminate against reverberation is unchanged (since the bandwidth and final pulse duration are unchanged). However, the sonar's ability to discriminate against noise is improved, due to the G factor increase in transmitted energy. This G factor causes an increase in the level of the target echo and reverberation, relative to the noise. In dB, that increase is $10 \log_{10}(G)$ rather than $5 \log_{10}(G)$.

The lesson to be learned here is that one must exercise great care in deciding whether the situation calls for $10 \log_{10}(\cdot)$ or $5 \log_{10}(\cdot)$.

2.4 PULSE COMPRESSION FILTERING BY DECONVOLUTION

A matched filter is optimum for target detection in the presence of flat-spectrum noise. However, if the goal of the filter is simply to shorten the pulse duration as much as possible, then the optimum solution is a deconvolution filter instead of a matched filter. This means that one would use a filter whose transfer function is $H(f) = 1/[X(f)]$ over the passband and zero outside it, instead of $H_{rcp}(f) = X^{*}_{rcp}(f)$. The objective is to produce an output spectrum that looks as much as possible like that of a bandlimited, ideal impulse function. Such an impulse has a unit valued Fourier transform over the passband; therefore, the filter's transfer function is taken to be the inverse of the incoming signal's Fourier transform.

However, for a CAFS waveform $|X(f)|$ is constant over the passband; indeed, it equals unity if the CAFS waveform is scale normalized, as has been assumed above. Thus, $1/[X(f)] = X^{*}(f)$ over the passband, so that the replica correlation (i.e., matched) filter *is* a deconvolution filter in that special case. (This is just another attractive feature of CAFS waveforms.)

2.5 THE CLASSICAL SIGNAL DESIGN PROBLEM

The signal design problem, in its classical form, is to fashion the sonar transmissions so that the replica gives the desired performance, as indicated by the entries in Table 2.1. The objective is to make the duration of the compressed pulse p(t) small enough to resolve targets at a specified range spacing, and of sufficient magnitude to make targets obvious even in the presence of noise. The former is purely a function of bandwidth, and the latter can be achieved simply by scaling up the transmitted pulse power. (NOTE: Scaling up the transmitter power does not affect $x_{rcp}(t)$ as we have normalized it in Eqs. (2.27) - (2.28); however, one may assume that it effectively reduces the noise level N_0 in Table 2.1.)

Since a tone burst can have arbitrarily large bandwidth, what is the advantage of using a large time-bandwidth product transmission, instead of a tone burst of the same bandwidth and energy? There are at least two possible

advantages of a large time-bandwidth product.

(1) To permit the use of a low power transmitter, by employing a broadband waveform of long duration (i.e., low power but high energy) that can be compressed to a duration on the order of $1.5/B_e$, with a corresponding increase in amplitude. A tone burst would need to have a very short duration to achieve the same range-resolving power, and its peak instantaneous power would then have to be extremely large to attain the same pulse energy. (An example has already been considered at the end of Section 2.3.3, above.)

(2) To spread out the energy of transmission, in both time and spectrum, to avoid detection by those who cannot exploit a processing gain of $5 \log_{10}(B_e \cdot T_e)$. (They cannot enjoy the benefit of a replica correlation filter because they do not know the exact waveform.)

In carrying out the design it is often assumed, for the sake of simplicity, that the frequency response of the sonar receiver will be designed to "pre-whiten" the noise at the receiver output $x(t)$, and that the sonar transmission will be tailored so that $x_{rep}(t)$ has a flat spectrum, so that it can be a CAFS waveform. The signal design problem then appears to be straightforward, guided by Table 2.1. However, for various reasons the replica correlation filter may not work in full conformance with Table 2.1. One such reason is distortion.

2.6 DISTORTION

The replica correlation filter will not perform to the specifications of Table 2.1 if the receiver signal $x(t)$ has been distorted. If the target is not an ideal target then its echo will already have been affected by the target's own impulse response. For example, a very small pebble will act as a Rayleigh scatterer, taking the derivative of the incident waveform in the process of reflecting it. The edges of a hard cylinder will apply 45° and 135° phase shifts to the echo (Lacker and Henderson, 1990). Targets that are mechanically resonant will extend the pulse, as will targets that promote circumferential waves.

Extended targets will produce even more complex distortions, sometimes stretching the pulse in a way that defies being compressed to any duration less than $2L/c$, where L is the down range extent of the target. Nevertheless, in such cases it may be useful to use a very large bandwidth transmission that "over-resolves" the target to reduce the false alarm rate on reverberation clutter (for example). One would then choose a detection time constant to match the down range extent of the target being sought, even though this might be much greater than $1.5/B_e$.

Another type of distortion is "flutter". It is the primary subject of this report; it is defined in Section 3.

2.7 IMPERFECT PULSE COMPRESSION

Section 2.3.3 discussed the performance of a replica correlator as used for pulse compression filtering. The most important result was Eq. (2.33), which can also be written as

$$\textbf{Proc. Gain} \cong 5 \log_{10}\left[\frac{T}{T_{pc}}\right], \tag{2.34}$$

where T and T_{pc} denote the effective durations of an ideal (point target) echo, as measured at the input and output, respectively, of the pulse compression filter. If the filter does its job perfectly, then $T_{pc} = 1.5/B_e$ according to Table 2.1. (Actually, when that value is substituted for T_{pc} in Eq. (2.34) there is a 0.88 dB discrepancy between Eqs. (2.33) and (2.34); however, this discrepancy is within the implied approximation tolerance.) The formula measures the insertion gain of the pulse compression filter for a CAFS transmitted pulse, as discussed in Section 2.3.4.

It turns out that this formula is approximately correct even when the action of the pulse compression filter is imperfect, provided T_{pc} expresses the actual duration at the output, even though it might be larger than $1.5/B_e$. In the context of our analysis, "imperfect" means that phase distortion in the sonar echo has

caused it to be mismatched to the filter's impulse response. Flutter is one potential cause of this distortion, as will be discussed extensively in the remainder of this report. Most of the entries in the "OUT" column of Table 2.1 remain correct despite this type of imperfection, assuming the energy spectrum of the sonar echo has not been significantly altered by the phase distortion, except that the duration of the output pulse will be greater than $1.5/B_e$ and the time-bandwidth product will be greater by the same factor.

Under ideal circumstances, the signal from the output of the pulse compression filter should be fed to a square-law device, followed by a sliding-window integrator whose window is matched to the ideal compressed pulse duration, and then to a threshold comparator whose threshold is adjusted to give the desired combination of detection probability and false alarm rate. If the pulse compression filter works imperfectly, producing a compressed duration T_{pc} that is larger than $1.5/B_e$, then one must lengthen the integration window to match T_{pc} and readjust the threshold. Despite these readjustments the detection performance will be degraded unless the amplitude of the sonar echoes is increased by some independent means (assuming the noise level remains constant). For example, this might be done by increasing the transmitter power or the directional gain of the hydrophone array. The amount, in dB, by which the echo energy must be increased to restore the detection performance is a measure of the loss attributable to imperfections in pulse compression.

A similar concept can be used to define the processing gain of the pulse compression filter itself, whether perfect or imperfect. To do this, one imagines that the pulse compression filter is removed and replaced by a simple wire (or a simple, unity-gain, bandpass filter matched to the signal bandwidth) that does no compression whatever. The integration window of the energy detector will then have to be lengthened to the full duration of the transmitted pulse. *The processing gain of the pulse compression filter is the amount, in dB, by which the energy of the sonar echoes would have to be externally increased to restore the original detection performance, assuming appropriate readjustment of the detection threshold.*

In order to use this definition for processing gain one must be able to assess the performance of an energy detector as a function of its integration window. In general, when an energy detector of bandwidth W and integration window T_{det} is used to detect a signal in the presence of white noise whose (two-sided) power spectral density is N_0, the signal energy E_s required to achieve the desired performance can be expressed in terms of a function $\lambda(\cdot)$ of the various detector parameters,

$$E_s = \lambda(Q_d, FAR, W, T_{det}) \times N_0 , \tag{2.35}$$

where Q_d denotes the desired probability of detection when the signal is truly present, and FAR denotes the desired false alarm rate. By definition, FAR is the probability of threshold exceedance when no signal is present, divided by T_{det}. It is expressed in units of inverse seconds.

The function $\lambda(\cdot)$ of Eq. (2.35) cannot be expressed in closed form. However, Urkowitz (1967) has provided a set of formulas to compute the false alarm probability, $Q_0 = FAR \cdot T_{det}$, for any specified detection threshold, and to compute Q_d for any specified value of λ (i.e., E_s/N_0), assuming that the values of W and T_{det} have been provided. Urkowitz's Eqs. (34)-(37) give these results in terms of the central chi-squared distribution, which is computable by standard routines. Using his formulas one can write a two-step routine to compute $\lambda(Q_d, FAR, W, T_{det})$ for any given values of Q_d, FAR, W, and T_{det}. The first step is to solve, iteratively, for the detection threshold that gives the false alarm probability $Q_0 = FAR \cdot T_{det}$. The second step is to solve, iteratively, for the value of λ (i.e., E_s/N_0) that gives the specified detection probability Q_d, using the detection threshold determined from the first step. Thus, although the function $\lambda(\cdot)$ of Eq. (2.35) cannot be expressed in closed form, it is computable by a straightforward routine.

From the definition of processing gain given above it follows that one can use the function $\lambda(\cdot)$ to calculate

$$\textbf{Proc. Gain} = 10 \log_{10}\left[\frac{\lambda(Q_d, FAR, W, T)}{\lambda(Q_d, FAR, W, T_{pc})}\right], \tag{2.36}$$

in which the value used for W should be B_e, the effective bandwidth of the received echo. An example will illustrate the use of this formula. Suppose a 300 kHz sonar is to be used for detection of acoustically reflective objects, with the desired detection probability specified as $Q_d = 0.8$, and the desired false alarm rate specified as $FAR = 0.02/s$. Suppose, for unknown reasons, it has been decided to use a transmitted pulse of bandwidth $B_e = 60$ kHz and duration $T = 500$ ms, giving a time-bandwidth product of 30,000. Ideally, the pulse compression filter should compress the duration to $1.5/B_e = 0.025$ ms. However, in non-ideal circumstances the compressed pulse might be of longer duration. Suppose, for example, the compressed duration T_{pc} takes the representative values 50 ms, 5 ms, 0.5 ms, and 0.05 ms. Using Eq. (2.36) and the routine for computing λ that was described above, the processing gains for these T_{pc} values are found to be 4.04 dB, 8.27 dB, 11.63 dB, and 14.03 dB, respectively. Notice that the simple formula

$$\textbf{Proc. Gain} \cong 4 \log_{10}\left[\frac{T}{T_{pc}}\right] \tag{2.37}$$

fits these four selected T_{pc} values to within a tolerance of 0.37 dB, over the four decades of pulse compression ratios that they span.

With a somewhat larger tolerance, this approximation holds surprisingly well when the sonar operating parameters are varied over the wide range of realistic values for high resolution sonar applications. Thus, Eq. (2.37) is applicable to a broad range of sonar examples, not just the single example for which it was derived. Certainly this simplified formula is handier for analysis purposes, since Eq. (2.36) has to be implemented by an iterative computational routine.

To satisfy tradition, however, the processing gain analyses in the remainder of this report will use Eq. (2.34) instead of Eq. (2.37). The two formulas are identical except that a "5" is substituted in place of the "4". This is done merely to be in conformance with processing gain formulas that are often found in the literature (Urick, 1983). Because of this acquiescence to tradition,

the formulas in the remainder of this report overestimate the processing gain by about 25%, but that has negligible impact upon the general conclusions of the report.

2.8 USE OF COMPLEX SIGNALS

As noted in the introduction, complex signals will be used throughout this report; e.g., $e^{j2\pi f_0 t}$ will be used instead of $\cos(2\pi f_0 t)$. The imaginary part cannot actually be transmitted and received, but it can be reconstructed at the receiver. For analysis purposes this reconstruction is assumed to consist of taking the Hilbert transform of the real part, i.e., of the signal that is received (Burdic, 1984). The process of reconstructing and adding the imaginary portion of the original complex waveform can also be expressed in terms of the Fourier transform: the Fourier transform of the real part is taken, its negative frequency portion is set to zero, and then the inverse transform is taken. The resulting time domain signal, after doubling its amplitude (to compensate for the energy lost by masking out the negative frequencies), is the reconstructed signal. Its real part is the received signal, and its imaginary part is the Hilbert transform of the real part. An equivalent operation can be done by complex carrier demodulation, using quadrature (i.e., sine and cosine) carrier signals generated by a special local oscillator designed for that purpose.

This reconstruction is exact in the case of a pure tone, since $\sin(2\pi f_0 t)$ is the Hilbert transform of $\cos(2\pi f_0 t)$. However, it is not exact in the case of a wave burst. For example, the real part of the complex tone burst $\Pi(t/T)e^{j2\pi f_0 t}$ is $\Pi(t/T)\cos(2\pi f_0 t)$, but its Hilbert transform is not exactly equal to $\Pi(t/T)\sin(2\pi f_0 t)$. This is because there are transient oscillations of short duration at the endpoints of its Hilbert transform (it does not turn "on" and "off", instantaneously). However, experience has shown that this inexactitude is not responsible for serious discrepancies between sonar system analysis and actual performance, and this is especially true for a waveform whose center frequency is several times bigger than its bandwidth, and/or whose time-bandwidth product is large. (Hardware imperfections usually cause larger discrepancies.) Indeed, cruder methods of reconstructing the imaginary

component are often acceptable (such as simply delaying the received signal by $1/(4f_0)$).

2.9 SECTION SUMMARY

This section has provided a tutorial review of such sonar related issues as replica correlation and time-bandwidth product theory. The concept of a normalized constant amplitude flat spectrum (CAFS) waveform has been introduced, and the implications of using such a waveform were described in Table 2.1. Processing gain was discussed in Section 2.3.4.

3. FLUTTER

Anyone who has listened to piano music reproduced by a poor quality cassette player has heard *flutter*. The sound is garbled in a way that is quite different from the distortive effects of additive noise, harmonics, or long decay reverberation. The distortion is caused by rapid variations in the speed of the tape as it slides across the playback head. Slower speed fluctuations produce an effect that sounds a bit different but is mathematically the same (it is called *wow*), but we make no such distinctions here.

3.1 CHARACTERIZING FLUTTER

From an analytical point of view, flutter (or wow) results from a perturbation of the time axis:

$$t \rightarrow t + \varepsilon(t) , \tag{3.1}$$

so that a signal $x(t)$ is perceived as $x[t + \varepsilon(t)]$. Audio engineers understandably put greater emphasis upon developing mechanical means to avoid flutter than mathematical means to study it. A more analytical approach has been taken by researchers intent upon developing more stable oscillators for precision timing standards (e.g., "atomic clocks"). In that context the phenomenon expressed in Eq. (3.1) is called *phase noise* (Lesage and Audoin, 1979; Allan, 1987; Boileau and Picinbono, 1976). The theoretical development of the next section closely parallels their approach.

3.1.1 Normalized Frequency Deviation $y(t)$

One consequence of characterizing the distortion by Eq. (3.1) is that the perturbation $\varepsilon(t)$ has the dimensions of time. However, the distortion can also be characterized in terms of the derivative

$$y(t) = \frac{d}{dt} \varepsilon(t) , \tag{3.2}$$

which is a dimensionless quantity that has been termed the *normalized* or *fractional frequency deviation* in the literature. The reason for this terminology is simple enough: Suppose a complex pure tone, $x(t) = e^{j2\pi f_0 t}$, is distorted by a perturbation of the time axis of the form of Eq. (3.1), yielding a distorted waveform

$$\tilde{x}(t) = e^{j2\pi f_0[t+\varepsilon(t)]} . \tag{3.3}$$

By definition, the instantaneous frequency $f_{inst.}$ is the time derivative of the accumulated phase, divided by 2π :

$$f_{inst.} = \frac{1}{2\pi}\frac{d}{dt}\left\{2\pi f_0\left[t+\varepsilon(t)\right]\right\} = f_0 + f_0\, y(t) . \tag{3.4}$$

It follows that the deviation of the instantaneous frequency from the nominal frequency is just $f_0\, y(t)$, which reduces to $y(t)$ when normalized by the nominal frequency f_0. Thus $y(t)$ is the normalized frequency deviation. (For example, the instantaneous frequency is deviated by 15% when $y(t)$ equals 0.15.)

3.1.2 Flutter as a Random Process: $S_y(f)$ and $S_\varepsilon(f)$

In addition to being dimensionless, $y(t)$ is somewhat more amenable to being characterized as a stationary random process (in the case of random flutter). For example, one can characterize $y(t)$ in terms of its power spectral density

$$S_y(f) = \underset{\tau\rightarrow f}{\mathcal{F}.\mathcal{T}.} \left\{ E\left[y(t)y(t+\tau)\right] \right\}, \tag{3.5}$$

where E denotes the expectation. Since the Fourier transform decomposes the fluctuations in $y(t)$ into component sinusoidal oscillations of frequencies represented by the argument f of $S_y(f)$, it is appropriate to refer to f as the *flutter frequency* in that context.

Lesage and Audoin (1979) state, "Since the class of noise processes for

which $y(t)$ is stationary is broader than that for which phase is stationary, $S_y(f)$ should be preferentially used in mathematical analyses." In effect, $\varepsilon(t)$ is a Brownian motion type of process (for a precision clock), whereas $y(t)$ represents the random agitating force that causes $\varepsilon(t)$ (via integration). The time axis distortion formalized in Eq. (3.1) can thus be re-expressed as

$$t \rightarrow t + \int^t y(t)\, dt, \tag{3.6}$$

in which the lower limit of the integral is left arbitrary since its only effect is to produce a constant time offset, which is of little consequence in the analysis of flutter. Furthermore, in most cases of interest (for flutter analysis) $y(t)$ is a zero-mean random process. To see this, suppose that a constant mean value y_0 were added to $y(t)$ in Eq. (3.6). The result, upon integrating the constant, would be

$$t \rightarrow (1+y_0)t + \int^t y(t)\, dt, \tag{3.7}$$

meaning that there would be a scaling of the time axis in addition to the randomizing of the time axis. To a sonar engineer the factor $(1+y_0)$ in Eq. (3.7) merely indicates the effect of constant Doppler. Its effect upon the sonar is well known, and theoretically it can be compensated for; i.e., constant Doppler is of little interest in flutter analysis. Hence, we assume that $y(t)$ has zero mean.

In sonar applications $\varepsilon(t)$ may not really be a Brownian-type process. Indeed, if it is the type of flutter that is induced by turbulence in the propagation medium (see Section 4), then the time axis perturbation cannot wander off to infinity, assuming the sound path does not deform into coils of infinite length! Thus, $\varepsilon(t)$ may be a well-behaved random process in its own right, with a power spectral density $S_\varepsilon(f)$. Since by definition $y(t)$ is the derivative of $\varepsilon(t)$, the following simple relation would then apply:

$$S_y(f) = (2\pi f)^2 S_\varepsilon(f) . \tag{3.8}$$

The reader who is familiar with communication theory will see that the choice of $y(t)$ or $\varepsilon(t)$ in our analysis of flutter effects is analogous to the choice of frequency modulation or phase modulation inputs in the analysis of communication systems. Both $y(t)$ and $\varepsilon(t)$ will be used in this report when appropriate. Either may correctly be referred to as "the flutter process".

A slightly modified version of $y(t)$ that is not dimensionless is defined in the next section. It has a useful physical interpretation.

3.1.3 Equivalent Observer Velocity $cy(t)$ and Acceleration $c\dot{y}(t)$

A plane wave signal propagating with speed c may be expressed as $x(t - c^{-1}\xi)$, where ξ represents the positional coordinate of the observer measured along the path of propagation. If flutter-distortion of the form of Eq. (3.1) occurs, then the distorted signal can be expressed as

$$\begin{aligned} \tilde{x} &= x(t + \varepsilon(t) - c^{-1}\xi) \\ &= x\left(t + \int^t y(t)\, dt - c^{-1}\xi\right) \\ &= x\left(t - c^{-1}\left[\xi - \int^t cy(t)\, dt\right]\right), \end{aligned} \tag{3.9}$$

so that the time perturbation is equivalent to a positional perturbation:

$$\xi \rightarrow \xi - \int^t cy(t)\, dt . \tag{3.10}$$

The term under the integral, $cy(t)$, can be interpreted as a velocity that,

when integrated, gives an equivalent observer displacement that could account for the distortion of the time axis. Thus, it is appropriate to call the product $cy(t)$ an *equivalent observer velocity.* Although it is related to the normalized frequency deviation $y(t)$ by a trivial constant factor, its physical interpretation makes it more meaningful in some cases. It has the units of m/s, and its power spectral density is $c^2 S_y(f)$.

The instantaneous frequency deviation for a pure tone at frequency f_0 can be obtained from the equivalent observer velocity by dividing by the wave propagation speed c and multiplying by f_0 (since $f_0 y(t)$ is the instantaneous frequency deviation). (Since the speed of electromagnetic waves in the atmosphere is larger than that of sound in water by a factor of 2×10^5, it turns out that, for the same equivalent observer velocity, the frequency deviation of a 100 kHz sonar due to flutter is ten times as large as that of a 2 GHz radar.)

The derivative of the equivalent observer velocity is $c\dot{y}(t)$, the equivalent observer acceleration. As is traditional with measurement of acceleration, it may be appropriate to express it in "gee" units (i.e., as a ratio of $c\dot{y}(t)/g$ where g is the acceleration of gravity).

3.1.4 The Subsonic Flutter Assumption

For purposes of analysis it will be assumed that the normalized frequency deviation $y(t)$ is small in magnitude:

$$|y(t)| \ll 1, \tag{3.11}$$

i.e., the instantaneous frequency deviation of a pure tone, due to the flutter, is a small percentage of the tone frequency. Another interpretation is that the magnitude of the equivalent observer velocity, $|cy(t)|$, is much less than the speed of sound c. In that sense the flutter is said to be *subsonic.* Thus, "violent" flutter, such as might be caused by a supersonically vibrating source or reflecting surface, is excluded from the analysis.

One consequence of Eq. (3.11) is that the perturbation of the time axis,

$t \rightarrow t+\varepsilon(t)$ is monotonic; i.e., it does not cause points on the time axis to overlap and become disordered. This monotonicity is assured because $1+y(t)$, which is the derivative of $t+\varepsilon(t)$, must be strictly positive by Eq. (3.11).

The subsonic flutter assumption can be expressed in statistical terms as

$$\langle y^2(t) \rangle \ll 1, \tag{3.12}$$

or, equivalently,

$$\sqrt{\langle (cy(t))^2 \rangle} \ll c \tag{3.13}$$

Notice that the left-hand side is the root mean square value of the equivalent observer velocity $cy(t)$. Since the mean square value of a random process can be obtained by integrating the power spectral density, Eq. (3.12) is also equivalent to

$$\int_{-\infty}^{+\infty} S_y(f)\, df \ll 1, \tag{3.14}$$

which is equivalent to

$$\int_{-\infty}^{+\infty} f^2 S_\varepsilon(f)\, df \ll \frac{1}{4\pi^2}, \tag{3.15}$$

since $S_y(f) = (2\pi f)^2 S_\varepsilon(f)$. Notice that Eq. (3.15) implies that $S_\varepsilon(f)$ has to roll off faster than f^{-3} for large f.

3.1.3 Additivity of Cascaded Flutter

Suppose that there are two flutter processes $\varepsilon_1(t)$ and $\varepsilon_2(t)$ that act in cascade, so that a signal $x(t)$ is first distorted to $\tilde{x}(t)$ and then distorted to $\tilde{\tilde{x}}(t)$:

$$\tilde{x}(t) = x\big(t+\varepsilon_1(t)\big), \tag{3.16}$$

$$\tilde{\tilde{x}}(t) = \tilde{x}\big(t+\varepsilon_2(t)\big) = x\Big(t+\varepsilon_2(t) + \varepsilon_1\big(t+\varepsilon_2(t)\big) \Big). \tag{3.17}$$

This cascaded effect can also be expressed as a net perturbation of the time axis

$$t \rightarrow t + \varepsilon_2(t) + \varepsilon_1\big(t+\varepsilon_2(t)\big) . \tag{3.18}$$

It will now be argued that this perturbation can be replaced by

$$t \rightarrow t + \varepsilon_2(t) + \varepsilon_1(t) \tag{3.19}$$

as a good approximation. The argument starts with the first order approximation

$$\varepsilon_2(t) + \varepsilon_1\big(t+\varepsilon_2(t)\big) \cong \varepsilon_2(t) + \varepsilon_1(t) + \frac{d\big(\varepsilon_1(t)\big)}{dt}\,\varepsilon_2(t). \tag{3.20}$$

By definition, $d\varepsilon_1(t)/dt$ is simply $y_1(t)$, so the last term in Eq. (3.20) is $y_1(t)\varepsilon_2(t)$. Thus, since $|y_1(t)| << 1$ (assuming the flutter processes are subsonic), it follows that the last term is negligible compared to the first term $\varepsilon_2(t)$. As a consequence, the time axis perturbation formula of Eq. (3.18) can be replaced by that of Eq. (3.19).

The final result, Eq. (3.19), says that flutter effects are additive. (It implies, for example, that the combined effect of flutters $\varepsilon_1(t)$ and $\varepsilon_2(t)$ during recording and playback of a magnetic tape is indistinguishable from a single, playback-only flutter that is equal to their sum.)

It follows that the normalized frequency deviations $y_1(t)$ and $y_2(t)$ are also additive, since they are just the derivatives of $\varepsilon_1(t)$ and $\varepsilon_2(t)$.

3.1.6 Spectral Broadening of a Pure Tone

Flutter can also be characterized in terms of what it does to a pure tone of arbitrary frequency f_0,

$$x(t) = e^{j(2\pi f_0 t + \theta)} , \tag{3.21}$$

where θ is a random, uniformly distributed, initializing phase that is included to make $x(t)$ a stationary random process. Flutter distorts the tone into

$$\tilde{x}(t) = x\big(t + \varepsilon(t)\big) = e^{j\{2\pi f_0[t + \varepsilon(t)] + \theta\}} , \tag{3.22}$$

which can also be written in the form

$$\tilde{x}(t) = q_0(t) e^{j(2\pi f_0 t + \theta)} , \tag{3.23}$$

where the angle modulation phasor $q_0(t)$ is

$$q_0(t) = \exp[j\,2\pi f_0 \varepsilon(t)] = \exp\left[j \int^t m(t)\, dt\right] , \tag{3.24}$$

with $m(t)$ being defined in terms of the normalized frequency deviation as

$$m(t) = 2\pi f_0\, y(t) . \tag{3.25}$$

Equations (3.23) and (3.24) describe a basic frequency modulation (FM) process that has been studied thoroughly in the context of radio communication theory. In that application $m(t)$ is regarded as the modulating input that carries the information, rather than as a corruptive distortion of the time axis. Despite extensive research in FM theory, no analytical method has been found to compute the spectrum of the FM wave $\tilde{x}(t)$ exactly, except for sinusoidal modulation, for which it can be computed in terms of Bessel functions (Peebles, 1976). However, good approximations to the spectrum can be obtained in the

cases of *narrowband FM* and *wideband FM*. Luckily, the boundary between these categories is rather sharp, so that in most situations one or the other of these approximations can be used.

The behavior of the phasor $q_0(t)$ determines whether the FM is wideband or narrowband. If $q_0(t)$ wraps several cycles around the origin before it unwraps, then the modulation is categorized as wideband. If, instead, the phasor $q_0(t)$ tends to be confined to an angular sector of limited width (up to one radian), and never (or rarely) wraps around the origin, then the modulation is categorized as narrowband. In the latter case one can use the approximation $\exp(jA) \cong 1 + jA$, with the result that $q_0(t)$ can be approximated (at least over moderately short periods of time) as

$$q_0(t) = \left(1 + j\int^t m(t)\,dt\right) Q_0 \ , \tag{3.26}$$

where Q_0 is a complex constant. The modulated tone $\tilde{x}(t)$ can then be approximated as

$$\tilde{x}(t) \cong \left(1 + j\int^t m(t)\,dt\right) Q_0\, e^{j(2\pi f_0 t + \theta)} \ , \tag{3.27}$$

or, in the context of the time-perturbation $\varepsilon(t)$,

$$\tilde{x}(t) \cong \left[1 + j\,2\pi f_0\, \varepsilon(t)\right] Q_0\, e^{j(2\pi f_0 t + \theta)} \ . \tag{3.28}$$

This is almost the same as the classical formula for amplitude modulation (AM), except for the imaginary factor on $\varepsilon(t)$. Indeed, the narrowband FM modulation of Eq. (3.28) has a pair of sidebands just like regular AM, but they are 90° out of phase with respect to the pure tone "carrier" at frequency f_0.

However, this carrier-plus-sidebands characterization of the spectral spreading of the pure tone only applies when the flutter is weak, i.e., when the value of $2\pi f_0 \varepsilon_{rms}$ does not exceed about a half-radian of angle, so that the

phasor $q_0(t)$ does not swing around very much. Such weak flutter would not significantly alter the phase of a sonar waveform centered around frequency f_0, and therefore would do little damage to the replica correlation process.

For the flutter to have a pronounced effect on sonar transmissions it must be *strong* flutter, which can be loosely characterized by the condition

$$2\pi f_0 \varepsilon_{rms} >> 1 \ . \tag{3.29}$$

This condition ensures that the phasor $q_0(t)$ twirls around the origin vigorously, giving wideband FM in the radio analogy. The power spectral density $S_{\tilde{x}}(f)$ of the signal $\tilde{x}(t)$ can then be approximated (Peebles, 1976; Taub and Schilling, 1971; Blachman and McAlpine, 1969):

$$S_{\tilde{x}}(f) \cong 2\pi \rho_m\big(2\pi(f-f_0)\big) \ , \tag{3.30}$$

where $\rho_m(\cdot)$ is the probability density function of $m(t)$. The term 2π that appears as the leading factor on the right-hand side is required to make the integral of $S_{\tilde{x}}(f)$ equal to unity, since $\tilde{x}(t)$ has unit power. Since the complex factor $e^{j(2\pi f_0 t + \theta)}$ in Eq. (3.23) merely shifts the spectrum by f_0, it follows from Eq. (3.30) that the power spectral density of $q_0(t)$ obeys an even simpler rule:

$$S_0(f) \cong 2\pi \rho_m\big(2\pi f\big) \ . \tag{3.31}$$

The results are more useful when expressed in terms of the probability density $\rho_y(\cdot)$ of $y(t)$. Since $m(t) = 2\pi f_0 y(t)$ (by definition), it follows that

$$\rho_m(\alpha) = \frac{1}{2\pi f_0} \rho_y\left(\frac{\alpha}{2\pi f_0}\right) \ . \tag{3.32}$$

Substitution into Eq. (3.30) then gives

$$S_{\tilde{x}}(f) \cong \frac{1}{f_0} \rho_y\left(\frac{f-f_0}{f_0}\right) \ , \tag{3.33}$$

which shows how the point statistics of the normalized frequency deviation of the flutter cause spectral broadening around the tone frequency f_0.

The bandwidth of this spectral broadening is an important measure of the strength of the flutter. It will be denoted as $B_{\tilde{f}_0}$. To compute $B_{\tilde{f}_0}$ one may use the effective-bandwidth formula of Eq. (2.2), with $S_{\tilde{x}}(f)$ used in place of the energy spectrum, i.e.,

$$B_{\tilde{f}_0} = \frac{\left[\int_{-\infty}^{+\infty} S_{\tilde{x}}(f)\, df\right]^2}{\int_{-\infty}^{+\infty} S_{\tilde{x}}^2(f)\, df} = \frac{1}{\int_{-\infty}^{+\infty} S_{\tilde{x}}^2(f)\, df} . \qquad (3.34)$$

(The numerator has unit value because $\tilde{x}(t)$ has unit power.) After substituting for $S_{\tilde{x}}(f)$ from Eq. (3.33) and simplifying the variable of integration, one obtains

$$B_{\tilde{f}_0} = \frac{f_0}{\int_{-\infty}^{+\infty} \rho_y^2(\alpha)\, d\alpha} . \qquad (3.35)$$

In many sonar operating environments the flutter can be expected to have Gaussian statistics, especially if it is induced by the medium, so that

$$\rho_y(\alpha) = \frac{1}{y_{rms}\sqrt{2\pi}} \exp\left[-\frac{(\alpha-\bar{y})^2}{2(y_{rms})^2}\right] . \qquad (3.36)$$

(NOTE: The mean value $\bar{y}$ would normally be assumed to be zero, although this is not mandatory.) When this density is substituted into Eq. (3.35) and the integration is carried out, the result is

$$B_{\tilde{f}_0} = 2\sqrt{\pi}\, y_{rms}\, f_0 . \quad \text{(Gaussian Flutter)} \qquad (3.37)$$

Suppose, rather than being Gaussian, $y(t)$ is distributed uniformly within some interval of length K, so that its probability density function is

$$\rho_y(\alpha) = \frac{1}{K}\,\Pi\left(\frac{\alpha-\bar{y}}{K}\right) . \tag{3.38}$$

This would apply to flutter having a sawtooth or triangular wave pattern of oscillation, for example. The uniform distribution of Eq. (3.38) can also be expressed in terms of the root mean square (rms) value (i.e., standard deviation) of $y(t)$, which is $y_{rms} = K/\sqrt{12}$:

$$\rho_y(\alpha) = \frac{1}{y_{rms}\sqrt{12}}\,\Pi\left(\frac{\alpha-\bar{y}}{y_{rms}\sqrt{12}}\right) . \tag{3.39}$$

When this is substituted into Eq. (3.35), the result is

$$B_{\tilde{f}_0} = 2\sqrt{3}\,y_{rms}\,f_0 . \quad \text{(Uniform Flutter)} \tag{3.40}$$

On the other hand, suppose that the flutter exhibits sinusoidal variations; i.e., the normalized frequency deviation is

$$y(t) = \bar{y} + \sqrt{2}\,y_{rms}\sin(2\pi f_f t + \eta) , \tag{3.41}$$

where f_f is the flutter frequency and η is a random starting phase (to make $y(t)$ a stationary random process). The probability density function is (Papoulis, 1965)

$$\rho_y(\alpha) = \frac{1}{\pi\sqrt{2y_{rms}^2-\alpha^2}}\,\Pi\left(\frac{\alpha-\bar{y}}{2^{3/2}y_{rms}}\right), \tag{3.42}$$

which exhibits infinitely tall cusps at $\pm\sqrt{2}\,y_{rms}$, because a sinusoid tends to linger near its maxima and minima. When this density is substituted into Eq. (3.35), the integral fails to converge. However, in this particular case there is an easy alternative for computing the duration. From Eq. (3.33) it is clear that the power spectral density of the fluttered tone $\tilde{x}(t)$ has the form

$$S_{\tilde{x}}(f) \cong \frac{1}{f_0} \rho_y(\alpha)_{\alpha \to \frac{f-f_0}{f_0}}, \tag{3.43}$$

and that means that $S_{\tilde{x}}(f)$ is confined to an interval whose endpoints are punctuated by tall cusps at values of f that satisfy

$$\frac{f-f_0}{f_0} = \bar{y} \pm \sqrt{2}\, y_{rms}, \tag{3.44}$$

i.e., at

$$f = (1+\bar{y}) f_0 \pm \sqrt{2}\, y_{rms} f_0, \tag{3.45}$$

which implies that the bandwidth $B_{\tilde{f}_0}$ is the width of that interval:

$$B_{\tilde{f}_0} = 2\sqrt{2}\, y_{rms} f_0. \qquad \text{(Sinusoidal Flutter)} \tag{3.46}$$

It is interesting that the formulas for the three different types of flutter statistics are almost the same; indeed, one can write

$$B_{\tilde{f}_0} = 2 \times \left\{\sqrt{2}, \sqrt{3}, \text{ or } \sqrt{\pi}\right\} y_{rms} f_0, \tag{3.47}$$

where $\sqrt{2}, \sqrt{3}, \text{or} \sqrt{\pi}$ is selected depending upon whether the flutter is sinusoidal, uniformly distributed, or Gaussian. The shapes of the fluttered-tone spectra are different in these three cases, however. Gaussian flutter gives a Gaussian-shaped spectrum, uniformly distributed flutter gives a flat spectrum, and for sinusoidal flutter the spectrum has two distinct peaks, with a trough of reduced level between them.

It should be noted that the term "flutter statistics" has been used here in reference to the normalized frequency deviation y(t), rather than the time axis perturbation $\varepsilon(t)$. If y(t) is sinusoidal or has Gaussian statistics then the same can probably be said for $\varepsilon(t)$. However, if y(t) looks like a triangular or sawtooth wave, so that its probability density is uniform, then $\varepsilon(t)$ will exhibit parabolic

arcs, and will not have a perfectly uniform distribution. (Since y(t) is the derivative of $\varepsilon(t)$, it follows that $\varepsilon(t)$ is the integral of y(t), and straight lines integrate to parabolic arcs.) The simple truth is that spectral broadening is more intimately related to y(t)than to $\varepsilon(t)$.

It is interesting to note that for the pure tone, spectral broadening of a 100 kHz sonar due to flutter is ten times as large as that of a 1 GHz radar, for the same equivalent observer velocity. (See discussion in Section 3.1.3.)

3.2 SOURCES OF FLUTTER IN ACTIVE SONAR

3.2.1 Motions of the Sonar Target

A sonar target resting upon the seafloor in a moderate current would probably not vibrate enough to cause appreciable flutter. However, a self-propelled target would be subject to turbulent forces (similar to the forces that cause cable strumming), possibly inducing enough random velocity of the acoustic reflecting boundary to distort the sonar echo. If the *only* source of flutter is random vibration or quivering of the sonar target, then the value of the normalized frequency deviation y(t)of the flutter is

$$y(t) = \frac{2\, v_{tgt}\left(t - \frac{1}{2}\tau_{del}\right)}{c}, \qquad (3.48)$$

where c denotes the speed of sound, τ_{del} is the round trip echo delay (from pulse transmission to echo reception), and $v_{tgt}(t)$ is the target's vibrational velocity component toward the sonar at time t. This formula may be verified by integrating both sides of Eq. (3.48), whereupon the left side becomes the time displacement $\varepsilon(t)$, and the right side becomes twice the target displacement due to vibration (i.e., the decrease in the round trip sound path) divided by the speed of sound. The time axis distortion seen in the arriving echo at time t was, in reality, induced when the sound was reflected from the target at time $t - \frac{1}{2}\tau_{del}$.

A simpler interpretation of Eq. (3.48) is that the equivalent observer

velocity $cy(t)$ is twice the target velocity, with an appropriate delay.

3.2.2 Including the Effects of Platform Motion

If the sonar platform is a moving vehicle, then it may undergo more turbulent random motions than the target. If random motion of the sonar platform is added to Eq. (3.49) the result is

$$y(t) = \frac{v_{son}(t - \tau_{del})}{c} + \frac{2\, v_{tgt}(t - \frac{1}{2}\tau_{del})}{c} + \frac{v_{son}(t)}{c}, \qquad (3.49)$$

where $v_{son}(t)$ is the platform's random velocity component toward the target at time t. The first and third terms on the right characterize the time axis distortion induced at the times of transmission and reception, respectively. The summation of contributions in Eq. (3.49) is based upon the additivity of cascaded flutter, as discussed above in Section 3.1.5.

It should be noted that some minor approximations have been made in Eq. (3.48). For example, the instant of reflection may not fall precisely at the middle of the echo delay τ_{del}, if the platform is in motion. Furthermore, the directions to and from the target could be time varying, and the directions of the pertinent ray paths ought to be used for exactness. However, since the random velocities $v_{tgt}(t)$ and $v_{son}(t)$ can only be quantified in statistical terms anyway, all of these approximations should be negligible (barring violent platform and target velocities on the order of the speed of sound in water).

It should be evident that the subsonic flutter assumption of Section 3.1.4 has a more tangible interpretation when the flutter is caused by target and/or platform motion. As expressed by Eq. (3.13), the subsonic flutter assumption means that the mean square value of the equivalent observer velocity $cy(t)$ is much less than c^2, and that the mean square perturbational velocities of the target and/or platform are, through Eq. (3.49), much less than c^2. To put it another way, making the subsonic flutter assumption is equivalent to supposing that the average, random motion kinetic energy of the object (target or platform) is much less than what its kinetic energy would be if it were traveling at the speed of sound in water.

3.2.3 Likely Motional Spectra for Sonar Platform and Target

The power spectral density $S_y(f)$ due to turbulence-induced motions of the platform and/or target will exhibit the same spectral characteristics as their velocities do. Due to mass loading and various dissipative processes these spectra should roll off rapidly with increasing frequency (although that assumption may be violated when resonant phenomena dominate).

As noted above in Section 3.1.4, for subsonic flutter the spectrum $S_\varepsilon(f)$ has to roll off faster than f^{-3} for large f. Unfortunately, data on the random perturbational motion spectra of sonar platforms and targets are not readily available. However, Blake (1986), in his book on flow-induced sound and vibration, provides the following formula for the mean square vibrational velocity of a plate excited by hydrodynamic flow, measured in a bandwidth Δf centered around frequency f:

$$\langle V^2 \rangle \propto \frac{U_\infty^2}{\eta_T}\left(\frac{\rho_0}{\rho_p}\right)^2\left(\frac{\delta^*}{h}\right)^3\left(\frac{U_\infty}{f\delta^*}\right)^n \frac{U_\infty}{c_l}\left(\frac{\Delta f}{f}\right) C_f^2 \,. \qquad (3.50)$$

The formula is valid for $f >> f_h$, where

$n \cong 4$,
f_h = hydrodynamic coincidence frequency (akin to resonance),
U_∞ = average free-stream velocity,
η_T = total loss factor,
ρ_0 = fluid (water) density,
ρ_p = plate density,
δ^* = boundary (shear) layer displacement thickness,
h = plate thickness,
c_l = longitudinal wave speed, and
C_f = friction coefficient.

If the sonar transducers are mounted on such a plate (the plate being, in

effect, the sonar platform) and if it is assumed that the velocity V in Eq. (3.50) is represented by the $v_{son}(t)$ of Eq. (3.49), then the component of the power spectral density $S_y(f)$ contributed by platform motion at the time of reception will obey

$$S_y(f) \propto \left(\frac{1}{c}\right)^2 \frac{U_\infty^2}{\eta_T}\left(\frac{\rho_0}{\rho_p}\right)^2\left(\frac{\delta^*}{h}\right)^3\left(\frac{U_\infty}{f\delta^*}\right)^n \frac{U_\infty}{c_l}\left(\frac{1}{f}\right) C_f^2 , \qquad (3.51)$$

for $f >> f_h$. Since $S_y(f) = (2\pi f)^2 S_\varepsilon(f)$ and $n \cong 4$, the rolloff characteristics of $S_\varepsilon(f)$ at high flutter frequencies will be described by

$$S_\varepsilon(f) \propto f^{-7}. \qquad (3.52)$$

The flutter contribution at the time of transmission would be similar.

Strictly speaking, Eq. (3.52) will apply only to the flutter contributed by flow-induced vibration of a transducer mounting plate; however, similar behavior might apply to other types of mounting configurations. On the other hand, Eq. (3.52) would not apply to gross, rigid-body motions of the sonar platform (or the target). If the turbulent, fluctuational force on the sonar platform were assumed to have a "white" spectrum, then the power spectral density of the rigid-body velocity components of the vehicle would roll off as f^{-2} at high flutter frequencies, due to the force-integrating effect of the inertial mass. This means that $S_y(f)$ would roll off like f^{-2} as well, with the result that

$$S_\varepsilon(f) \propto f^{-4}. \qquad (3.53)$$

The condition required by the subsonic flutter assumption, namely, that $S_\varepsilon(f)$ must roll off faster than f^{-3}, is satisfied by both Eqs. (3.52) and (3.53). In practice, the truth may lie somewhere between the two.

3.3 BEHAVIOR AT LOW FLUTTER FREQUENCIES

The subsonic flutter assumption, as expressed in Eq. (3.14) and repeated here for convenience,

$$\int_{-\infty}^{+\infty} S_y(f)\, df \;<<\; 1\,, \tag{3.54}$$

demands that $S_y(f)$ cannot grow as fast as $1/f$ at vanishingly low frequencies, because the integral would otherwise be infinite. Since $S_y(f) = (2\pi f)^2 S_\varepsilon(f)$, this means that $S_\varepsilon(f)$ cannot grow as fast as $1/f^3$ at low frequencies.

Since the mean square value of $\varepsilon(t)$, i.e., ε^2_{rms}, is the integral of $S_\varepsilon(f)$, it follows that ε^2_{rms} will be infinite if $S_\varepsilon(f)$ grows as fast as $1/f$ at low frequencies. However, for flutter that is due to random vibratory motion of a moving sonar platform it may be proper for $\varepsilon(t)$ to exhibit the characteristics of Brownian-type random process, including an infinite value of ε^2_{rms} (since the positional error due to micro-navigational imperfections may, indeed, grow without bound). In such cases it is better to use $y(t)$ and $S_y(f)$ than $\varepsilon(t)$ and $S_\varepsilon(f)$.

Yet, for the type of medium-induced flutter that is studied in Section 4, the time axis perturbations cannot exhibit the characteristics of a Brownian-type random process, since propagational variations in the medium will not cause the sound path to grow or shrink without bound. Indeed, the experimental results to be surveyed in Section 4 indicate that the time axis perturbations virtually never exceed a few milliseconds. For this kind of flutter it must be true that ε^2_{rms} is finite, and that $S_\varepsilon(f)$ cannot grow as fast as $1/f^3$ at low frequencies.

3.4 SECTION SUMMARY

Flutter has been defined and described in terms of a time axis perturbation $\varepsilon(t)$, a normalized frequency deviation $y(t)$ (the time derivative of $\varepsilon(t)$), an equivalent observer velocity $cy(t)$, and an equivalent observer

acceleration $c\dot{y}(t)$. Its characteristics have been discussed in terms of power spectral densities $S_\varepsilon(f)$ and $S_y(f)$, where f denotes the flutter frequency, and in terms of the spectral broadening that it impresses upon a pure tone. Several properties and bounds for the flutter parameters have been introduced for later use.

An argument has been offered that flutter induced by sonar platform motion will probably be characterized by a dramatic rolloff in the spectral density $S_\varepsilon(f)$, with asymptotic behavior lying somewhere between f^{-4} and f^{-7}; however, no data were available to estimate the magnitude of flutter from this source. Flutter induced by turbulence in the medium is examined in the next section.

4. FLUTTER CONTRIBUTED BY THE PROPAGATION MEDIUM

The ocean medium may contain sound speed inhomogeneities that move across the sonar's line-of-sight. This will be the case if the sonar is looking across a river's outflow, for example, or if the sonar platform is moving rapidly through a region of pronounced temperature inhomogeneities. Time axis distortions may then occur due to rapid variations in the speed of sound along the acoustic path. At first glance it might appear that the rather extensive body of literature on wave propagation through random media (e.g., Ishamaru, 1978) would provide ample tools to characterize this type of distortion. Unfortunately, previous investigators have focused their attention upon many issues that are of limited interest here. Nevertheless, some useful information has been developed and experimental studies have been made. This section reviews some of that prior work, and attempts to interpret it in terms of contributions to flutter.

4.1 PROPAGATION IN AN INHOMOGENEOUS MEDIUM

Sound speed inhomogeneities in the ocean are caused by internal waves, layering (including fresn water boundary layers), and turbulence. The word "fluctuation" is commonly used to describe the variations in sound speed (or, equivalently, the refractive index) that result, as well as the variations in acoustic phase and/or amplitude. However, in much of the mathematical literature this fluctuation is regarded either as a variation with spatial position, or as a statistical ensemble of possible outcomes, rather than as a time dependence. Caution must therefore be exercised to correctly interpret the term "spectrum", since it oftens refers to a spatial spectrum rather than a temporal one. Temporal spectra *are* used in experimental studies of the effects of internal waves and tides, and caution must be used in interpreting their results because of a notational peculiarity: In that literature the symbol ω is often used to denote cycles-per-unit-time rather than radians-per-unit-time, presumably implying a $\sin(2\pi\omega t)$ oscillation. This atrocity is usually camouflaged to some degree by the choice of hours as time units, so that ω is expressed in cycles per hour (cph). The reader will be pleased to note that the material presented in this report has been sanitized, using f where appropriate instead of ω.

The traditional approach to accommodate inhomogeneities can be loosely characterized as follows: In the absence of soundspeed inhomogeneities a spherical wave propagates from the source without perturbation, its amplitude decaying according to the law of spherical spreading; however, in the presence of (fixed) homogeneities the wavefront is distorted by bumps and dimples. These bumps and dimples obviously cause phase perturbations, but they also affect the amplitude because they alter the natural progression of spreading loss (by locally de-focusing or re-focusing the wavefront). The usual viewpoint taken by mathematical analysts is to assume that the inhomogeneities and the pattern of bumps and dimples are spatially random, but fixed in time. An exception is sometimes made to allow for the measurement of "scintillation drift", where the frozen pattern of medium inhomogeneities drifts slowly across the field of view.

Another limitation of the literature is that the analysis is always geared toward transmission of pure tones rather than broadband signals. It is also generally true that phase fluctuations are not considered without including amplitude fluctuations as well. Indeed, phase fluctuations are given scanty treatment when prediction of sonar detection ranges is the primary goal. The reader is also cautioned that virtually all the work has assumed one-way propagation, but the results obviously extrapolate to round trip propagation, within some degree of approximation.

4.2 DUDA *et al.*

4.2.1 Theoretical Results of Duda *et al.*

Duda, Flatté, and Creamer (1988) considered two anisotropic, *fine scale* models of sound speed fluctuation (the Garret-Munk ocean internal wave spectrum and a simple power law, wavenumber spectrum for spatial dependence of sound speed), and an isotropic *microscale* model (based upon a "Kolmogorov-type isotropic inertial-convective scalar subrange spectrum") to account for variations over distances of 1 m or less. They assumed weak fluctuations in the *unsaturated* regime, in which the scintillation index σ_I^2 was

less than 0.3 (which allowed the Rytov approximation to be used). The index σ_I^2 is defined as the normalized variance of sound intensity I:

$$\sigma_I^2 = \frac{\mathbf{E}\left(I^2\right) - \left[\mathbf{E}(I)\right]^2}{\left[\mathbf{E}(I)\right]^2}, \qquad (4.1)$$

where $\mathbf{E}$ denotes the expectation operator. Using the Garret-Munk model, they concluded that the unsaturated regime included all cases where the product of frequency and the square of the (one-way) range is less than 10^{11} m^2/s, which is met (for example) by 90 kHz at 1.1 km range.

4.2.2 Experimental Results of Duda *et al.*

Duda *et al.'s* experimental results were quite interesting. They conducted propagation studies by lowering transducers through holes cut in ice floes floating between Greenland and Elsmere Island, where the water was 380 m deep. They used 1 ms pulses at frequencies of 10, 20, 30, 60, and 75 kHz propagated (one way) horizontally across ranges of 270, 551, 820, and 1077 m. As mentioned above, they regarded the depth dependence of acoustic intensity as "fluctuations". Indeed, their assumption that the random fluctuations of both sound speed inhomogeneities and acoustic field parameters were frozen in time was evident in their experimental procedure: They raised their transducer through a depth span of 60 m at a rate of 0.5 m/s while recording sampled intensity values, and declared that "because the time required for each profile was short compared with the evolution time scale for the ocean sound speed perturbation spectrum, these [data] can be treated as instantaneous vertical profiles of sound pressure intensity I from a fixed source."

No phase data were recorded by Duda *et al.*, but it is noteworthy that their measured scintillation indices were well under 0.3. In fact, they were less than 0.1 in most cases even at the 1.1 km range. This observed constancy of amplitude, on the order of ±1 dB, suggests a rather stable propagation path (except that we must always remind ourselves that the stability is with respect to position, not necessarily with respect to time).

4.3 FARMER *et al.*

Fortunately for our purposes, phase data *were* recorded by Farmer *et al.*, in their experimental studies in the Cordova channel between Vancouver Island and James Island (Farmer and Clifford, 1986; Farmer, Clifford, and Verrall, 1987).

4.3.1 Test Environment of Farmer *et al.*

Their experiment used a pair of receivers placed upon one slope of the channel at a depth of 15 m, and a transmitter on the opposing slope of the channel at the same depth, at a distance of 660 m. The channel was 34 m deep at the center, so that the line-of-sight was approximately at mid-depth where it crossed the center of the channel. The two receivers were spaced 99.3 cm apart, along a horizontal line that was orthogonal to the sound path; i.e., they were positioned to intercept the incident wavefront simultaneously. The two receivers were used to measure the spatial correlation of the incident field, from which it was intended to infer the flow rate of the inhomogeneities across the sound path, caused by tidal cycles. Their computational method had been established in prior work (Clifford and Farmer, 1983).

Farmer *et al.* were apparently quite successful in their attempts to develop a remote method of cross-flow measurement. However, of greater interest to us is the fact that they measured phase (and amplitude) histories for the two receivers separately, and supported their study with extensive oceanographic recordings and analyses. A conductivity/temperature/depth (CTD) probe was used at 15 min intervals to determine sound speed as a function of depth (as inferred from temperature and salinity). Due to tidal mixing there was little or no gross bending of the sound ray across the channel, so that it remained essentially horizontal. However, there were microscale irregularities in the sound speed profiles that were adequate to cause fluctuations. Current meters were moored at three points in the channel. The tidal flow rates were roughly sinusoidal with a period of one day, with peak currents of about ±1 m/s. The investigators provided the following summary of

oceanographic data (Farmer, Clifford, and Verrall, 1987):

> "When the current is strong and the water well mixed, only a high-frequency [i.e., rapidly-varying with depth] temperature fluctuation of small amplitude appears on the CTD record. As slack water approaches, warmer, fresher water appears near the surface, giving way to a well-mixed layer bounded by stratification above and beneath. ... There is less variability within the enclosed mixing layer at slack water, but this subsequently increases until the profile again becomes relatively homogenized. The variability in the time series observation, however, remains substantially greater during the flood tide than during the ebb. Moreover, [CTD] profiles obtained during the flood tide display a significantly greater variability than corresponding ebb profiles."

4.3.2 Instrumental Technique of Farmer *et al.*

The acoustic transmissions were centered at 86 kHz (giving a wavelength of 1.72 cm), and the projector's nominal (circular) beamwidth was 10°. The main pulse was of 25.4 ms duration, consisting of 127 consecutive "bit intervals" of 200 μs duration each (Farmer and Clifford, 1986). These bit intervals were modulated by a maximal-length linear code sequence of length 127 bits (Dixon, 1984; Eaves and Reedy, 1987; Proakis, 1989). The 86 kHz carrier was on/off keyed by the binary code (Verrall, 1990). The autocorrelation of the complex envelope theoretically had the form of a triangular pulse whose base was of 400 μs duration. Experimental observations confirmed the theory (Farmer and Clifford, 1986). Indeed, after pulse compression (i.e., matched filtering by "multiplication of the [complex] detected signal with the corresponding code template"), the direct path signal amplitude displayed precisely that shape, but with a slightly rounded peak. A second arrival was also visible; its peak occurred about 600 μs later, roughly consistent with the predicted arrival time of surface and bottom reflected paths. (Since the sound path was at mid-depth, 15 m, in the center of the channel, the specular surface-bounce arrival should have arrived about 450 μs later, almost simultaneously with the bottom-bounce path.) After pulse compression filtering the received pulses were remarkably repeatable.

The coded pulse used by Farmer *et al.* had interesting properties. They actually used two additional 127-bit length transmissions, packed around the main pulse to act as "guard codes to improve the signal-to-noise ratio, [but] the useful signal was derived only from the center sequence." Thus the transmission consisted of "three identical consecutive 127-bit maximal linear coded sequences". Since the three compressed pulses would then be separated by 25.4 ms intervals, there was no danger of confusing them. The complete 76.2 ms (= 3X25.4) pulse train was transmitted five times a second, and the received data were recorded on an almost continuous basis for the duration of the experiment. Although the transmission consisted of three consecutive copies of the binary code sequence, the matched filter used only one copy, and applied the binary code as (-1,+1) multiplying factors (i.e., as phase-reversal keying), rather than as on/off keying in the manner used for transmission (Verrall, 1990). The purpose was to obtain a compressed pulse having a well-isolated central peak, surrounded by a (theoretically) zero-valued pedestal that extended 25.4 ms in either direction to the guard-code peaks, although a nonzero range-lobe structure was present beyond the peaks.

4.3.3 Phase Fluctuation Data of Farmer *et al.*

Farmer *et al.* have published phase data in two different journal articles. Each sample of phase data was taken as the argument of the complex envelope at the output of the matched filter, sampled when the magnitude reached its peak, with no smoothing having been done (Verrall, 1990). A simple phase-unwrapping algorithm was used to track the phase changes. The transmitting and receiving electronics were connected by cable to the data recording electronics, so there was no difficulty in maintaining a common phase reference. The phases were measured independently in the two hydrophone output channels. The two phases always tracked each other fairly closely, even though the hydrophones were spaced 99.3 cm apart.

In their JGR article (Farmer, Clifford, and Verrall, 1987) the researchers plotted 11 min phase histories for a quiescent period on 26 August 1984, which they characterized as "very well-mixed conditions during a weak flood (current ≈ 0.1 m/s)", and a more turbulent condition on 28 August 1984, described as

"stronger flow at a time of intense mixing (current ≈ 0.8 m/s)". For the quiescent data the phase changed very slowly and very little. It showed random undulations of about ±15° over periods of 30 s, with a slight long term drift. (The pulse transit time was observed to vary by 250 μs during each tidal cycle, which corresponds to 21.5 cycles or 7740° of accumulated phase shift. This works out to about 5° of phase drift per minute, assuming that the variation is roughly constant between flood tide and ebb tide.) The phase plots from the two hydrophones were almost identical, except for a phase offset that was due to a slight misalignment of the transducer pair relative to the incident wavefront.

For the more turbulent condition on 28 August the phase history showed greater and more rapid variation. In the 11 min plot there was one full cycle of roughly sinusoidal variation of phase of about ±180°, numerous small variations of about ±70° occurring over periods of about 20 s, and smaller variations over shorter periods. Only occasionally did the phase vary by more than 30° within a 10 s span.

Phase plots covering a different 11 min period, on 25 August 1984, were published in the IEEE paper (Farmer and Clifford, 1986). The current was not specified, but the condition appears to be that of moderate turbulence, although not quite so much as for the 28 August data.

One of their phase plots was hand digitized by the present author, and is shown in Fig. 4.1.

4.3.4 Calculations Using the Data of Farmer *et al.*

The data of Fig. 4.1 can be divided by 360° and multiplied by the carrier period (11.628 μs) to get the time perturbation $\varepsilon(t)$, then numerically differentiated with respect to time to get the normalized frequency deviation $y(t)$, and finally multiplied by the speed of sound (1490 m/s) to get the equivalent observer velocity $cy(t)$. The result is plotted in Fig. 4.2. (One outlier, probably due to noise that was introduced by the present author's hand-digitization, was off-scale and is not shown.)

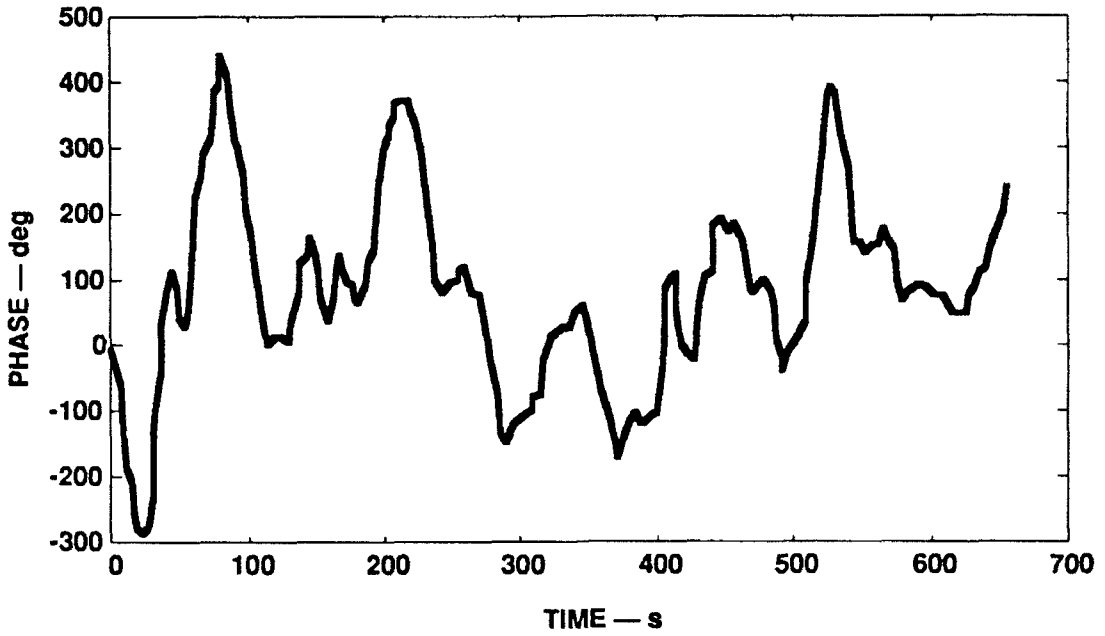

FIGURE 4.1
86 kHz PHASE VARIATIONS AT 660 m OVER AN 11 min PERIOD, TAKEN FROM FARMER AND CLIFFORD (1986)

What is significant about Fig. 4.2 (see next page) is that the equivalent observer velocity is so small. The root mean square of the data shown in the figure is only 0.0634 cm/s. To put this in perspective, suppose that a self-propelled sonar platform has a 4-blade propeller turning at 600 rpm (i.e., 5 Hz), with a stationary strut located so close to the propeller that it impedes the flow to some degree. As each blade passes the strut it will temporarily lose efficiency, so that there will be a negative force pulsation at a rate of 20 Hz (= 4 X 5 Hz). Suppose this force produces a peak acceleration of 0.01 g, which is the threshold of perception for a human observer, at 20 Hz, under ideal quiescent conditions (Harris, 1988). Then the root mean square vibrational velocity will be

$$v_{rms} = \frac{0.01 \times 9.8 \text{ m/s}}{\sqrt{2} \times 2 \times \pi \times 20 \text{ Hz}} \approx 0.055 \text{ cm/s} \qquad (4.1)$$

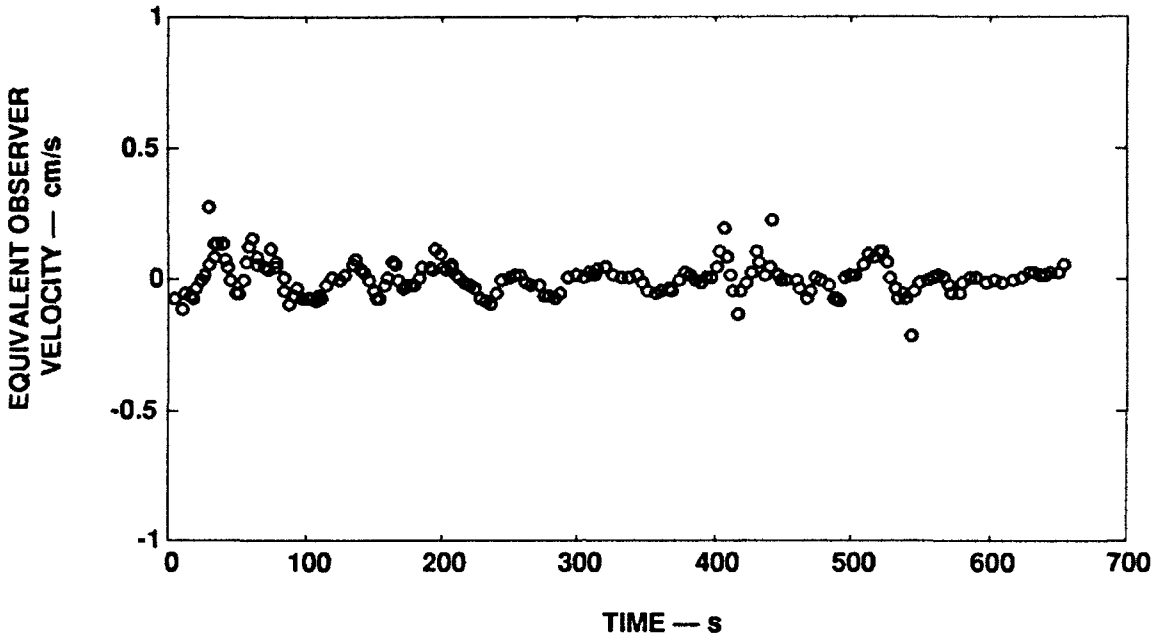

FIGURE 4.2
EQUIVALENT OBSERVER VELOCITY CALCULATED BY THE PRESENT AUTHOR FROM THE PHASE DATA OF FARMER *et al.*

which is almost as large as the overall 0.0634 cm/s equivalent observer velocity shown in Fig. 4.2, and greatly exceeds its components of comparable frequency (observe that most of the 0.0634 cm/s amplitude of Fig. 2.3 is due to oscillatory energy at much lower frequencies, of the order 0.02 Hz). Recall, also, that the data of Fig. 4.2 were for a relatively turbulent condition. During quiescent conditions the fluctuations were much less, by at least an order of magnitude. What this example indicates is that the propagational fluctuations due to medium instabilities are equivalent to very small platform vibrations, so small as to be insensible to human observers (but perhaps not insensible to a sonar).

4.4 EWART *et al.*

The Cobb Seamount experiment, done in 1971, had a transmit/receive geometry similar to that of Farmer *et al.*, but on a larger scale. The following

summary paraphrases the one given by Ewart (1976).

4.4.1 Test Environment of Ewart *et al.*

The transmitter and receiver towers (each 15 m high) were positioned at depths of 973 m and 951 m, respectively, on the slopes of opposing seamounts at a separation of 17.2 km. The seafloor dropped off to a depth of about 3000 m between the two seamounts. Extensive oceanographic data were recorded, including temperature, salinity, and sound velocity profiles using dropped probes and the self-propelled underwarter research vehicle (SPURV). Ray tracing analysis indicated that the main refracted path was concave-upward, with its lowest point at about 1200 m depth. Currents were measured periodically at the transmitter and receiver locations. The largest observed current was 12 cm/s, but most of the time it was less than 5 cm/s.

4.4.2 Instrumental Technique of Ewart *et al.*

The experiments were conducted at two frequencies: 4.166 kHz and 8.333 kHz. The receiver consisted of three hydrophones positioned along a horizontal line that was approximately orthogonal to the sound path. The hydrophones were spaced so as to permit correlation studies at separations of 5, 10, and 15 m. The transmitter had a strong vertical directivity, with a beamwidth of 22° at 4.166 kHz and 11° at 8.333 kHz. The receiving hydrophones also had strong vertical directivity, with beamwidths of 30° and 15° at the two frequencies.

The transmissions consisted of eight cycles of 4.166 kHz, or 16 cycles of 8.333 kHz, giving pulse durations of 1.92 ms in both cases. The transmissions were repeated every 15.72864 s, with alternation of the choice of frequency, giving a complete pair of transmissions (both frequencies) every 31.45728 s. The received waveforms were digitized (9 bits plus sign) at 65.666 kHz, stored in a temporary memory, and then telemetered to the data recording ship. The telemetery was in two stages: by a short range acoustic link (at 45 kHz carrier frequency), and then by a buoy-to-ship radio link (at 253.1 MHz carrier frequency). Since there was no wire link between the transmitter and receiver, reliance had to be placed upon a pair of precise electronic clocks to maintain

instrumental phase synchronism. The clocks were tested for six months prior to the experiment, establishing that their timing frequencies agreed to within one part in 10^9. A total of 16,500 pulse transmissions of each frequency were recorded during 85% of a 144.5 h period.

The first millisecond of each received pulse was examined to extract phase (and amplitude data). It should be noted that Ewart (1976) used the word "phase" to refer to what we have called the time perturbation $\varepsilon(t)$ in Section 3.1. We shall use our terminology in paraphrasing his results.

4.4.3 Experimental Results of Ewart *et al.*

Ewart extracted the time perturbation $\varepsilon(t)$ from the following three independent calculations.

"(1) From the discrete Fourier transform of the pulse evaluated at the acoustic center frequency and the two frequencies adjacent to it,

(2) graphically from digital computer plots of every 50th pulse (the time between 50 pulses is less than the correlation time of the phase), and

(3) by a one-parameter least squares fit of the observed pulse axis crossings to the expected axis crossings using the time delay as the parameter."

The values of $\varepsilon(t)$ were computed for each of the three hydrophones, for each of the two pulse center frequencies, and for each transmission, i.e., every 15.72864 s. The amplitudes of the received pulses were also determined. This was done by adjusting the amplitude of an ideal sine wave (of duration 480 μs), offset in time by the value of $\varepsilon(t)$ that was already determined, to achieve a least squares fit to the received data. Ewart, in his Fig. 8 (Ewart, 1976), plotted the measured values of $\varepsilon(t)$ for hydrophone 1, for the entire 144 h period of the experiment, for both center frequencies (4.166 kHz and 8.333 kHz). There were some gaps in the plots, totaling about 20 h. During about half of this gap-time the telemetry was lost, and during the other half the data were censored

because there was deemed to be multipath interference. The first 88 h of 8 kHz data were hand-digitized from Ewart's Fig. 8 by the present author, and are presented here as Fig. 4.3, with the gaps filled in by straight lines.

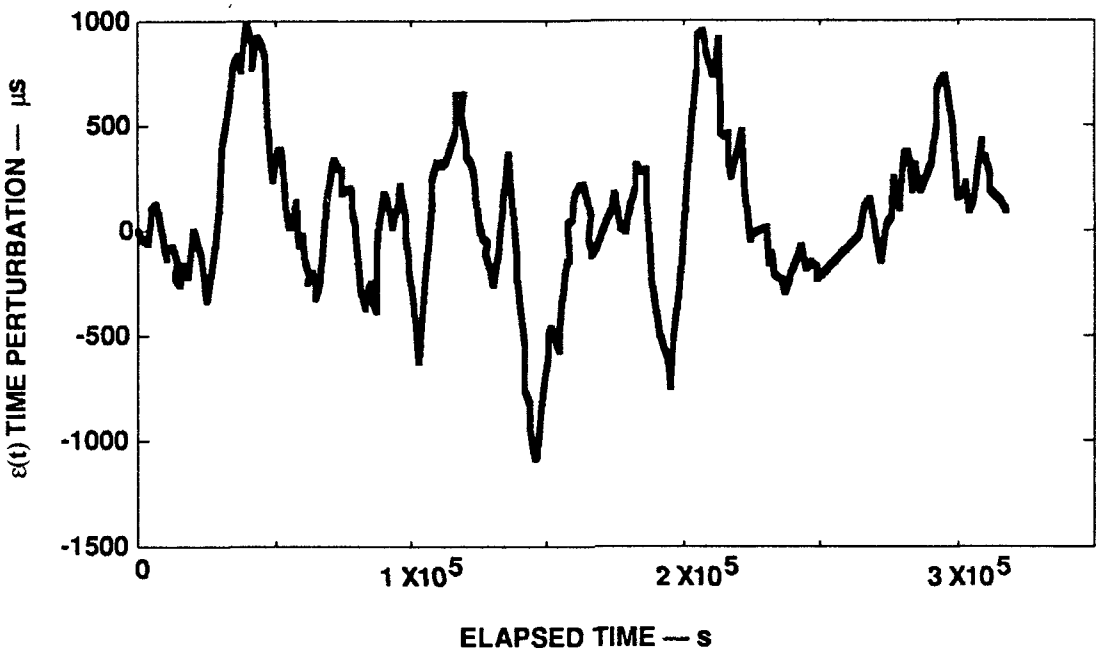

FIGURE 4.3
TIME PERTURBATIONS OF AN 8 kHz PULSE AT 17.2 km DURING AN 88 h PERIOD, TAKEN FROM EWART (1976)

In this plot ε(t) looks like a typical random process exhibiting low frequency emphasis. In fact, it looks rather like the phase data of Farmer *et al.* that were shown in Fig. 4.1, except that the Farmer *et al.* data covered only a span of 11 min instead of 88 h, and showed a maximum perturbation of only about 13 μs (400° at 86 kHz) instead of ±1000 μs. However, the reader will recall that Farmer *et al.* reported a 250 μs variation in pulse time of arrival over the course of the tidal cycle; furthermore, their sound was transmitted over a 660 m span as opposed to the 17.2 km span of Ewart. If these differences are taken into account, the two experimental results exhibit a modicum of similarity.

4.4.4 Analysis of Ewart's Data

For high resolution sonar applications the phase variations that occur within seconds are much more important than those that occur over several hours or days. Unfortunately, $\varepsilon(t)$ was only sampled every 31 s in Ewart's experiment. However, it may be possible to extrapolate the statistics from long term to shorter term variations by using Ewart's studies of the power spectral density of $\varepsilon(t)$. In our notation this density is denoted as $S_\varepsilon(f)$, where f denotes the flutter frequency (see Section 3). Ewart estimated $S_\varepsilon(f)$ by computing a 16,384-point, discrete Fourier transform of $\varepsilon(t)$ with a Hamming window, and then applying logarithmic smoothing to the resultant periodogram. For 4.166 kHz as well as 8.333 kHz transmissions, $S_\varepsilon(f)$ rolled off like f^{-3}. To study this behavior more carefully, Ewart plotted a flattened version of the power spectral density, $f^3 S_\varepsilon(f)$, in his Fig. 16. The present author has hand digitized his plot; it appears below as Fig. 4.4.

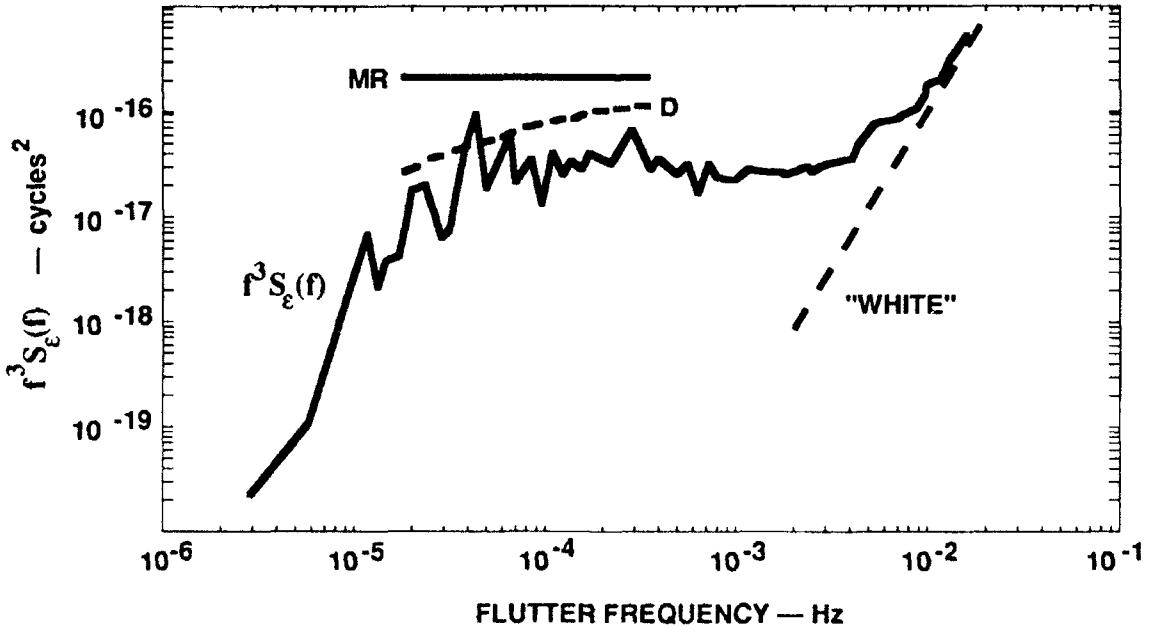

FIGURE 4.4
CUBIC-FREQUENCY SCALED POWER SPECTRAL DENSITY OF TIME PERTURBATIONS OF 8 kHz PULSE, FROM EWART (1976)

There are a number of comments to be made regarding Fig. 4.4:

(1) Ewart used cycles per hour (cph) for his flutter frequency axis. To get Hz in Fig. 4.4, his abscissas had to be divided by 3600 s/h .

(2) Ewart expressed $S_\varepsilon(f)$ in units of $(\mu s)^2/(cph)$, so he naturally expressed $f^3 S_\varepsilon(f)$ in units of $(\mu s)^2 \cdot (cph)^2$. To get Fig. 4.4, his ordinates had to be divided by $[(10^6 \mu s/s) \cdot (3600 s/h)]^2$, which resulted in ordinates having the dimensions of squared cycles, the time units having canceled out. The time units actually canceled out in the ordinates of Ewart's plot, of course, but it had not been obvious.

(3) The first three peaks (i.e., local maxima) in the spectrum are not artifacts; they are tidal effects. They are the diurnal frequency of 1.16 X 10^{-5} Hz (period = 24 h), the semidurnal frequency of 2.24 X 10^{-5} Hz (period = 12.4 h), and the quarter-diurnal frequency of 4.48 X 10^{-5} Hz (period = 6.2 h).

(4) The solid line marked "MR" and the dashed line marked "D" represent theoretical predictions that Ewart attributes to other researchers, namely, Munk and Rosenbluth (MR), and Desaubies (D). The lines are drawn over an applicable range of flutter frequencies, from the "inertial frequency" of 1.68 X 10^{-5} Hz (period = 16.5 h), to the Väisälä frequency at 1000 m depth, namely 2.41 X 10^{-4} Hz (period = 1.15 h).

(5) Wherever the cube-frequency-scaled spectrum curve in Fig. 4.4 is approximately level, it means that $S_\varepsilon(f) \sim f^{-3}$. This is clearly the case for frequencies in the range from 2.2 X 10^{-5} Hz to 4 X 10^{-3} Hz. On the other hand, wherever $S_\varepsilon(f)$ remains constant, the curve of $f^3 S_\varepsilon(f)$ as plotted in Fig. 4.4 exhibits a positive slope of three decades per decade. Such a slope is indicated by the dashed line marked "white".

4.4.5 White Noise Artifact in Ewart's Data

Certainly, any contributions to the $\varepsilon(t)$ that are random and uncorrelated from sample to sample will add a "white noise floor" to $S_\varepsilon(f)$, and produce an

upward slope parallel to the line marked "white". Evidence of such behavior is strongly indicated in Fig. 4.4. Such uncorrelated perturbations can come from at least two sources:

Type 1 — measurement errors due to additive random noise within the receiver passband, including electronic noise and "sea state noise", and

Type 2 — the combined effect of all fluctuations in $\varepsilon(t)$ that occur at a rate faster than 0.032 Hz (which is the sampling frequency, i.e., the reciprocal of 31 s).

Contributions of type 2 can be regarded as the result of aliasing due to the 0.032 Hz sampling rate of Ewart's experiment; i.e., the higher frequency fluctuations of $\varepsilon(t)$ were randomly mapped into the low frequency domain. Contributions of type 1 are not part of $S_\varepsilon(f)$; they merely contaminate the measurements of $\varepsilon(t)$ and inflate the periodogram estimate of $S_\varepsilon(f)$.

Ewart concluded that the white noise portion of the periodogram estimate of $S_\varepsilon(f)$ contributed about $(2.2\ \mu s)^2$ to the variance of $\varepsilon(t)$, whereas the *total* variance of $\varepsilon(t)$ was $(374\ \mu s)^2$ for the 8.333 kHz pulse transmissions. This means that

$$2\int_{0.032\ Hz}^{\infty} S_\varepsilon(f)\ df \quad \leq \quad (2.2\ \mu s)^2\ , \tag{4.2}$$

whereas

$$2\int_{0\ Hz}^{\infty} S_\varepsilon(f)\ df \quad = \quad (374\ \mu s)^2\ . \tag{4.3}$$

(The factor "2" is needed to account for both positive and negative frequencies, since $S_\varepsilon(f)$ is a two-sided, symmetric, power spectral density of the real valued random process $\varepsilon(t)$.)

Based upon prior experimental simulations and pre-experiment tests of his electronic apparatus, Ewart concluded that the "white" contribution to the variance, $(2.2\ \mu s)^2$, was due to type 1 errors. Thus, he concluded that the upturn in the curve of $f^3 S_\varepsilon(f)$ in the right-hand portion of Fig. 4.4 was an artifact of the measurement limitations (i.e., noise and sampling rate).

4.4.6 An Approximate Formula for $S_\varepsilon(f)$, from Ewart's Data

One might assume, therefore, that $f^3 S_\varepsilon(f)$ actually remains flat beyond 10^{-3} Hz, at about the value 10^{-13} (cycles)^2. The power spectral density of the time axis perturbations $\varepsilon(t)$ could then be approximated as

$$S_\varepsilon(f) \cong |f|^{-3} \times 10^{-13}, \tag{4.4}$$

which gives a result in units of s^2/Hz if the flutter frequency f is expressed in Hz.

Ewart's experiment established Eq. (4.4) only from flutter frequencies of about 2×10^{-5} Hz to 4×10^{-3} Hz, with extension to 0.032 Hz by virtue of the "white noise" explanation. To get to the higher flutter frequencies that might impair replica correlation in a high resolution sonar, where transmissions of up to tens of seconds might be used to achieve large time-bandwidth products, one would have to extrapolate Eq. (4.4) upwards by at least a few orders of magnitude in f.

In the spirit of this extrapolation one might also consider reductions in range from Ewart's 17.2 km. One way to do this is to assume that each portion of the propagation path makes equal contribution to the variance, at all frequencies, i.e., $S_\varepsilon(f)$ grows linearly with range. In that case, for operation of an active sonar at range R_{son}, Eq. (4.4) would generalize to

$$S_\varepsilon(f) \cong \left(\frac{2 \times R_{son}}{17.2\ km}\right) |f|^{-3} \times 10^{-13}. \tag{4.5}$$

[NOTE: This can be no more than a crude approximation. There is reason to suspect that $S_\varepsilon(f)$ would not shrink exactly linearly with range, because all portions of the propagation path may not contribute equally to the variance.

Indeed, as noted in Farmer *et al.* (1987), the inhomogeneities near the receiver have greater effect upon the wave-structure function that determines phase fluctuation statistics. Nevertheless, the approximation of Eq. (4.5) may suffice down to some inner range limit. Furthermore, one should remember that f^{-3} dependence cannot extend to arbitrarily large f. It must roll off faster than that because of the subsonic flutter assumption; see Section 3.1.4.]

It will be recalled from Section 3.1.3 that the equivalent observer velocity is $cy(t)$, where $y(t)$ is the derivative of $\varepsilon(t)$, so that $S_y(f) = (2\pi f)^2 S_\varepsilon(f)$. Thus, if Eq. (4.5) is true then the power spectral density of the equivalent observer velocity is given by

$$c^2 S_y(f) \cong (2\pi \times 1500 \text{ m/s})^2 \times \left(\frac{2 \times R_{son}}{17.2 \text{ km}}\right) |f|^{-1} \times 10^{-13}, \qquad (4.6)$$

with the result having units of $(m/s)^2/Hz$. To get the root mean square value of the equivalent observer velocity, one would integrate the right-hand side of Eq. (4.6) over the appropriate range of flutter frequencies, $f_1 \le f \le f_2$, then double it (to account for positive and negative frequencies), and finally take the square root. The result is that the root mean square equivalent observer velocity is

$$\{cy(t)\}_{rms} \cong \sqrt{\left(\frac{R_{son}}{17.2 \text{ km}}\right) \log_e\left(\frac{f_2}{f_1}\right)} \times 0.298 \text{ cm/s}. \qquad (4.7)$$

4.4.7 Application of the Formula Based on Ewart's Data to the Results of Farmer *et al.*

As an example of the application of Eq. (4.7), let us see how well it predicts the equivalent observer velocity curve of Fig. 4.2 that was obtained from the Cordova Channel experiment of Farmer *et al.* (admittedly in more turbulent water). Since Eq. (4.7) was tailored for active sonar (i.e., for round trip propagation), the 660 m span of the Cordova Channel experiment must be divided by 2. The observations of Fig 4.2 were for a period of 11 min (660 s), so that any fluctuation having a longer period would not have been seen. Thus,

it is appropriate to set f_1 as 1/660 ≈ 0.0015 Hz. The selection of the upper limit is less obvious, but luckily Eq. (4.7) is rather insensitive to it. The sampling rate (transmissions per second) of Farmer *et al.* was five samples per second, so a natural choice for f_2 is 5 Hz. The result of calculating Eq. (4.7) with these values is a root mean square velocity of 0.118 cm/s. In comparison, the root mean square velocity of the data in Fig. 4.2, from the Cordova Channel experiment, was 0.06345 cm/s.

This agreement, to within a factor of 2, is truly remarkable. In fact, such close agreement was probably accidental, given the substantial extrapolations and approximations involved, and the dependence of the Cordova Channel propagation statistics upon weather conditions.

4.4.8 Dependence of Ewart's Data upon Tone Center Frequency

All of the analysis just presented was based upon Ewart's power spectral density data for the 8.333 kHz transmissions. The 4.166 kHz data provided generally similar results, although there were differences in the spectra above the Väisälä frequency (2.41×10^{-4} Hz) that could have been due to a shift in the noise floor. The nature of "true" flutter, as it has been defined above in Section 4.1, is such that the time axis perturbation $\varepsilon(t)$ is independent of the center frequency of the pulse transmission. Ewart stated that the 4.166 kHz and 8.333 kHz data "produced almost identical [$\varepsilon(t)$] time series". Indeed, this was true as regards gross fluctuations that occurred over time spans on the order of an hour or more. However, when the present author made a transparency from Ewart's Fig. 8 and overlaid it on his plot so as to align the 4.166 kHz and 8.333 kHz $\varepsilon(t)$ time series, there were visible discrepancies on the order of at least ±30 μs. Furthermore, Ewart reported that the overall variance for the 4.166 kHz data was $(384\ \mu s)^2$, as compared to $(374\ \mu s)^2$ for the 8.333 kHz data. Thus, they were only approximately identical.

The noise floor fluctuations discussed above would have been independent in the two time series; however, Ewart determined that those fluctuations only inflated the variance of $\varepsilon(t)$ by $(2.2\ \mu s)^2$, which would have accounted for a difference variance of $2 \times (2.2\ \mu s)^2$, i.e., a root mean square

difference of about 3 μs between the ε(t) time series for the two transmitting frequencies. This is significantly smaller than the 30 μs discrepancy noted above. Thus, evidence remains that the fast-rate fluctuations were nonidentical for the two frequencies. Actually, this discrepant behavior is in conformance with the fine-scale and microscale theory of inhomogeneities, wherein the size of the inhomogeneity in comparison to the acoustic wavelength determines the degree to which it perturbs the propagating wavefront (Ishimaru, 1978).

4.4.9 Later Analysis by Ewart *et al.*

In a later paper (Ewart *et al.*, 1983), the Cobb Seamount experiment was discussed again, with an aim toward resolving some of the discrepancies in amplitude fluctuation statistics between theory and experiment. However, the authors stated, "We do not discuss the phase (transit time) [i.e., the ε(t) data of the 1971 Cobb Seamount experiment] because predictions on the basis of the Rytov or Born approximation as in Desaubies and Flatté *et al.* are very close to the observations. Ishimaru has shown that the Rytov approximation for the phase is valid for large range into the region of saturation." Thus, the phase data of Ewart (1976) stand.

4.5 CHRISTOFF *et al.*

Christoff *et al.* (1982) reported a study of acoustic phase stability in shallow water in St. Andrews Bay, near Panama City, Florida.

4.5.1 Test Environment of Christoff *et al.*

The tests were made at the eastern end of the remaining west span of the old Hathaway Bridge (the center span having been removed many years earlier). The water was nominally 12 m deep, with tidal variations of ±0.6 m. The transmitter was mounted atop an upright 4 m aluminum beam, whose base was anchored rigidly by a 3000 lb concrete clump. The receiver was 48 m away, mounted on a platform of adjustable depth that was locked into position for each set of measurements. Phase histories were published for the receiver at 3, 4, and 9 m above the bottom.

4.5.2 Instrumental Technique of Christoff *et al.*

A 100 kHz tone burst of 140 μs duration was transmitted every second. The direct path pulse arrived cleanly, 250 μs ahead of the bottom-bounced pulse. In-phase and quadrature components of the first part of the received pulse were sampled, digitized, and processed by a small computer. The "phase noise" of the system was measured to be less than 1/100th of a cycle (i.e., 0.1 μs). (From their plots it appears that this is a very conservative upper limit.) Phase was computed by rectangular-to-polar conversion of the complex data.

4.5.3 Experimental Results of Christoff *et al.*

Christoff *et al.* published plots of phase history that were recorded over 20-32 min periods in June 1979, at a receiver elevation of 3 m; in November 1980, at 4 m elevation; and again in November 1980, at 9 m elevation. The author has hand-digitized the last of these; the result appears as Fig. 4.5.

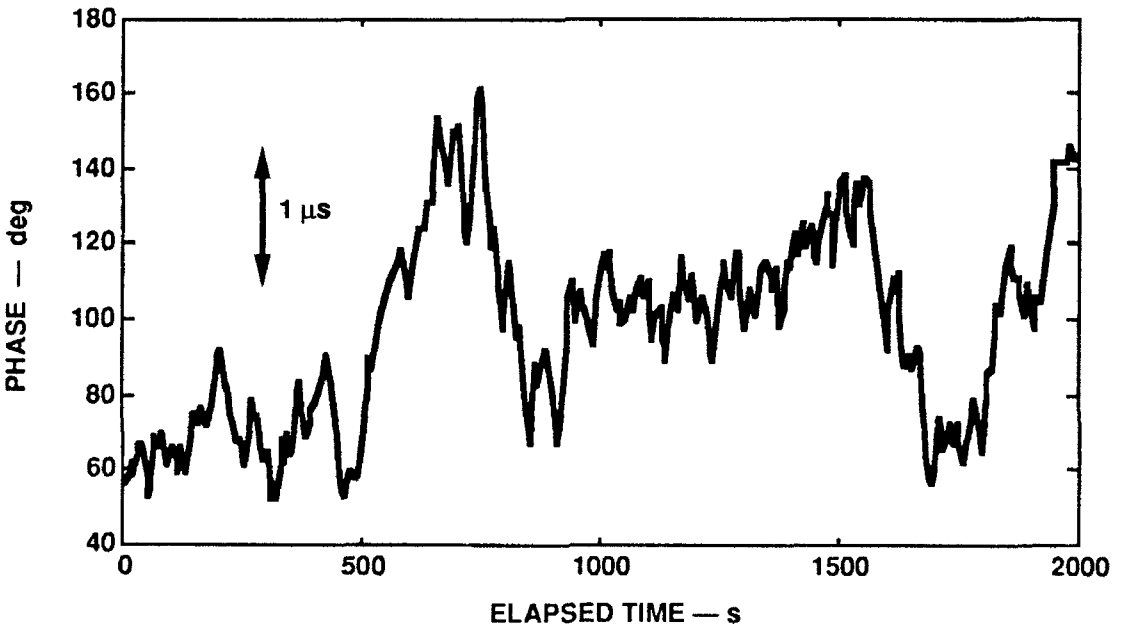

FIGURE 4.5
100 kHz PHASE VARIATION AT 48 m OVER A 33 min PERIOD, TAKEN FROM CHRISTOFF *et al.*

Their other two phase plots for the lower receiver altitudes showed much less variation, by an order of magnitude. Indeed, it appears to the present author that the most significant phase variations in those data (not shown here) were occasional transient events on the order of 30 s duration, possibly due to biological entities.

4.5.4 Calculations from the Results of Christoff *et al.*

The data of Fig. 4.5 can be represented as a time axis perturbation $\varepsilon(t)$ by multiplying the ordinates by (10 μs)/360. The variation in $\varepsilon(t)$ has a span of about 3 μs, with a standard deviation of 0.698 μs. The equivalent observer velocity $cy(t)$ can then be computed by taking the derivative of $\varepsilon(t)$ and multiplying by $c = 1490$ m/s. The result is plotted as Fig. 4.6.

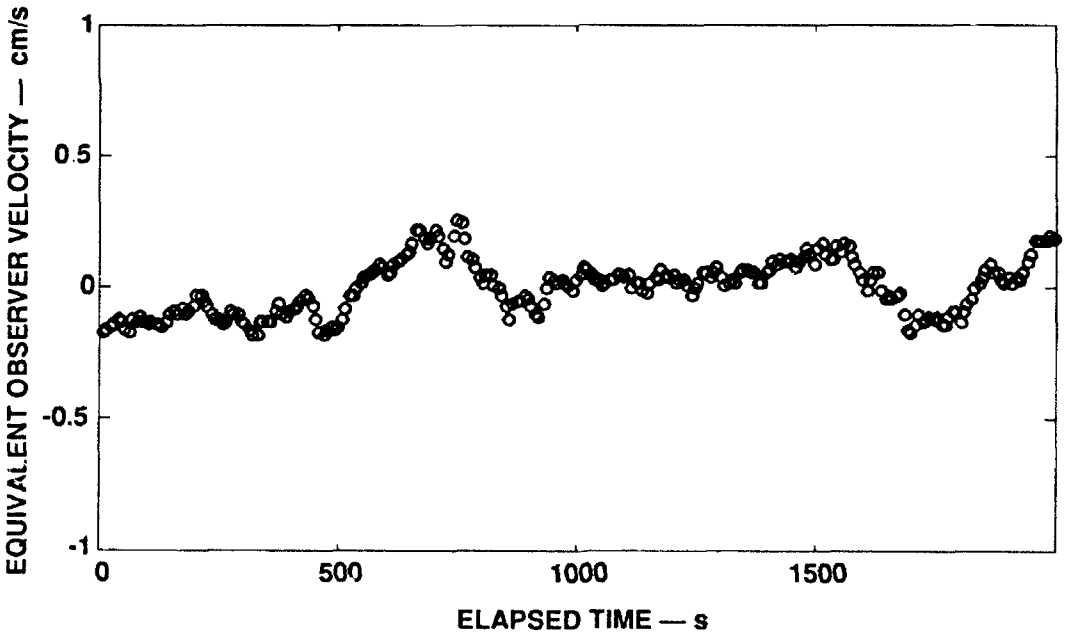

FIGURE 4.6
EQUIVALENT OBSERVER VELOCITY CALCULATED BY THE PRESENT AUTHOR FROM THE DATA OF CHRISTOFF *et al.*

The plot of Fig. 4.6, which is for 86 kHz transmissioins at 660 m range, is very comparable to Fig. 4.2, which showed the results of a similar calculation for the data of Farmer *et al.* for 100 kHz at 48 m.

The power spectral density $S_\varepsilon(f)$ was calculated from the $\varepsilon(t)$ data by the present author using the Welch method, employing Hanning-windowed blocks of 256 s duration. This resulted in a distortion (flattening) of the spectrum below 0.01 Hz, but those very low frequencies were not of primary interest. The resulting plot appears below as Fig. 4.7

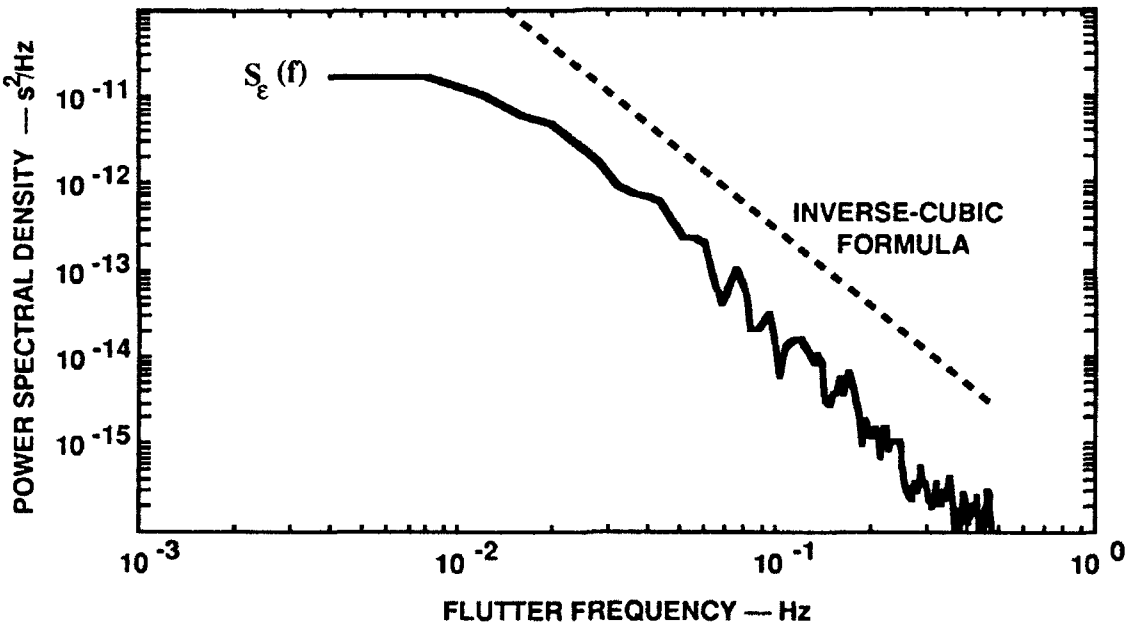

FIGURE 4.7
POWER SPECTRAL DENSITY OF TIME PERTURBATIONS OF A 100 kHz PULSE, TAKEN FROM CHRISTOFF *et al.* (1982)

The dashed line marked "inverse-cubic formula" is a plot of the approximate extrapolation formula of Eq. (4.5) that was obtained from Ewart's data in the manner described above in Section 4.4.6. In that formula the value of R_{son} was set at 24 m (= 48/2), since the formula was designed for active sonar (round trip path). The agreement is fairly good except for a difference in level.

The actual time perturbations measured by Christoff *et al.* were about 1/3 of what the formula predicted (giving a power spectral density about 1/10 as high). It should be remembered, however, that the other two phase perturbation plots of Christoff *et al.* showed fluctuations whose amplitudes were smaller by an order of magnitude. This would correspond to two orders of magnitude reduction in the power spectrum of Fig. 4.7.

It is to be expected that the level of the fluctuation spectrum should be highly variable, and depends upon environmental conditions. What is significant is that the *shape* of the fluctuation spectrum consistently rolls off approximately as f^{-3}, as confirmed by data from experiments with parameters that differed by a wide margin. Actually, the spectrum in Fig. 4.7 rolls off a bit faster than f^{-3} at the higher flutter frequencies, perhaps by as much as f^{-4}.

4.5.7 Conclusions of Christoff *et al.*

The motivation behind the experiment of Christoff *et al.* was to determine whether the fluctuations in the medium would limit the operation of a 100 kHz synthetic aperture sonar operating at modest ranges. Since the observed phase fluctuations were so small, rarely varying by more than 20° in a 2 min window, they concluded that the fluctuations would be no problem. Similarly, we can conclude that the fluctuations would not have interfered with replica correlation, even if the transmitted waveforms had been of 2 min duration.

4.6 BARTELS

Bartels (1989) performed a propagation phase-stability experiment near the bottom of Lake Travis (at Lake Travis Test Station) in 1988.

4.6.1 Test Environment of Bartels

The transmitter and receiver were both TR-225 transducers. Each was mounted upright at the center of a heavy, steel 2 ft x 2 ft anchor plate. The transducers were separated by 110 m, at depths of 30 and 37 m. The lake floor between the tranducers was known to be free of obstructions. Severe thermal

gradients are the norm for this lake in July, but they do not usually extend below 15 m; the region near the lake floor at 30 m is thought to be relatively isothermal. The current was negligible, and the sound path was only a few inches above the lake floor. All data reported here were collected between 12:30 AM and 2:10 AM on 19 July 1988.

4.6.2 Instrumental Technique and Experimental Results of Bartels

Tone bursts, consisting of 2 ms duration of 40 kHz, were transmitted at a rate of 1, 2, or 4 times per minute (the rate varied during the data recording period). The received signal was digitized at a 2 MHz rate and decimated by one half for computer storage. Windows of 8 ms of data were stored for each tone burst. Each window was then truncated to a 1.82 ms sub-window that contained only the direct path arrival. The phase (and amplitude) were extracted from the 40 kHz complex component of the discrete Fourier transform. The phase history for the 100 min data collection period is shown in Fig. 4.8.

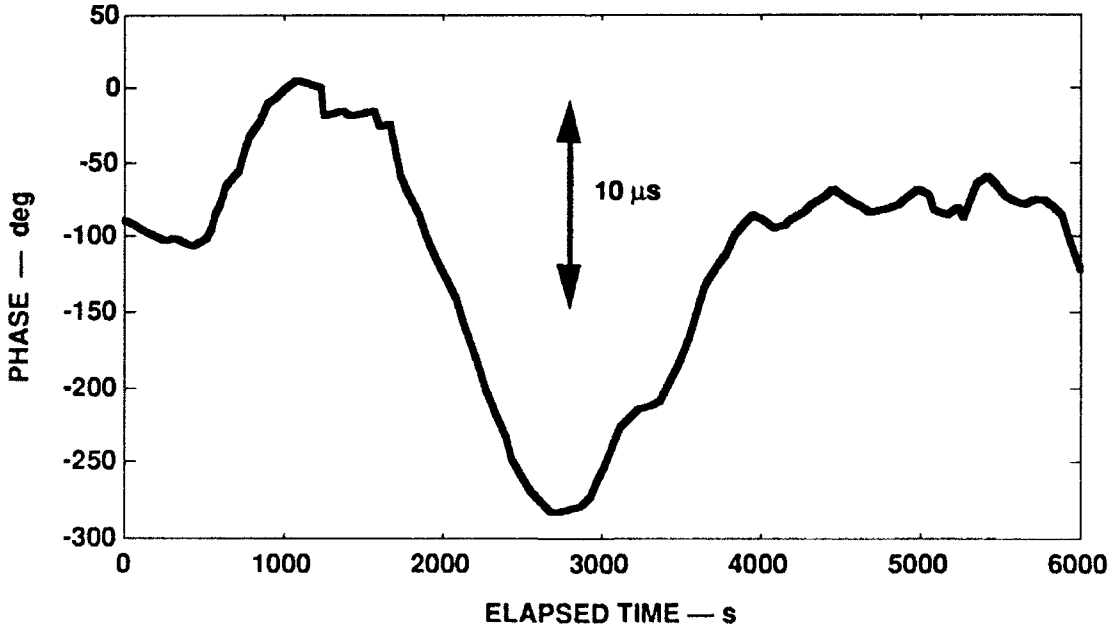

FIGURE 4.8
40 kHz PHASE VARIATION AT 110 m OVER A 100 min PERIOD, TAKEN FROM BARTELS (1989)

4.6.3 Calculations from the Results of Bartels

The data of Fig. 4.8 can be represented as a time axis perturbation $\varepsilon(t)$ by multiplying the ordinates by (25 μs)/360°. The variation in $\varepsilon(t)$ is much greater than for the data of Christoff *et al.*, but it was recorded over a much longer interval, and it consisted of much slower processes.

This fact that the flutter is dominated by very low frequencies can also be seen in the power spectral density $S_\varepsilon(f)$, which is shown in Fig. 4.9. The plotted spectrum $S_\varepsilon(f)$ was computed by the Welch method, as described above for Fig. 4.7. As before, the dashed line marked "inverse-cubic formula" is a plot of the approximate extrapolation formula of Eq. (4.5). In that formula the value of R_{son} was set at 55 m (= 110/2), since the formula was designed for active sonar (round trip path). As before, the leveling off of the curve at the left end is an artifact due to the window size.

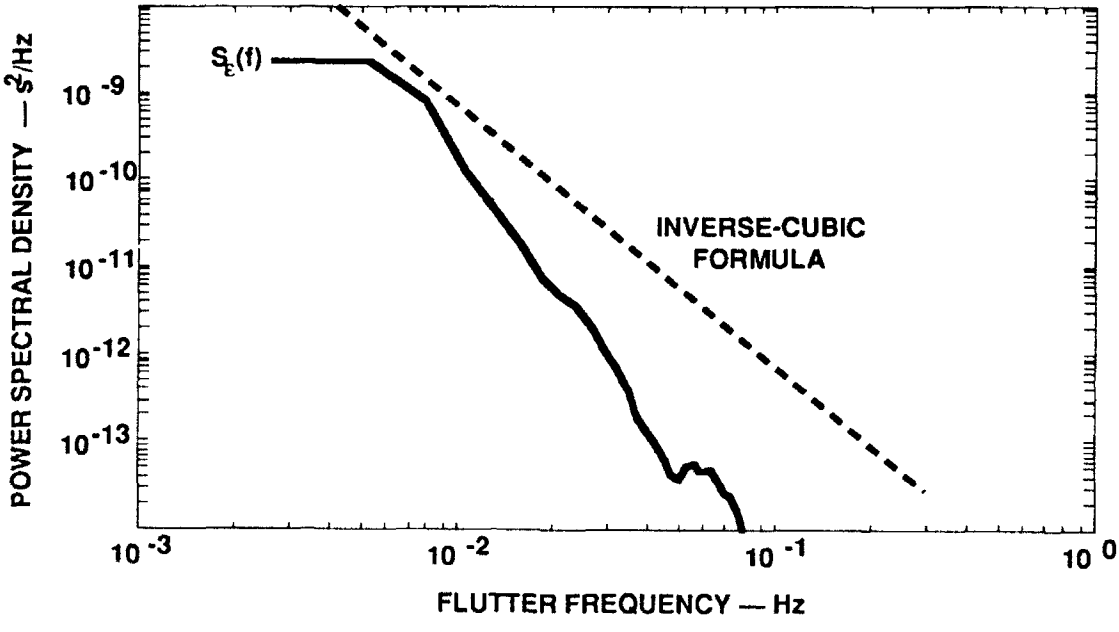

FIGURE 4.9
POWER SPECTRAL DENSITY OF TIME PERTURBATIONS OF A 40 kHz PULSE, TAKEN FROM BARTELS (1989)

The plotted spectrum of Fig. 4.9 obviously falls off more rapidly than f^{-3}. Indeed, it falls off as rapidly as f^{-4} or f^{-5}. This behavior is also indicated by the relative smoothness of the phase history, compared with that of Christoff *et al.*

4.6.4 Conclusions of Bartels

The motivation for Bartels' study was to determine the limits that Lake Travis would impose upon the use of an active sonar with a large time-bandwidth product. He concluded that a time-bandwidth product of 10,000 was feasible for short range use. Bartels also recorded amplitude variations, and looked at the locus traced out in the complex plane by the "phasor" of amplitude and phase. The amplitude seemed to remain fairly constant while the phase gradually rotated, but the amplitude shifted when the phase reversed its direction of rotation. However, this observation is based upon very little data.

4.7 GOUGH AND HAYES

4.7.1 Test Environment and Technique of Gough and Hayes

Gough and Hayes performed a study of propagation path phase stability in Loch Linnhe, Scotland, using a synthetic aperture sonar as both transmitter and receiver. The target was a 4 ft diam air-filled steel sphere, held on the seafloor by blocks of concrete at a distance from the transmitter/receiver of 66 m. The water depth at the target position was 7-10 m, depending upon the tidal state.

The sonar was held in place by taut wires. It used an FM wave burst of 0.8 s duration (repeated continuously), sweeping from 15 to 30 kHz, giving a time-bandwidth product of 12,000. Each (demodulated) echo was divided into 20 ms contiguous "frames" and individual Fourier transforms were taken.

4.7.2 Experimental Results and Conclusions of Gough and Hayes

Phase information was extracted by Gough and Hayes from their complex data. They plotted phase histograms in their paper, as well as a

15 min history of phase variation. It showed a monotonic phase variation of about 70° during that period.

The fact that this was a monostatic sonar test made it unique among published studies of phase stability. However, it also meant that the signal-to-noise ratio (in this case signal-to-clutter) could not be made high simply by increasing the transmitter power. They estimated that their 15 dB signal-to-noise ratio would give a standard deviation of 10°.

From their test they concluded that the medium posed no fundamental barrier to the operation of their synthetic aperture sonar.

4.8 KENNEDY

Kennedy (1969) reported a propagation experiment conducted 30 miles south of Bermuda in October 1967.

4.8.1 Test Environment and Instrumental Technique of Kennedy

The transmitter was buoyed 2000 ft above the seafloor, at a depth of about 9300 ft. The receiving array was 25 miles away, also buoyed from the seafloor. It consisted of 11 vertically spaced hydrophones spaced from 100 ft to 400 ft above the seafloor, at a depth of about 14,000 ft. Ray trace analysis indicated that the refracted sound path would be concave downward, with its uppermost point being only 125 ft below the surface! The transmission consisted of a 20 ms tone burst at a center frequency of 800 Hz, repeated every 6 min, for an experiment duration of 48 h. The recording equipment was linked by wire with the transmitter and receiving array, and a stable oscillator was used to assure phase synchronism.

4.8.2 Experimental Results of Kennedy

The time axis perturbation, $\varepsilon(t)$, was measured by a zero crossing method that Kennedy deemed to be very reliable, with an instrumental error whose standard deviation had been measured to be 66 μs. Kennedy plotted

the $\varepsilon(t)$ history for his topmost hydrophone in his Fig. 4, covering the entire 48 h period. It showed long term undulations that he was not interested in, so he subjected his raw data to a 10 Hz high pass filter. The filtered $\varepsilon(t)$ plot, shown in his Fig. 5 (but not shown here), was remarkably similar in appearance to Ewart's $\varepsilon(t)$ history that was depicted in our Fig. 4.3 (which the reader may wish to consult). However, although the amplitudes of Ewart's $\varepsilon(t)$ plot and Kennedy's filtered $\varepsilon(t)$ plot were similar, the rate of fluctuation in Kennedy's plot was more rapid. In fact, the entire 88 h plot of Ewart looked like about 15 h of Kennedy's data. (The more rapid fluctuations in Kennedy's data were also evident before the high pass filtering, but they were riding on a low frequency undulation that may have been due to tidal effects.) The $\varepsilon(t)$ fluctuations of Kennedy's (filtered) data had a standard deviation that ranged from 596 to 646 μs over the 11 hydrophones (compare to 374 μs for Ewart's 8 kHz data).

4.8.3 Conclusions Regarding Kennedy's Data

Although Kennedy did provide plots of fluctuation estimated spectra and autocorrelation functions, the data were deemed to be of little value in assessing the effects of ocean propagation flutter on high resolution, large time-bandwidth sonar for the following reasons.

(1) The propagation path was heavily refracted and too long: 25 miles.
(2) The data sampling rate was too low: 0.00277 Hz.
(3) The transmission frequency was too low: 800 Hz.
(4) The source and receiver were not rigidly attached to the seafloor.
(5) The instrumental error was too large: $\sigma_{sys}[\varepsilon(t)] = 66$ μs.

4.9 SECTION SUMMARY

The experimental studies of phase fluctuations in ocean propagation agree in several important respects: The power spectral density $S_\varepsilon(f)$ of the flutter always goes down with increasing frequency, usually as f^{-3} or f^{-4}, or even as fast as f^{-5} on occasion. The time axis perturbation $\varepsilon(t)$ virtually never exceeds a few milliseconds. The equivalent observer velocity is typically on the order of a few millimeters per second. It is the conclusion of several investigators that phase fluctuations in the medium itself rarely impose any

severe limits upon high resolution sonar as we have defined it; indeed, rarely does the medium induce enough phase shift to degrade (for example) the performance of a replica correlator, if the sonar and target remain stationary and the operating frequency is not too high.

It should be acknowledged that efforts to develop a successful synthetic aperture sonar have met with greater difficulties than parallel efforts in the development of synthetic-aperture radar, and the blame has always been placed upon phase incoherence. Nevertheless, the experimental studies would seem to indicate that the fault lies not with the phase fluctuations inherent to the medium but, rather, to flutter caused by (especially) sonar platform motions. Since the coherent phase processing that is done in a synthetic aperture sonar is virtually identical to replica correlation (except that the linear motion of the platform is taken into account in constructing the replica), it follows that whatever affects synthetic aperture sonar also affects replica correlation (in a large time-bandwidth product sonar). Platform motion-induced flutter, including uncompensated micro-navigational meanderings, would seem to be the main limitation to both techniques.

On the other hand, it would be foolish to suppose that the medium poses no limitation whatever to large time-bandwidth product sonar. For transmitted waveforms of especially long duration at relatively high frequencies, the effect can be deadly. If $\varepsilon(t)$ oscillates slowly between limits of ± 200 μs, and the sonar center frequency is 200 kHz, then the phase variation will be $\pm 14{,}000°$ if the transmitted sonar pulse lasts long enough to experience it. This is enough phase variation to kill replica correlation several times over.

The point to remember is that the effect of platform motion is probably even worse. A ± 200 μs time axis deviation corresponds to a platform motion of about 6 in. (as measured in the target direction, for two-way propagation). The reader should ask himself or herself the following question: Which is likely to happen sooner, a variation in propagation time of ± 200 μs (which may require many minutes or even hours), or an accumulated micro-navigational error of 6 in.? For moving platforms, it is hard to escape the conclusion that the latter is the more likely.

5. THE EFFECT OF FLUTTER ON AN FM WAVE BURST

Although the effect of flutter upon a few specific types of active sonar transmissions can be simulated by computer, it is good to have theoretical results as well. It is, for example, hard to plan and interpret simulation studies without the aid of theory. This section addresses, from a theoretical point of view, the effect of flutter upon a replica correlation sonar, for what is perhaps the most flutter resistant type of transmission: a linear FM waveform.

5.1 AN INTEGRAL FOR CALCULATING THE EFFECT OF FLUTTER

Equation (2.15) is repeated here for convenience:

$$z(t) = \int_{-\infty}^{+\infty} x_{rep}^{*}(\lambda)\, x(\lambda+t)\, d\lambda\,. \tag{5.1}$$

This equation gives the output of the replica correlation filter for an arbitrary received signal input $x(t)$. If the received input $x(t)$ is a perfect echo from an ideal target of unit strength then $x(t) = x_{rep}(t)$ and the filter output $z(t)$ will be the ideally compressed pulse $p(t)$, i.e., it will be the autocorrelation function of the replica as given by Eq. (2.19):

$$p(t) = x_{rep}^{*}(-t) \otimes x_{rep}(t) = \int_{-\infty}^{+\infty} x_{rep}^{*}(\lambda)\, x_{rep}(\lambda + t)\, d\lambda\,. \tag{5.2}$$

However, if the received signal $x(t) = x_{rep}(t)$ in Eq. (5.1) is distorted by flutter,

$$\tilde{x}(t) = \tilde{x}_{rep}(t) = x_{rep}\big(t+\varepsilon(t)\big), \tag{5.3}$$

then the output will be a correspondingly distorted compressed pulse,

$$\tilde{p}(t) = x^*_{rep}(-t) \otimes \tilde{x}_{rep}(t) = \int_{-\infty}^{+\infty} x^*_{rep}(\lambda)\, \tilde{x}_{rep}(\lambda+t)\, d\lambda . \qquad (5.4)$$

If the received input is a superposition of echoes from many targets, then the component echoes will be compressed into different versions of $\tilde{p}(t)$, because of the different times of arrival of the echoes and the time-varying nature of the random process $\varepsilon(t)$ that perturbs the time axis. However, it is only necessary to study the effect of flutter upon an isolated compressed pulse of the form of Eq. (5.4) to gain a general understanding of how all of the pulses will be corrupted.

It should be noted that the round trip acoustic path still represents a linear system even if corrupted by flutter, and the linear superposition principle still applies. The time axis distortion does prevent it from being an ideal linear-*time-invariant* (LTI) system, however. (The replica correlation filter is an LTI system even when flutter is present; that is why its output can be represented as a convolution integral of its flutter-corrupted input. The convolution integral appears in disguised form in Eq. (5.4), because of a change of variables that was intended to reveal its correlative nature.)

It is difficult to carry the analysis forward from Eq. (5.4) without assuming a particular type of replica waveform, because of the non-integrable form that results when one substitutes $\tilde{x}_{rep}(\lambda+t) = x_{rep}(\lambda+t+\varepsilon(\lambda+t))$ under the integral. For that reason, the rest of this section is devoted to the analysis of the FM wave burst in particular.

5.2 APPLICATION TO AN FM WAVE BURST

The sonar waveform that is most commonly used to obtain a large time-bandwidth product is the FM wave burst. In particular, let $x_{rep}(t)$ be of duration T, starting at instantaneous frequency $f_0 - \frac{1}{2}\Delta f$ and ending at frequency $f_0 + \frac{1}{2}\Delta f$; i.e.,

$$x_{rep}(t) = \sqrt{\frac{\Delta f}{T}}\,\Pi\left(\frac{t}{T}\right) e^{j2\pi\beta(t)}, \tag{5.5}$$

where the quadratically varying phase $\beta(t)$ is given by

$$\beta(t) = f_0 t + \frac{\Delta f}{2T} t^2 . \tag{5.6}$$

Equation (5.5) is the same as the FM wave burst that was considered above as Eq. (2.7), with different notation and a scaling factor to make it a normalized constant amplitude, flat spectrum (CAFS) waveform (see Section 2.3.1). The reader may also recall from Section 2.1.2 that its bandwidth satisfies the approximation $B_e \cong \Delta f$ when the time-bandwidth product $\Delta f \times T$ is large.

The fluttered version of $x_{rep}(t)$ is

$$\tilde{x}_{rep}(t) = \sqrt{\frac{\Delta f}{T}}\,\Pi\left(\frac{t+\varepsilon(t)}{T}\right) e^{j2\pi\beta(t+\varepsilon(t))} , \tag{5.7}$$

which can be written as

$$\tilde{x}_{rep}(t) = \sqrt{\frac{\Delta f}{T}}\,\Pi\left(\frac{t+\varepsilon(t)}{T}\right) e^{j2\pi\beta(t)}\, e^{j\phi(t)} , \tag{5.8}$$

wherein $\phi(t)$, the *instantaneous phase deviation due to the flutter*, is defined as

$$\phi(t) = 2\pi\left[f_0 + \frac{t}{T}\Delta f + \frac{\varepsilon(t)}{2T}\Delta f\right]\varepsilon(t) . \tag{5.9}$$

Then, replacing $t \rightarrow \lambda + t$ in Eq. (5.8) and substituting into Eq. (5.4), one gets

$$\tilde{p}(t) = \frac{\Delta f}{T}\int_{-\infty}^{+\infty} \Pi\left(\frac{\lambda}{T}\right) e^{-j2\pi\beta(\lambda)}\,\Pi\left(\frac{\lambda+t+\varepsilon(\lambda+t)}{T}\right) e^{j2\pi\beta(\lambda+t)}\, e^{j\phi(\lambda+t)}\, d\lambda . \tag{5.10}$$

Substitution of $\tau = \lambda + t$ as the variable of integration yields

$$\tilde{p}(t) = \frac{\Delta f}{T}\int_{-\infty}^{+\infty} \Pi\left(\frac{\tau - t}{T}\right) \Pi\left(\frac{\tau+\varepsilon(\tau)}{T}\right) e^{j\phi(\tau)}\, e^{j2\pi[\beta(\tau)-\beta(\tau-t)]}\, d\tau . \qquad (5.11)$$

Using Eq. (5.6) and a little algebra one can establish that

$$[\beta(\tau) - \beta(\tau - t)] = -\beta(-t) + \left(\frac{\Delta f}{T}\right) t\tau . \qquad (5.12)$$

Upon substituting this into Eq. (5.11) and pulling the τ-independent terms out of the integral, one obtains

$$\tilde{p}(t) = \left(\frac{\Delta f}{T}\right) e^{-j2\pi\beta(-t)} \int_{-\infty}^{+\infty} \Pi\left(\frac{\tau - t}{T}\right) \Pi\left(\frac{\tau+\varepsilon(\tau)}{T}\right) e^{j\phi(\tau)}\, e^{-j2\pi f_t \tau}\, d\tau , \qquad (5.13)$$

where f_t is defined as

$$f_t = -\frac{t}{T}\Delta f . \qquad (5.14)$$

Equation (5.13) will be developed further in Section 5.4, for the general case.

5.3 CHECKING THE FORMULA FOR THE NO-FLUTTER CASE

It is instructive to test Eq. (5.13) for the case of no flutter, i.e., where $\varepsilon(t)$ is identically zero, and $\phi(t)$ consequently vanishes (see Eq. (5.9)). Equation (5.13) then gives an undistorted, compressed pulse $p(t)$:

$$p(t) = \left(\frac{\Delta f}{T}\right) e^{-j2\pi\beta(-t)} \left\{ \int_{-\infty}^{+\infty} \Pi\left(\frac{\tau - t}{T}\right) \Pi\left(\frac{\tau}{T}\right) e^{-j2\pi f_t \tau}\, d\tau \right\} . \qquad (5.15)$$

The two rectangle functions (i.e., the Π functions) merely limit the range of integration to the interval $[L_1, L_2]$, where L_2 and L_1 are defined as

$$\left\{\begin{array}{l} L_2 = \min\left\{t+\frac{T}{2},+\frac{T}{2}\right\} \\ L_1 = \max\left\{t-\frac{T}{2},-\frac{T}{2}\right\} \end{array}\right\}. \qquad (5.16)$$

A null integral results if $L_1 > L_2$, i.e., if $|t| >> T$. Thus

$$p(t) = \left(\frac{\Delta f}{T}\right)\Pi\left(\frac{t}{2T}\right)e^{-j2\pi\beta(-t)}\int_{L_1}^{L_2} e^{-j2\pi f_t\tau}\,d\tau\ . \qquad (5.17)$$

The integration is facilitated by the formula

$$\int_a^b e^{-j2\pi f\tau}\,d\tau = (b-a)\,\mathrm{sinc}[(b-a)f]\,e^{-j\pi(b+a)f}\ , \qquad (5.18)$$

which is valid for any a and b. In applying it one makes use of the fact that $L_2 - L_1 = T-|t|$, whereas $L_2 + L_1 = t$. These results come directly from the definitions of Eq. (5.16). Thus, Eq. (5.17) becomes

$$p(t) = \left(\frac{\Delta f}{T}\right)\Pi\left(\frac{t}{2T}\right)e^{-j2\pi\beta(-t)}(T-|t|)\,\mathrm{sinc}[(T-|t|)f_t]\,e^{-j\pi f_t t}\ . \qquad (5.19)$$

This can be simplified by substituting for f_t from Eq. (5.14) and $\beta(t)$ from Eq. (5.6), and making use of the triangle function $\Lambda(t)$ (see Eq. (2.9)):

$$p(t) = \Delta f \times \Lambda\left(\frac{t}{T}\right)\mathrm{sinc}\left[\Lambda\left(\frac{t}{T}\right)\Delta f\,t\right]\ e^{j2\pi f_0 t}\ . \qquad (5.20)$$

The answer agrees with the autocorrelation function of an FM wave burst as given by Rihaczek (1969). The central peak has an amplitude of $\Delta f\ (\cong B_c)$ in accordance with the filter performance specifications of Table 2.1. The duration of the pulse is determined almost entirely by the sinc function. For small t the approximation

$$\operatorname{sinc}\left[\Lambda\left(\frac{t}{T}\right)\Delta f\, t\right] \;\cong\; \operatorname{sinc}(\Delta f\, t) \tag{5.21}$$

is satisfied, giving a duration of $T_e = 1.5/\Delta f$ by Eq. (2.11). This compressed pulse duration is also in agreement with Table 2.1.

5.4 SIMPLIFYING THE INTEGRAL FOR THE FLUTTERED FM WAVE

The no-flutter case provides a model for attacking the integral of Eq. (5.13) in the flutter-corrupted case. The first step is to convert the rectangle functions into a set of integration limits. The first rectangle function, $\Pi[(\tau\text{-}t)/T]$, switches "on" whenever the variable of integration τ satisfies the inequality

$$-\frac{T}{2} + t \;\le\; \tau \;\le\; \frac{T}{2} + t \;, \tag{5.22}$$

and the second one, $\Pi[(\tau+\varepsilon(t))/T]$, switches "on" whenever

$$-\frac{T}{2} \;\le\; \tau + \varepsilon(\tau) \;\le\; \frac{T}{2} \;. \tag{5.23}$$

This latter inequality would fail to define a simple interval were it not for the subsonic flutter assumption. Because of that assumption (which was made and defended in Section 3.1.4) the time-perturbing transformation, $t \rightarrow t+\varepsilon(t)$, is monotonic and invertible, so a pair of unique numbers τ_1 and τ_2 exist that satisfy the equations

$$\tau_1 + \varepsilon(\tau_1) \;=\; -\frac{T}{2} \;, \tag{5.25}$$

$$\tau_2 + \varepsilon(\tau_2) \;=\; +\frac{T}{2} \;. \tag{5.26}$$

These numbers τ_1 and τ_2 can be used to replace Eq. (5.23) by the following equivalent inequality (the monotonicity of $\tau+\varepsilon(\tau)$ makes it equivalent):

$$\tau_1 \;\le\; \tau \;\le\; \tau_2 \;. \tag{5.27}$$

It is therefore possible to combine Eqs. (5.22) and (5.27) into one inequality that defines the τ-interval over which both rectangle functions of Eq. (5.13) will be switched "on":

$$\tilde{L}_1 \leq \tau \leq \tilde{L}_2 \ , \tag{5.28}$$

where $\tilde{L}_1$ and $\tilde{L}_2$ are perturbed versions of the numbers L_1 and L_2 that were defined in Eq. (5.16), i.e.,

$$\left\{ \begin{array}{l} \tilde{L}_2 = \min\left\{t+\frac{T}{2}, \tau_2\right\} \\ \tilde{L}_1 = \max\left\{t-\frac{T}{2}, \tau_1\right\} \end{array} \right\} . \tag{5.29}$$

The integral of Eq. (5.13) will vanish unless the condition $\tilde{L}_2 > \tilde{L}_1$ is satisfied. That condition can also be expressed as

$$\max\left\{t, \tau_1+\frac{T}{2}\right\} - \min\left\{t, \tau_2-\frac{T}{2}\right\} < T \ , \tag{5.30}$$

i.e.,

$$\tau_1 - \frac{T}{2} < t < \tau_2 + \frac{T}{2} \ . \tag{5.31}$$

A rectangle function can be constructed to switch "on" when Eq. (5.31) is satisfied:

$$I_\varepsilon(t) = \Pi\left[\frac{t - \frac{1}{2}(\tau_1+\tau_2)}{T + \tau_2 - \tau_1}\right] . \tag{5.32}$$

With these preparations complete, it is possible to express the integral of Eq. (5.13) as

$$\tilde{p}(t) = \left(\frac{\Delta f}{T}\right) e^{-j2\pi\beta(-t)} I_\varepsilon(t) \int_{\tilde{L}_1}^{\tilde{L}_2} e^{j\phi(\tau)} e^{-j2\pi f_1 \tau} \, d\tau \ . \tag{5.33}$$

5.5 BREAKING UP THE INTEGRAL

In Section 5.12 it will be shown that $\tilde{L}_1$ and $\tilde{L}_2$ are very close to their unperturbed versions, L_1 and L_2, that were defined in Eq. (5.16). In anticipation of that behavior it is useful to break up the integral into three pieces,

$$\int_{\tilde{L}_1}^{\tilde{L}_2} d\tau = \int_{\tilde{L}_1}^{L_1} d\tau + \int_{L_1}^{L_2} d\tau + \int_{L_2}^{\tilde{L}_2} d\tau , \qquad (5.34)$$

in which the first and third integrals make small contributions. Then Eq. (5.33) can be expressed as

$$\tilde{p}(t) = \left(\frac{\Delta f}{T}\right) e^{-j2\pi\beta(-t)} I_\varepsilon(t) \left[\tilde{p}_1(t) + \tilde{p}_2(t) \right] , \qquad (5.35)$$

in which $\tilde{p}_1(t)$ and $\tilde{p}_2(t)$ are the *primary* and *secondary* components of the fluttered autocorrelation. They are defined as follows:

$$\tilde{p}_1(t) = \int_{L_1}^{L_2} e^{j\phi(\tau)} e^{-j2\pi f_t \tau} d\tau , \qquad (5.36)$$

and, for the small contributions of the first and third integrals in Eq. (5.34),

$$\tilde{p}_2(t) = \int_{\tilde{L}_1}^{L_1} e^{j\phi(\tau)} e^{-j2\pi f_t \tau} d\tau + \int_{L_2}^{\tilde{L}_2} e^{j\phi(\tau)} e^{-j2\pi f_t \tau} d\tau . \qquad (5.37)$$

5.6 THE PRIMARY COMPONENT OF THE FLUTTERED PULSE $\tilde{p}_1(t)$

The tedious task of verifying the negligibility of $\tilde{p}_2(t)$, as compared to $\tilde{p}_1(t)$, is postponed until Section 5.12. This is done to avoid obfuscation of the main theme of development, and to permit a small but necessary preliminary result to be developed first. For the time being, the reader is requested to

assume that the secondary component $\tilde{p}_2(t)$ in Eq. (5.35) can, indeed, be neglected, so that development theme can continue uninterrupted. Attention thus shifts to the primary component $\tilde{p}_1(t)$.

Using a window function that switches "on" in the domain $L_1 < \tau < L_2$, where L_1 and L_2 are as defined in Eq. (5.16), one can express Eq. (5.36) as

$$\tilde{p}_1(t) = \int_{-\infty}^{+\infty} \Pi\left[\frac{\tau - t/2}{T - |t|}\right] e^{j\phi(\tau)} e^{-j2\pi f_t \tau}\, d\tau . \tag{5.38}$$

It is helpful to change the variable of integration to $\tau' = \tau - t/2$. After this is done the prime notation can be dropped, giving the result

$$\tilde{p}_1(t) = e^{-j\pi f_t t} \int_{-\infty}^{+\infty} \Pi\left[\frac{\tau}{T - |t|}\right] e^{j\phi(\tau + t/2)} e^{-j2\pi f_t \tau}\, d\tau . \tag{5.39}$$

The value of the variable t affects the integral in three different ways:

Effect 1: It affects the window length, $T-|t|$, of the rectangle function.

Effect 2: It shifts the argument of the ϕ function, which, from the definition given in Eq. (5.9), is

$$\phi(t) = \left[1 + \left(\frac{\varepsilon(t)}{2T}\right)\left(\frac{\Delta f}{f_0}\right) + \left(\frac{t}{T}\right)\left(\frac{\Delta f}{f_0}\right)\right] 2\pi f_0 \varepsilon(t) . \tag{5.40}$$

Effect 3: It is a subscript-parameter on the term f_t that, from Eq. (5.14), is defined as

$$f_t = -\frac{t}{T}\Delta f . \tag{5.41}$$

It turns out that effect 3 is by far the most significant, especially for small t values. (This simplification is justified in the next section.) Since small values of t need to be explored to see how the pulse deteriorates in the presence of

flutter, this is a very useful simplification. In this regard, it is noteworthy that in the absence of flutter (i.e., where ϕ is identically zero) the $\tilde{p}_1(t)$ pulse of Eq. (5.39) is

$$p_1(t) = e^{-j\pi f_t t}(T-|t|)\,\mathrm{sinc}[(T-|t|)f_t] \tag{5.42}$$

$$= T\,e^{-j\pi f_t t}\,\Lambda\left(\frac{t}{T}\right)\mathrm{sinc}\left[\Lambda\left(\frac{t}{T}\right)\Delta f\, t\right], \tag{5.43}$$

which has a duration of $1.5/\Delta f$. (This is in accordance with Eqs. (5.20) and (5.35), wherein the secondary component vanishes in the absence of flutter.) When flutter is present the pulse deteriorates, and it is necessary to examine a wider range of t values to see what happens to it. For example, one might wish to explore a domain one hundred times as large as the pulse's original duration:

$$|t| < \left(\frac{1.5}{\Delta f}\right)\times 50 = \left(\frac{75}{T\,\Delta f}\right)T\ . \tag{5.44}$$

5.7 A USEFUL SIMPLIFICATION FOR SMALL t VALUES

In this section it is established that effect 1 and effect 2 can, indeed, be neglected for sufficiently small t values. Certainly, if t is small enough to satisfy $|t| << T$, then effect 1 can be ignored; i.e., $T-|t|$ can be replaced by T in the denominator of the Π function in Eq. (5.39). Indeed, for a sonar whose time-bandwidth product is very large, the hundredfold-expanded domain that is defined in Eq. (5.44) would satisfy $|t| << T$ with room to spare, easily justifying the replacement of $T-|t|$ by T. This replacement is harmless because the integral can be interpreted as a Fourier transform of an almost stationary random process, for which the window length is not a critical parameter. (If it were, i.e., if the Fourier spectrum were sensitive to slight alterations in the window length, then FFT analyzers would not be as popular as they are.)

To confirm that the random process $e^{j\phi(\tau+t/2)}$ is "almost-stationary", as it was implied to be in the foregoing paragraph, one can use the following line of

reasoning: For high resolution sonars the ratio $\Delta f/f_0$ typically ranges from 0.1 to 0.3, and it can never exceed unity. For a very large time-bandwidth sonar T would be on the order of seconds, or (at least) hundreds of milliseconds. The experimental studies of Section 3 suggest that the time-axis perturbation is not likely to exceed a millisecond. Thus the second term in the square brackets of Eq. (5.40) must be less than 0.001, and can be neglected in comparison to the first term (i.e., the "1"), giving the very accurate approximation

$$\phi(t) \cong \left[1 + \left(\frac{t}{T}\right)\left(\frac{\Delta f}{f_0}\right) \right] 2\pi f_0 \varepsilon(t) \ . \qquad (5.45)$$

Furthermore, assuming that the ratio $\Delta f/f_0$ is between 0.1 to 0.3 and that t varies over the range $-T/2<t<+T/2$, it is clear that the number in square brackets applies a very gradual, ramp-type amplitude modulation, changing the amplitude from -5% to +5% in the case of $\Delta f/f_0 = 0.1$, or from -15% to +15% in the case of $\Delta f/f_0 = 0.3$. This slow amplitude modulation has very little impact; thus, the random process $\phi(t)$ can be treated like a stationary random process with a slowly time-varying power spectral density.

Effect 2 cannot be dismissed as easily; some preparatory work is required. The first step is to rewrite Eq. (5.39) in the form

$$\tilde{p}_1(t) \cong e^{-j\pi f_t t} \int_{-\infty}^{+\infty} e^{j\Psi(\tau)} \Pi\left[\frac{\tau}{T}\right] e^{j\phi(\tau)} e^{-j2\pi f_t \tau} \, d\tau \ , \qquad (5.46)$$

where the angle $\Psi(\tau)$ is defined as

$$\Psi(\tau) = \phi(\tau+t/2) - \phi(\tau) \ . \qquad (5.47)$$

By application of Eq. (5.45) and algebraic simplification one obtains the very accurate approximation

$$\Psi(\tau) \cong 2\pi f_0 \left[1 + \left(\frac{\tau}{T}\right)\left(\frac{\Delta f}{f_0}\right) \right] [\varepsilon(\tau+t/2) - \varepsilon(\tau)] + \left(\frac{\pi \Delta f t}{T}\right) \varepsilon(\tau+t/2) \ . \qquad (5.48)$$

(It is a very accurate approximation because Eq. (5.45) is very accurate.) The angle $\Psi(\tau)$ vanishes as t goes to zero. Certainly, if t is sufficiently small then $\Psi(\tau)$ will be so small that the approximation $e^{j\Psi(\tau)} \cong 1$ can be made in Eq. (5.46), which is equivalent to neglecting effect 2. But how small does t have to be?

To get the answer, one first constructs an upper bound from Eq. (5.48), based upon the fact that $|a+b|_{rms} \leq |a|_{rms}+|b|_{rms}$:

$$|\Psi(\tau)|_{rms} \lesssim 2\pi f_0[1.5]|\varepsilon(\tau+t/2)-\varepsilon(\tau)|_{rms} + \left(\frac{\pi\Delta f}{T}\right)|\varepsilon(\tau+t/2)|_{rms}|t|. \quad (5.49)$$

The $[1.5]$ term represents the upper bound for the first bracketed term in Eq. (5.48), since $\Delta f/f_0$ is always less than unity and $|\tau| \leq T/2$.

It can be assumed that the approximation $e^{j\Psi(\tau)} \cong 1$ will be valid if Ψ_{rms} is on the order of a two-tenths of a radian, or less. To ensure this condition, one can require that each of the two terms on the right-hand side of Eq. (5.49) be less than 0.1; i.e., for the first term,

$$|\varepsilon(\tau+t/2)-\varepsilon(\tau)|_{rms} < \frac{0.1}{2\times 1.5\pi f_0} \cong \frac{0.0106}{f_0}, \quad (5.50)$$

and, for the second term of Eq. (5.49),

$$|t| < \left\{\frac{0.1\,T}{\pi\Delta f\,|\varepsilon(\cdot)|_{rms}}\right\} \cong \left(\frac{1.5}{\Delta f}\right)\left\{\frac{0.0212\,T}{|\varepsilon(\cdot)|_{rms}}\right\}. \quad (5.51)$$

As it stands, Eq. (5.50) is difficult to apply. However, the quantity $\varepsilon(\tau+t/2)-\varepsilon(\tau)$ that appears in it can be regarded as having been produced by a linear system whose input is $\varepsilon(\tau)$ and whose system-transfer function is

$$H(f) = e^{j2\pi(t/2)f} - 1. \quad (5.52)$$

(In this interpretation τ is the "time" variable and t is a fixed constant.) The power spectral density of its output is

$$|H(f)|^2 S_\varepsilon(f) = \left\{\sin[\pi(t/2)f]\right\}^2 S_\varepsilon(f)\,, \tag{5.53}$$

and the mean-square value of $\varepsilon(\tau+t/2)-\varepsilon(\tau)$ can thus be equated to the integral of that power spectral density:

$$\mathbf{E}\left[\,|\varepsilon(\tau+t/2)-\varepsilon(\tau)|^2\,\right] = \int_{-\infty}^{+\infty} \sin^2[\pi(t/2)f]\,S_\varepsilon(f)\,df\,. \tag{5.54}$$

Since $\sin^2 x \le x^2$, this leads to the upper bound

$$\mathbf{E}\left[\,|\varepsilon(\tau+t/2)-\varepsilon(\tau)|^2\,\right] \le \frac{t^2}{16}\int_{-\infty}^{+\infty} (2\pi f)^2\,S_\varepsilon(f)\,df\,. \tag{5.55}$$

It will be recalled from Section 3.1.2 that, since the normalized frequency deviation y is the derivative of the time-axis perturbation ε, the power spectral densities are related by $S_y(f)=(2\pi f)^2 S_\varepsilon(f)$. It follows that the integral in Eq. (5.55) is simply the mean square value of y. Using this fact, and taking square roots to obtain root mean square values, one determines that

$$|\varepsilon(\tau+t/2)-\varepsilon(\tau)|_{rms} \le \frac{1}{4}|t|\,y_{rms}\,. \tag{5.56}$$

Thus, to ensure that Eq. (5.50) is satisfied, one needs only to require that the right-hand side of Eq. (5.56) be less than the right-hand side of Eq. (5.50), i.e., that

$$\frac{1}{4}|t|\,y_{rms} \le \frac{0.0106}{f_0}\,, \tag{5.57}$$

i.e., t must be small enough that

$$|t| \le \frac{0.0424}{f_0\,y_{rms}} = \left(\frac{1.5}{\Delta f}\right)\times\left\{\left[\frac{\Delta f}{f_0}\right]\left[\frac{42.4\ m/s}{c\,y_{rms}}\right]\right\}\,. \tag{5.58}$$

Note that the parameter cy_{rms} in Eq. (5.58) is the root mean square value of the equivalent observer velocity of the flutter, as discussed in Section 3.1.3. Also, the quantity in curved braces is the expansion factor of the permitted "observation window", relative to the unfluttered pulse duration of $1.5/\Delta f$. For example, to allow an observation window with a hundredfold expansion factor, for a sonar having a 10% bandwidth (i.e., $\Delta f/f_0 = 0.1$), Eq. (5.58) would require that cy_{rms} be less than 4.24 cm/s.

Equation (5.58) replaces Eq. (5.50), and in combination with Eq. (5.51) provides the necessary assurance that $\Psi(\tau)$ is small enough to set $e^{j\Psi(\tau)} \cong 1$ in Eq. (5.46). The result of making that approximation is that effects 1 and 2 can be ignored in Eq. (5.39); i.e.,

$$\tilde{p}_1(t) \cong e^{-j\pi f_t t} \int_{-\infty}^{+\infty} \Pi\left[\frac{\tau}{T}\right] e^{j\phi(\tau)} e^{-j2\pi f_t \tau}\, d\tau \ . \qquad (5.59)$$

To recapitulate, the conditions for validity of this approximation are that $|t| << T$, and that Eqs. (5.51) and (5.58) be satisfied. In reality, the size of the observation window that is allowed by these limits is probably too conservative; i.e., larger values of t could likely be permitted without severely violating the approximation of Eq. (5.59).

5.8 PULSE SPREADING AS A PERIODOGRAM

One can express Eq. (5.59) in another way by interpreting the integral as a Fourier transform and using the definition of $f_t = -\Delta f t/T$ as given in Eq. (5.14):

$$\tilde{p}_1(t) \cong e^{j\pi \Delta f t^2/T} \left(\underset{\tau \to f}{\mathcal{F.T.}} \left\{ \Pi\left[\frac{\tau}{T}\right] e^{j\phi(\tau)} \right\} \right)_{f \to -\Delta f \frac{t}{T}} \ . \qquad (5.60)$$

In this regard, it should be noted that the phase of $\tilde{p}_1(t)$ is not really important for determining the pulse spreading. It is sufficient to look at the power envelope of $\tilde{p}_1(t)$.

$$|\tilde{p}_1(t)|^2 \cong \left| \underset{\tau \to f}{\mathcal{F.T.}} \left\{ \Pi\left[\frac{\tau}{T}\right] e^{j\phi(\tau)} \right\} \right|^2_{f \to -\Delta f \frac{t}{T}} . \qquad (5.61)$$

However, this still requires a separate computation for each new flutter history $\varepsilon(t)$ that is considered. What is needed is a way of predicting the pulse spreading based upon the statistical characteristics of the flutter.

The first step toward describing the pulse spreading process in statistical terms is to let $\Phi_T(f)$ denote the unsmoothed, continuous periodogram spectral estimate (Papoulis, 1984) of the random process $e^{j\phi(t)}$, based upon a sample of length T; i.e.,

$$\Phi_T(f) = \frac{1}{T} \left| \underset{\tau \to f}{\mathcal{F.T.}} \left\{ \Pi\left[\frac{\tau}{T}\right] e^{j\phi(\tau)} \right\} \right|^2 . \qquad (5.62)$$

Then Eq. (5.61) can be expressed in terms of the power envelope $|\tilde{p}_1(t)|^2$ as

$$|\tilde{p}_1(t)|^2 \cong T\, \Phi_T\left(-\Delta f \frac{t}{T}\right) . \qquad (5.63)$$

This says that the power envelope of the fluttered and compressed pulse looks like a single periodogram estimate of the power spectral density of the random process $e^{j\phi(t)}$, if one views it through the correspondence $f \leftrightarrow -\Delta f t/T$ between the frequency domain and time domain. Using this correspondence, the duration and shape of the fluttered and compressed pulse can be inferred from the bandwidth and frequency distribution of the spectrum of $e^{j\phi(t)}$.

This interpretation leads immediately to two questions that will be addressed in the next two sections:

(1) What is the nature of the random process $e^{j\phi(t)}$, and what is its power spectral density?

(2) How accurately is that power spectral density approximated by a single periodogram estimate?

5.9 THE POWER SPECTRAL DENSITY OF $e^{j\phi(t)}$

It will be recalled from the definition given in Eq. (5.9) that $\phi(t)$ is the instantaneous phase deviation (of the received FM wave burst pulse echo) due to flutter. The time-varying phasor that expresses this phase deviation will be denoted as $q(t)$; i.e.,

$$q(t) = e^{j\phi(t)} . \tag{5.64}$$

It will also be recalled from Eq. (5.45) that the very accurate approximation

$$\phi(t) \cong A_t 2\pi f_0 \varepsilon(t) , \tag{5.65}$$

can be made, in which A_t is defined as

$$A_t = 1 + \left(\frac{t}{T}\right)\left(\frac{\Delta f}{f_0}\right) . \tag{5.66}$$

This factor A_t can be regarded as a slow growth, linear ramping factor that ranges from

$$A_{min} = 1 - \tfrac{1}{2}\left(\Delta f/f_0\right) \tag{5.67}$$

to

$$A_{max} = 1 + \tfrac{1}{2}\left(\Delta f/f_0\right) \tag{5.68}$$

as t goes from $-T/2$ to $+T/2$, giving an average value of unity. Assuming $\Delta f/f_0$ is less than 0.3 (since a larger value is difficult to attain and of questionable utility), A_t may, at most, vary from 0.85 to 1.15 (this is the ±15% that was discussed in Section 5.7). Thus $A_t \cong 1$ to a rough approximation, and it follows that $q(t)$ can be expressed to a similarly rough approximation as

$$q(t) \cong q_0(t) = \exp\left[j2\pi f_0 \varepsilon(t)\right] , \tag{5.69}$$

where $q_0(t)$ is the same as originally defined in Eq. (3.24); i.e., $q_0(t)$ is the phasor that expresses the instantaneous phase deviation, due to flutter, of a *pure tone* at frequency f_0. It will also be recalled from Section 3.1.6 that when the flutter is sufficiently strong to produce a significant effect then, from Eqs. (3.31) and (3.32), the power spectral density $S_0(f)$ of $q_0(t)$ is well approximated by

$$S_0(f) \cong \frac{1}{f_0}\rho_y\left(\frac{f}{f_0}\right), \tag{5.70}$$

where $\rho_y(\cdot)$ is the probability density function of $y(t)$, the normalized frequency deviation of the flutter.

It follows that the power spectral density $S_q(f)$ of $q(t)$ is roughly approximated by the right-hand side of Eq. (5.70), in the same sense that the phasor $q(t)$ is roughly approximated by $q_0(t)$. However, it is possible to improve upon the approximation a bit. From Eq. (5.65) it is clear that the only thing that prevents $S_q(f)$ from being almost exactly the same as $S_0(f)$ is the factor A_t that is multiplied onto $\varepsilon(t)$ and, as a consequence, onto $y(t)$ (which is by definition the derivative of $\varepsilon(t)$). Certainly, if A_t had constant value (which would be very nearly true in the case of a high "Q" sonar, i.e., where $\Delta f/f_0 << 1$), then one could account for the effect of this scale factor by replacing $\rho_y(\cdot)$ by $\rho_{A_t y}(\cdot)$, the probability density of $A_t y(t)$, which is

$$\rho_{A_t y}(\alpha) = \frac{1}{A_t}\rho_y\left(\frac{\alpha}{A_t}\right). \tag{5.71}$$

Actually, however, as A_t varies linearly from A_{min} to A_{max}, the ensemble statistics of $A_t y(t)$ will become a smeared version of the ensemble statistics of $y(t)$, giving a mixture probability density $\bar{\rho}_y(\cdot)$ given by

$$\bar{\rho}_y(\alpha) \cong \frac{1}{A_{max}-A_{min}}\int_{A_{min}}^{A_{max}} \frac{1}{A}\rho_y\left(\frac{\alpha}{A}\right) dA . \tag{5.72}$$

This density can be substituted for $\rho_y(\cdot)$ to improve the right-hand side of Eq. (5.70) before it is used to approximate $S_q(f)$, the power spectral density of $e^{j\phi(t)}$:

$$S_q(f) \cong \frac{1}{f_0}\overline{\rho}_y\left(\frac{f}{f_0}\right) . \tag{5.73}$$

The reader may wish to verify for himself, or herself, that the mixture density $\overline{\rho}_v(\cdot)$ has a unit integral: i.e., it is a proper density function. Furthermore, if A_{min} and A_{max} are reasonably close to one another, the "smearing" that is described by Eq. (5.72) is exactly that: Sharp points are rounded off and cracks are filled, but features of the density that are already smooth are not significantly affected. Actually, in most cases the density $\rho_y(\cdot)$ will be smooth enough that the smearing can be disregarded, i.e., $\overline{\rho}_y(\cdot)$ may be replaced by $\rho_y(\cdot)$ in Eq. (5.73) for computational purposes.

5.10 IMPLICATIONS OF THE PERIODOGRAM REPRESENTATION

If the periodogram estimate $\Phi_T(f)$ defined in Eq. (5.62) were an accurate representation of the power spectral density $S_q(f)$ of $e^{j\phi(t)}$, then the power envelope $|\tilde{p}_1(t)|^2$ of the fluttered and compressed pulse could be expressed in terms of $S_q(f)$ through Eq. (5.63). However, because the unsmoothed periodogram is actually a rather noisy estimate of power spectral density, it bears further scrutiny.

In general, if $S_T(f)$ represents a raw periodogram estimate of a power spectral density $S(f)$, obtained from a sample of length T, then the expected value of the estimate is (Papoulis, 1984, with appropriate adjustments for his notation)

$$\mathbf{E}\left[S_T(f)\right] = S(f) \otimes T\,\mathrm{sinc}^2(Tf) , \tag{5.74}$$

and its variance about that mean value has a lower bound

$$\mathbf{var}\left[S_T(f)\right] \geq \left\{\mathbf{E}\left[S_T(f)\right]\right\}^2 . \tag{5.75}$$

From Eq. (5.74) one can see that $S_T(f)$ is really estimating a smoothed version of $S(f)$, i.e., the result of convolving $S(f)$ with the function $T\,\mathrm{sinc}^2(Tf)$. This means that any sharp spectral lines in the spectrum $S(f)$ (including any spike at the origin that represents concentration of energy at very low frequencies) will be smeared to a bandwidth of about $1/2T$. However, if T is large the smoothing effect will be rather modest, and negligible under most circumstances. Equation (5.75) has more serious consequences. It implies that the root mean square fluctuations in the estimate are as large as the quantity being estimated; i.e., the estimate's "noise" is as large as its "signal". (For that reason, spectrum analysts never use the periodogram estimate without applying some additional smoothing.)

In our particular application the periodogram estimate $\Phi_T(f)$ is not a deliberate attempt to do good spectral analysis; it is accidental. It presents itself as an uninvited guest, appearing as the power envelope $|\tilde{p}_1(t)|^2$ of the fluttered and compressed FM wave burst. From Eq. (5.63) the mean power envelope must be

$$\mathbf{E}\left[|\tilde{p}_1(t)|^2\right] \cong T\,\mathbf{E}\left[\Phi_T(f)\right]_{f \to -\Delta f \pm \frac{1}{T}}, \tag{5.76}$$

which, by Eq. (5.74) and the fact that $\Phi_T(f)$ is the periodogram estimate of $S_q(f)$, may be expressed as

$$\mathbf{E}\left[|\tilde{p}_1(t)|^2\right] \cong T\left[S_q(f) \otimes T\,\mathrm{sinc}^2(Tf)\right]_{f \to -\Delta f \pm \frac{1}{T}}. \tag{5.77}$$

This can be further approximated by

$$\mathbf{E}\left[|\tilde{p}_1(t)|^2\right] \cong T\left[S_q(f)\right]_{f \to -\Delta f \pm \frac{1}{T}} \tag{5.78}$$

if T is sufficiently large, i.e., if the aperture width $1/2T$ is small in comparison to the spectral features of $S_q(f)$, so that the smoothing effect of convolution by $T\,\mathrm{sinc}^2(Tf)$ is negligible. Indeed, if one uses the approximation of Eq. (5.73) for

$S_q(f)$, the smearing of the probability density in Eq. (5.72) should ensure a smooth spectrum unless T is unusually small. With the approximation of Eq. (5.73), Eq. (5.78) becomes

$$\mathbf{E}\left[\left|\tilde{p}_1(t)\right|^2\right] \cong T\left[\frac{1}{f_0}\bar{\rho}_y\left(\frac{f}{f_0}\right)\right]_{f \to -\Delta f \frac{t}{T}} \tag{5.79}$$

i.e.,

$$\mathbf{E}\left[\left|\tilde{p}_1(t)\right|^2\right] \cong \frac{T}{f_0}\bar{\rho}_y\left(-\frac{\Delta f}{f_0}\frac{t}{T}\right). \tag{5.80}$$

The "noisiness" of the power envelope is revealed in the fact that statistical variance of the power envelope is bounded from below by

$$\mathbf{var}\left[\left|\tilde{p}_1(t)\right|^2\right] \geq \left\{\mathbf{E}\left[\left|\tilde{p}_1(t)\right|^2\right]\right\}^2, \tag{5.81}$$

which follows from Eqs. (5.63) and (5.75). In effect, Eq. (5.80) tells us what the mean value of the power envelope looks like, but Eq. (5.81) warns us that the root mean square variations are at least as large as that mean value.

Alternatively, Eq. (5.80) can also be expressed in terms of the root mean square envelope of the fluttered and compressed pulse, by taking the square root:

$$\left|\tilde{p}_1(t)\right|_{rms} \cong \sqrt{\frac{T}{f_0}\bar{\rho}_y\left(-\frac{\Delta f}{f_0}\frac{t}{T}\right)}. \tag{5.82}$$

Since Eq. (5.80) is one of the most important results of this section, it is appropriate to review some of its aspects, as follows.

(1) The formula is valid for flutter that is strong enough to cause significant phase deviations at the frequency of operation; specifically, the formula is valid if $|f_0\varepsilon(t)|>1$ most of the time. The formula does not give the correct answer for vanishingly small flutter.

(2) Because of the slow growth, linear ramping factor A_t in Eq. (5.65), neither of the random processes $\phi(t)$ and $e^{j\phi(t)}$ is truly stationary, so that the use of a power spectral density $S_q(f)$ is only valid in an approximate sense. However, since $e^{j\phi(t)}$ is only seen within an observation window of duration T, its lack of stationarity does not have the opportunity to manifest itself in a dramatic way; i.e., it looks pretty stationary.

(3) The formula is valid within a range of t values that obey Eqs. (5.58) and (5.51).

(4) The formula depends only upon the point statistics of the random process $y(t)$, not upon its temporal statistics. However, it does depend upon the temporal characteristics of the time axis perturbation process $\varepsilon(t)$, because $y(t)$ is the time derivative of $\varepsilon(t)$.

(5) In most cases the density $\rho_y(\cdot)$ will be smooth enough that its "smearing" can be disregarded, i.e., $\bar{\rho}_y(\cdot)$ may be replaced by $\rho_y(\cdot)$ in Eq. (5.80) for computational purposes.

(6) The expected value of the power envelope, given by Eq. (5.80), *retains all of the energy of the unfluttered pulse.*

Assertion (6) can be verified by computing the energy in Eq. (5.80):

$$\int_{-\infty}^{+\infty} \mathbf{E}\left[\left|\tilde{p}_1(t)\right|^2\right] dt \;\cong\; \frac{T}{f_0}\int_{-\infty}^{+\infty} \bar{\rho}_y\left(-\frac{\Delta f}{f_0}\frac{t}{T}\right) dt \;=\; \frac{T^2}{\Delta f}\,, \qquad (5.83)$$

where the last step was achieved by simplifying the variable of integration and exploiting the fact that the integral of a probability density function has unit value. (It makes no difference whether $\bar{\rho}_y(\cdot)$ or $\rho_y(\cdot)$ is used.) This computed energy, $T^2/\Delta f$, is the same as the energy of the unfluttered pulse $p_1(t)$, where $p_1(t)$ is as given in Eq. (5.42):

$$\int_{-\infty}^{+\infty} |p_1(t)|^2\,dt \;=\; T^2 \int_{-\infty}^{+\infty} \left\{ \Lambda\left(\frac{t}{T}\right) \operatorname{sinc}\left[(\Delta f\, t)\, \Lambda\left(\frac{t}{T}\right) \right] \right\}^2 dt \qquad (5.84)$$

$$\cong\; T^2 \int_{-\infty}^{+\infty} \operatorname{sinc}^2(\Delta f\, t)\,dt \;=\; \frac{T^2}{\Delta f}\,. \qquad (5.85)$$

(Note that Eq. (5.85) was obtained by approximating $\Lambda(t/T) \cong 1$, which is certainly valid in the small central region where the unfluttered, compressed pulse has non-vanishing amplitude.)

5.11 THE FLUTTERED AND COMPRESSED PULSE DURATION

The duration (denoted **dur**) of the root mean square envelope of the flutter-corrupted pulse can be computed by plugging Eq. (5.82) into the definition of Eq (2.8), giving the result

$$\mathbf{dur}\left(|\tilde{p}_1(t)|_{rms}\right) \;\cong\; \frac{\left\{ \int_{-\infty}^{+\infty} \frac{T}{f_0}\, \bar{\rho}_y\!\left(-\frac{\Delta f}{f_0}\frac{t}{T}\right) dt \right\}^2}{\int_{-\infty}^{+\infty} \left\{ \frac{T}{f_0}\, \bar{\rho}_y\!\left(-\frac{\Delta f}{f_0}\frac{t}{T}\right) \right\}^2 dt}\,, \qquad (5.86)$$

which can be simplified by changing the variable of integration to $\alpha = -(\Delta f/f_0)(t/T)$, giving the result

$$\mathbf{dur}\left(|\tilde{p}_1(t)|_{rms}\right) \;\cong\; \frac{\left(\frac{f_0}{\Delta f}\right) T}{\int_{-\infty}^{+\infty} \bar{\rho}_y^2(\alpha)\,d\alpha}\,. \qquad (5.87)$$

If it is assumed that the density $\rho_y(\cdot)$ is already so smooth that $\bar{\rho}_y(\cdot)$ is

approximately equal to $\rho_y(\cdot)$, then the duration is

$$\mathbf{dur}\left(\left|\tilde{p}_1(t)\right|_{rms}\right) \cong \frac{\left(\frac{f_0}{\Delta f}\right)T}{\int_{-\infty}^{+\infty} \rho_y^2(\alpha)\, d\alpha}, \tag{5.88}$$

which, in light of Eq. (3.35), means that

$$\mathbf{dur}\left(\left|\tilde{p}_1(t)\right|_{rms}\right) \cong \frac{T}{\Delta f} B_{\tilde{f}_0}, \tag{5.89}$$

where $B_{\tilde{f}_0}$ is the fluttered tone bandwidth, i.e., it is the bandwidth of a pure tone at frequency f_0 after it has been corrupted by flutter. (Recall that the fluttered tone bandwidth, $B_{\tilde{f}_0}$, was one of several measures of flutter magnitude that were discussed in Section 3.)

The rather simple result expressed by Eq. (5.82) is not too surprising. It has already been pointed out, in the discussion following Eq. (5.70), that $S_q(f)$ is roughly the same as $S_0(f)$. (Recall that $S_q(f)$ is the spectrum of the flutter-deviation phasor $q(t)$ that is *impressed upon the FM wave burst*, whereas $S_0(f)$ is the spectrum of the flutter-deviation phasor $q_0(t)$ that would be *impressed upon a pure tone* at frequency f_0.) It then follows from Eq. (5.78) that the expected value of the power envelope has the shape of $S_q(f)$, with its frequency scale converted into a time scale by the substitution $f \rightarrow -\Delta f t/T$, i.e., by multiplying the frequency values by $T/\Delta f$ to get time values. Therefore, if the fluttered tone spectrum $S_q(f)$ exhibits a bandwidth $B_{\tilde{f}_0}$, then the root mean square envelope of the fluttered and compressed pulse $\tilde{p}_1(t)$ should exhibit a pulse duration equal to $(T/\Delta f) \times B_{\tilde{f}_0}$, which is in agreement with Eq. (5.89).

In view of Eq. (5.80), the shape of the spread pulse will depend upon the nature of the statistics of $y(t)$. In particular, if $y(t)$ has Gaussian statistics then $\left|\tilde{p}_1(t)\right|^2_{rms}$ will have a Gaussian shape; if $y(t)$ is uniformly distributed over an interval then $\left|\tilde{p}_1(t)\right|^2_{rms}$ will have a rectangular shape; and if $y(t)$ is sinusoidal

then $|\tilde{p}_1(t)|^2_{rms}$ will display two tall cusps with a trough of reduced level between them (see Section 3.1.6). Furthermore, it will be recalled from Eq. (3.47) of Section 3.1.6 that

$$B_{\tilde{f}_0} = 2\times\left\{\sqrt{2},\ \sqrt{3},\ \text{or}\ \sqrt{\pi}\right\} y_{rms}\, f_0\ , \tag{5.90}$$

where $\sqrt{2}$, $\sqrt{3}$, or $\sqrt{\pi}$ is selected depending upon whether the flutter y(t) is Gaussian, uniformly distributed, or sinusoidal. It follows from Eq. (5.89) that

$$\mathbf{dur}\left(|\tilde{p}_1(t)|_{rms}\right) \cong \left(\frac{T}{\Delta f}\right)\left[\ 2\times\left\{\sqrt{2},\ \sqrt{3},\ \text{or}\ \sqrt{\pi}\right\} y_{rms}\, f_0\ \right]. \tag{5.91}$$

Although this result looks fairly powerful as it stands, with a few adjustments it can be made even more useful and general. The first adjustment is mainly for simplicity: Since $\sqrt{2}$, $\sqrt{3}$, and $\sqrt{\pi}$ are so similar, it is well within the scope of the approximation to compromise upon the middle one, $\sqrt{3}$, for general use. Thus, Eq. (5.91) becomes

$$\mathbf{dur}\left(|\tilde{p}_1(t)|_{rms}\right) \cong \left(\frac{T}{\Delta f}\right)\left(\ 2\times\sqrt{3}\, y_{rms}\, f_0\ \right). \tag{5.92}$$

The second adjustment is more subtle. It addresses the case where the duration T of the FM wave burst is so brief that the *sample statistics* of the random process y(t) during that interval do not accurately reflect the *population statistics*; i.e., they give a distorted view of the behavior of y(t) that would be seen in a much larger interval. This is best illustrated with a simple example: Suppose that the bandwidth Δf of the FM wave is much less than the center frequency f_0, so that the instantaneous phase deviation, as defined in Eq. (5.9), is very accurately approximated by

$$\phi(t) \cong 2\pi f_0\, \varepsilon(t)\ . \tag{5.93}$$

(In Section 5.9 this was a rough approximation, but it is very accurate for this example.) Suppose, further, that y(t) has wide excursions but varies quite slowly (this will be the case if the flutter is due to sonar platform meandering that

has substantial velocity but small acceleration). Then $y(t)$ will be essentially constant during the interval of an FM wave burst whose duration T is very short (e.g., a few milliseconds):

$$y(t) \cong y(0) \quad \text{for} \left|t\right| \leq T/2 , \tag{5.94}$$

and the time axis perturbation $\varepsilon(t)$, which is by definition the derivative of $y(t)$, will be approximately linear,

$$\varepsilon(t) \cong \varepsilon(0) + y(0)\, t , \tag{5.95}$$

which upon substitution into Eq. (5.93) gives

$$\phi(t) \cong 2\pi f_0 \varepsilon(0) + 2\pi y(0) f_0 t . \tag{5.96}$$

This simplifies Eq. (5.59) to

$$\widetilde{p}_1(t) \cong e^{-j\pi f_t t}\, e^{j2\pi f_0 \varepsilon(0)} \int_{-\infty}^{+\infty} \Pi\left[\frac{\tau}{T}\right] e^{j2\pi y(0) f_0 \tau}\, e^{-j2\pi f_t \tau}\, d\tau , \tag{5.97}$$

so that

$$\left|\widetilde{p}_1(t)\right| \cong \left| \int_{-T/2}^{+T/2} e^{-j2\pi \tilde{f}_t \tau}\, d\tau \right| , \tag{5.98}$$

where $\tilde{f}_t$ defined as a shifted version of the parameter f_t of Eq. (5.14):

$$\tilde{f}_t = -\frac{t}{T}\Delta f - y(0) f_0 . \tag{5.99}$$

As applied to Eq. (5.97), the integral formula of Eq. (5.18) gives the result

$$\left|\widetilde{p}_1(t)\right| \cong \left|T \operatorname{sinc}(T \tilde{f}_t)\right| = \left|T \operatorname{sinc}\left\{\Delta f \left[t + \frac{T}{\Delta f} y(0) f_0\right]\right\}\right| , \tag{5.100}$$

which means that the original unfluttered duration, $1.5/\Delta f$, is actually preserved (approximately), but the pulse has a random time displacement, i.e., a "jitter", equal to

$$dt \cong \frac{T}{\Delta f} y(0) f_0 \ . \tag{5.101}$$

The fact that the pulse is not elongated would seem to contradict the pulse spreading formulas of Eqs. (5.80) and (5.92), but it really does not. Indeed, from Eq. (5.100) it follows that

$$\mathbf{E}\left[\left|\tilde{p}_1(t)\right|^2\right] \cong T^2 \mathbf{E}\left(\operatorname{sinc}^2\left\{T f_0 \left[\frac{\Delta f}{T f_0} t + y(0)\right]\right\}\right) , \tag{5.102}$$

which can be expressed in terms of $\rho_y(\cdot)$, the probability density function of $y(t)$, as

$$\mathbf{E}\left[\left|\tilde{p}_1(t)\right|^2\right] \cong T^2 \int_{-\infty}^{+\infty} \operatorname{sinc}^2\left\{T f_0 \left[\frac{\Delta f}{T f_0} t + \alpha\right]\right\} \rho_y(\alpha)\, d\alpha \ . \tag{5.103}$$

Then, making use of the fact that $\operatorname{sinc}^2(K\alpha) \cong K^{-1}\delta(\alpha)$ for large K, where $\delta(\cdot)$ is Dirac's delta function, one sees that

$$\begin{aligned} \mathbf{E}\left[\left|\tilde{p}_1(t)\right|^2\right] &\cong \frac{T}{f_0} \int_{-\infty}^{+\infty} \delta\left(\frac{\Delta f}{T f_0} t + \alpha\right) \rho_y(\alpha)\, d\alpha \\ &= \frac{T}{f_0} \rho_y\left(-\frac{\Delta f}{T f_0} t\right) , \end{aligned} \tag{5.104}$$

which is the same as Eq. (5.80), except that Eq. (5.104) does not use the smeared probability density $\bar{\rho}_y(\cdot)$. However, for our example it was assumed that the center frequency f_0 was much larger than the bandwidth Δf, which means that the linear ramping factor A_t defined in Eq. (5.66) varies over a small range, and the smeared density $\bar{\rho}_y(\cdot)$ defined in Eq. (5.72) is essentially the

same as $\rho_y(\cdot)$. Thus, Eq. (5.104) really *is* the same as Eq. (5.80), and there is no contradiction between the no-spreading ("jitter only") result of Eq. (5.101) and the pulse duration spreading results of Eq. (5.80) and, consequently, Eq. (5.92). Although a single pulse does not exhibit significant spreading, it does exhibit pulse-to-pulse "jitter", *and Eq. (5.92) predicts the root mean square envelope that must be used to cover the entire ensemble of randomly jittered pulses.*

The lesson of this short burst example is that Eqs. (5.80) and (5.92) describe average behavior over an ensemble of pulses, but for short duration transmissions they cannot be relied upon to predict single-pulse spreading. Still, if the FM wave burst lasts long enough that the flutter process $y(t)$ *does* exercise the full range of its population statistics, then Eqs. (5.80) and (5.92) will adequately predict single-pulse spreading.

There is a subtle way to adjust Eqs. (5.80) and (5.92) to make them predict single-pulse duration in both cases. (In most sonar applications single-pulse spreading would be the most important consequence of flutter, and pulse-to-pulse jitter would be of lesser importance.) One simply writes

$$\left|\tilde{p}_1(t)\right|^2_{\substack{\text{smoothed,}\\ \text{single pulse}}} \cong \frac{T}{f_0}\bar{\rho}_y^{(T)}\left(-\frac{\Delta f}{f_0}\frac{t}{T}\right) \tag{5.105}$$

in place of Eq. (5.80), and

$$\mathbf{dur}\left(\left|\tilde{p}_1(t)\right|_{\substack{\text{smoothed,}\\ \text{single pulse}}}\right) \cong \left(\frac{T}{\Delta f}\right)\left(2\times\sqrt{3}\, y_\sigma^{(T)} f_0\right), \tag{5.106}$$

in place of Eq. (5.92). In the right-hand sides of these expressions the superscript "(T)" designates that *sample statistics* for the interval of the FM wave burst are to be used rather than *population statistics*; e.g., $y_\sigma^{(T)}$ refers to the sample standard deviation, i.e., the root mean square average of the flutter process $y(t)$ during the specific interval $|t| \le T/2$ after subtracting the mean value over that same interval. Assuming the random process $y(t)$ is stationary (and ergodic), $y_\sigma^{(T)}$ converges to y_{rms} as T becomes infinite; i.e., $y_\sigma^{(\infty)} = y_{rms}$. However, for finite T the value of $y_\sigma^{(T)}$ may differ from y_{rms}. In particular, for a

very small T the interval will be so short that y(t) will be almost constant over the interval, so that the value of $y_\sigma^{(T)}$ will be small.

The substitution of $y_\sigma^{(T)}$ for y_{rms} can be defended by the following argument: Since y(t) is observed only during an interval of length T (when a single pulse is observed), it is possible to imagine that y(t) is a sample of a mythical random process whose population statistics match the observed sample statistics, including the sample mean and sample standard deviation $y_\sigma^{(T)}$. The left-hand sides of Eqs. (5.105) and (5.106) are then based upon averages over that mythical ensemble, and are marked with the subscripted notation smoothed, single pulse to emphasize that they do not describe average behavior over the true ensemble of fluttered pulses, in the sense that they do not account for pulse-to-pulse jitter. However, if T is long enough that the distinction between population statistics and sample statistics evaporates, i.e, so that $y_\sigma^{(T)}$ is certain to be close to y_{rms}, then Eqs. (5.105) and (5.106) become equivalent to Eqs. (5.80) and (5.92). For that case, the single-pulse spreading (which could also be loosely described as "within-the-pulse jitter") is so severe that it covers the full span of pulse-to-pulse jitter.

The reader will recall that Eq. (5.92) was our first adjustment to Eq. (5.91). Equation (5.106) constitutes our second adjustment. The third adjustment relates to the fact that the minimum duration is $1.5/\Delta f$ no matter how small the flutter is. (See the discussion following Eq. (5.21) for the no-flutter case.) Although this would seem to violate Eq. (5.106), there is really no contradiction because the discussion following Eq. (5.82) acknowledged that the pulse spreading formulas are only valid when there is significant flutter. When the formula of Eq. (5.106) gives a value less than $1.5/\Delta f$ it should not be believed. There is a simple way to "fix" this defect without seriously degrading the level of approximation: One merely adds $1.5/\Delta f$ to the right-hand side of Eq. (5.106). (This trick is somewhat analogous to the heuristic development of "Carson's Rule" for estimating the bandwidth of an FM transmission; see, for example, Stark and Tuteur (1979).) The result of this third and final adjustment is

$$\mathbf{dur}\left(\left|\tilde{p}_1(t)\right|\right)_{\substack{\text{smoothed,}\\ \text{single pulse}}} \cong \left(\frac{1.5}{\Delta f}\right)\left[1 + \left(2\times\sqrt{3}\, y_\sigma^{(T)}\right)\left(\frac{T f_0}{1.5}\right)\right] . \qquad (5.107)$$

The quantity in square brackets represents the pulse elongation factor due to the flutter. In terms of $cy_{\sigma}^{(T)}$, which expresses the strength of the flutter in terms of the standard deviation (about the sample mean) of the equivalent observer velocity during the FM wave burst's duration, the duration of the fluttered and compressed pulse is

$$\mathbf{dur}\left(\left|\tilde{p}_1(t)\right|\right)_{\substack{\text{smoothed,}\\ \text{single pulse}}} \cong \left(\frac{1.5}{\Delta f}\right)\left[1+(Tf_0)\left(\frac{cy_{\sigma}^{(T)}}{650\ \text{m/s}}\right)\right]. \qquad (5.108)$$

For example, for a 200 kHz sonar ($=f_0$) with a transmitted duration T equal to 1 s, the pulse elongation factor would be about 16.4 for flutter having a $cy_{\sigma}^{(T)}$ value of 5 cm/s.

If the flutter is strongly dominated by low frequency components, then

$$y(t) \cong y(0) + \dot{y}(0)t \quad \text{for} \left|t\right| \le T/2 \qquad (5.109)$$

if T is small enough. Since $y(t)$ is then uniformly distributed over the interval $[\,y(0)-\dot{y}(0)T/2,\ y(0)+\dot{y}(0)T/2\,]$, whose length is $\dot{y}(0)T$, it follows that the standard deviation about the sample mean is $\dot{y}(0)T/\sqrt{12}$, so that with some algebraic manipulations Eq. (5.108) can be replaced by

$$\mathbf{dur}\left(\left|\tilde{p}_1(t)\right|\right)_{\substack{\text{smoothed,}\\ \text{single pulse}}} \cong \left(\frac{1.5}{\Delta f}\right)\left[1+1.33\left(\frac{\frac{1}{2}gT^2}{\lambda_0}\right)\left(\frac{c\dot{y}(0)}{g}\right)\right], \qquad (5.110)$$

where g is the acceleration of gravity and λ_0 is the wavelength (in water) at the center frequency f_0. The last factor in Eq. (5.110) is the equivalent observer acceleration at time zero, measured in "gee" units (equivalent observer acceleration was briefly discussed in Section 3.1.3). The next to last factor has an amusing interpretation: It is the distance, measured in wavelengths, that a body would drop (in free fall) during the duration T of the FM wave burst.

This formula, which is valid for small T in the presence of flutter that has low frequency dominance, reveals that the pulse elongation has a *quadratic*

dependence upon T for small T. This behavior was not particularly evident from Eq. (5.108), and was certainly not evident in Eq. (5.92). It makes sense, though, and shows that the effect of flutter disappears when the duration drops below a threshold value. From Eq. (5.110) the threshold value of T for flutter is given (in seconds) approximately by

$$T_{thresh} \cong 0.4 \times \frac{\sqrt{\text{wavelength in meters}}}{\sqrt{\text{equivalent observer acceleration in "gee" units}}} . \qquad (5.111)$$

5.12 NEGLIGIBILITY OF THE SECONDARY COMPONENT $\tilde{p}_2(t)$

Much of the foregoing discussion has been predicated on the negligibility of the secondary component $\tilde{p}_2(t)$ of Eq. (5.37) in comparison with the primary component $\tilde{p}_1(t)$. The first step in verifying this negligibility is to examine the constants τ_1 and τ_2 that were defined through Eqs. (5.25) and (5.26). In particular, Eq. (5.26) can be written as

$$\tau_2 = +\frac{T}{2} - \varepsilon(\tau_2) . \qquad (5.112)$$

From the discussions of Sections 3 and 4 it can be concluded that the time axis perturbation $\varepsilon(t)$ is typically on the order of a few hundred microseconds, and would virtually never exceed a few milliseconds. For large time-bandwidth product sonars T will likely be at least a few hundred milliseconds. It follows that $|\varepsilon(t)| << T/2$ and, from Eq. (5.112), that τ_2 will be very close to T/2, i.e., within a few milliseconds, so close, in fact, that the approximation

$$\varepsilon(\tau_2) \cong \varepsilon(T/2) + (\tau_2 - T/2)\dot{\varepsilon}(T/2) \qquad (5.113)$$

$$= \varepsilon(T/2) + (\tau_2 - T/2)y(T/2) \qquad (5.114)$$

is extremely accurate. The reason is that the flutter is predominantly of such low frequency, and it certainly fits a straight line approximation for a few

milliseconds. Substituting Eq. (5.114) for $\varepsilon(\tau_2)$ in Eq. (5.112) and solving for τ_2 gives the extremely accurate approximation

$$\tau_2 \cong \frac{T}{2} + \frac{\varepsilon(T/2)}{1-y(T/2)} . \tag{5.115}$$

When the same approach is followed with Eq. (5.25), a corresponding result for τ_1 is obtained:

$$\tau_1 \cong -\frac{T}{2} + \frac{\varepsilon(-T/2)}{1-y(-T/2)} . \tag{5.116}$$

Equations (5.115) and (5.116) can be used in Eq. (5.29) to express the definitions of $\tilde{L}_1$ and $\tilde{L}_2$ in terms of very accurate approximations:

$$\left\{ \begin{array}{l} \tilde{L}_2 \cong \min\left\{t, \dfrac{\varepsilon(T/2)}{1-y(T/2)}\right\} + \dfrac{T}{2} \\ \tilde{L}_1 \cong \max\left\{t, \dfrac{\varepsilon(-T/2)}{1-y(-T/2)}\right\} - \dfrac{T}{2} \end{array} \right. . \tag{5.117}$$

The definitions of the unperturbed values L_1 and L_2 were given in Eq. (5.16), which can be rewritten as

$$\left\{ \begin{array}{l} L_2 \cong \min\{t, 0\} + \dfrac{T}{2} \\ L_1 \cong \max\{t, 0\} - \dfrac{T}{2} \end{array} \right. . \tag{5.118}$$

It follows that

$$\left|\tilde{L}_2 - L_2\right| \lesssim \left|\frac{\varepsilon(T/2)}{1-y(T/2)}\right| , \tag{5.119}$$

and

$$\left|\tilde{L}_1 - L_1\right| \lesssim \left|\frac{\varepsilon(-T/2)}{1-y(-T/2)}\right| . \qquad (5.120)$$

Because of the subsonic flutter assumption of Section 3.14, it must be true that $|y| << 1$, so that the denominators of both Eqs. (5.119) and (5.120) have nearly unit value. The numerators are very small, assuming the time axis perturbation $\varepsilon(t)$ is never larger than a few milliseconds (as suggested by the results of Sections 3 and 4). Thus, in both cases the quantities on the right are very small, and the assertion that was made in Section 5.5 is fully justified, namely, that $\tilde{L}_1 \cong L_1$ and $\tilde{L}_2 \cong L_2$.

Also, it follows from the definition of $\tilde{p}_2(t)$ given in Eq. (5.37) that

$$\left|\tilde{p}_2(t)\right| \leq \left|\int_{\tilde{L}_1}^{L_1} \left|e^{j\phi(\tau)} e^{-j2\pi f_t \tau}\right| d\tau\right| + \left|\int_{L_2}^{\tilde{L}_2} \left|e^{j\phi(\tau)} e^{-j2\pi f_t \tau}\right| d\tau\right| \qquad (5.121)$$

or, since the integrands have unit magnitude,

$$\left|\tilde{p}_2(t)\right| \leq \left|\tilde{L}_1 - L_1\right| + \left|\tilde{L}_2 - L_2\right| . \qquad (5.122)$$

The combination of Eq. (5.122) with Eqs. (5.119) and (5.120) then gives the result

$$\left|\tilde{p}_2(t)\right| \lesssim \left|\frac{\varepsilon(-T/2)}{1-y(-T/2)}\right| + \left|\frac{\varepsilon(T/2)}{1-y(T/2)}\right| . \qquad (5.123)$$

As was mentioned following Eq. (5.120), the subsonic flutter assumption implies that $|y| << 1$, so that both denominators have nearly unit value and the approximate inequality can be simplified to

$$\left|\tilde{p}_2(t)\right| \lesssim \left|\varepsilon(-T/2)\right| + \left|\varepsilon(T/2)\right| . \qquad (5.124)$$

Using the algebraic inequality $(a+b)^2 \leq 2a^2 + 2b^2$, it then follows that

$$|\tilde{p}_2(t)|^2 \;\tilde{<}\; 2|\varepsilon(-T/2)|^2 + 2|\varepsilon(T/2)|^2 . \qquad (5.125)$$

With this bound for the power of the secondary component $\tilde{p}_2(t)$ it is possible to demonstrate its weakness as compared to the primary component $\tilde{p}_1(t)$, in the central zone where the primary component is strong, i.e., within the interval over which the pulse has been spread by the effects of flutter. Recall that the expected energy of the primary component was computed in Eq. (5.83) to be $T^2/\Delta f$, and that its duration was computed to be $2\sqrt{3}\,(f_0/\Delta f)T\,y_{rms}$ (see Eq. (5.92)). Thus, the effective power of the primary component is

$$(\tilde{p}_1(t))_{power} \cong \frac{T^2/\Delta f}{2\sqrt{3}\,(f_0/\Delta f)T\,y_{rms}} = \frac{T}{2 f_0\, y_{rms}\sqrt{3}} . \qquad (5.126)$$

If the power of the secondary component $\tilde{p}_2(t)$ is less that 1% of the effective power of the primary component $\tilde{p}_1(t)$, then we might say that the secondary component is negligible. This condition will certainly be met if the upper bound given in Eq. (5.125) is less than 1/100th of the value given by Eq. (5.126):

$$2|\varepsilon(-T/2)|^2 + 2|\varepsilon(T/2)|^2 < \frac{0.01\,T}{2 f_0\, y_{rms}\sqrt{3}} . \qquad (5.127)$$

With a rearrangement of terms, this criterion for negligibility of the secondary component can be expressed as

$$(f_0\, y_{rms})\left(\frac{|\varepsilon(-T/2)|^2 + |\varepsilon(T/2)|^2}{T}\right) < 1.44\times 10^{-3} . \qquad (5.128)$$

As an example of the application of this criterion, consider a sonar with $f_0 = 200$ kHz and $T = 1$ s, in a flutter environment in which the maximum time axis perturbation is expected to be $\varepsilon(t) = 3$ ms, and the root mean square equivalent observer velocity of the flutter is limited to 10 cm/s, so that $y_{rms} = 10\,\text{cm/s} / 1500\,\text{m/s} = 6.67\times 10^{-5}$. Then the left-hand side of Eq. (5.128) evaluates to 2.4×10^{-4}, which meets the criterion easily.

The reader will recall that the secondary component and the primary component were added to give the flutter-corrupted, compressed pulse. as specified by Eq. (5.35), which is repeated here for convenience:

$$\tilde{p}(t) = \left(\frac{\Delta f}{T}\right) e^{-j2\pi\beta(-t)} I_{\varepsilon}(t) \left[\tilde{p}_1(t) + \tilde{p}_2(t) \right] . \qquad (5.129)$$

If the negligibility of the secondary component is assured, then

$$\tilde{p}(t) \cong \left(\frac{\Delta f}{T}\right) e^{-j2\pi\beta(-t)} I_{\varepsilon}(t)\, \tilde{p}_1(t) . \qquad (5.130)$$

5.13 PROCESSING GAIN

In terms of the sample standard deviation value of equivalent observer velocity $cy_{\sigma}^{(T)}$ (as sampled during the interval T of the sonar waveform) the pulse duration after pulse-compression filtering is, by Eq. (5.108),

$$\mathbf{dur}\left(\left|\tilde{p}_1(t)\right|\right)_{\substack{\text{smoothed,} \\ \text{single pulse}}} \cong \left(\frac{1.5}{\Delta f}\right)\left[1 + (Tf_0)\left(\frac{cy_{\sigma}^{(T)}}{650\ \text{m/s}}\right)\right] . \qquad (5.131)$$

In terms of the ratio of durations before and after filtering, the processing gain yielded by the pulse-compression operation (see Section 2.3.4) is $5\log_{10}\left(\text{dur}_{\text{before}} / \text{dur}_{\text{after}}\right)$. Since the duration was originally T, it follows that

$$\textbf{Proc. Gain} \cong 5\log_{10}\left[\frac{(\Delta f T)}{1 + (Tf_0)\left(\frac{cy_{\sigma}^{(T)}}{650\ \text{m/s}}\right)}\right] - 5\log_{10}(1.5), \qquad (5.132)$$

which may also be expressed as

$$\textbf{Proc. Gain} \cong 5\log_{10}\left[\frac{(\Delta f T)}{1 + \frac{(\Delta f T)}{K_T}}\right] - 0.88\,\text{dB}, \qquad (5.133)$$

where the the time-bandwidth product "ceiling value" K_T is defined as

$$K_T = \frac{650 \text{ m/s}}{Q\, c\, y_\sigma^{(T)}}, \tag{5.134}$$

and the "Q" of the sonar is

$$Q = \frac{f_0}{\Delta f} . \tag{5.135}$$

For large T the value of K_T converges to K_∞, defined as

$$K_\infty = \frac{650 \text{ m/s}}{Q\, c\, y_{rms}} . \tag{5.136}$$

If K_T were a constant, the dependence of processing gain upon time-bandwidth would be very easy to describe: The processing gain would then increase at a rate of 5 dB per decade of time-bandwidth product, approaching a "knee" at K_T, whereupon it would level off, gaining only 1.5 dB beyond the value it had at K_T. Such behavior is depicted in Fig. 5.1. The value $K_T = 21{,}666$ is merely an example for $Q = 3$, taking the root mean square value of equivalent observer velocity to be $c y_{rms} = 1$ cm/s, and assuming that T is large enough that $K_T \cong K_\infty$.

In a real sonar design exercise one can assume that the time-bandwidth product would be varied by increasing T, after the center frequency f_0 and the bandwidth Δf had been selected (thereby fixing the value of Q). It follows that K_T will generally converge downward to K_∞ with increasing T, because the sample standard deviation $y_\sigma^{(T)}$ will generally converge upward to $y_\sigma^{(\infty)} = y_{rms}$. (It is possible for $y_\sigma^{(T)}$ to be greater than than y_{rms} if the sonar waveform interval happens to catch the flutter process y(t) in a violent maneuver, e.g., at a point of discontinuity. An example of this will be presented in Section 7, using a flutter process $\varepsilon(t)$ that has sharp-pointed "cusps", at which $y(t) = \dot{\varepsilon}(t)$ exhibits discontinuities. However, such behavior is of a singular or pathological nature, and does not alter the truth of the statement that K_T will *generally* converge

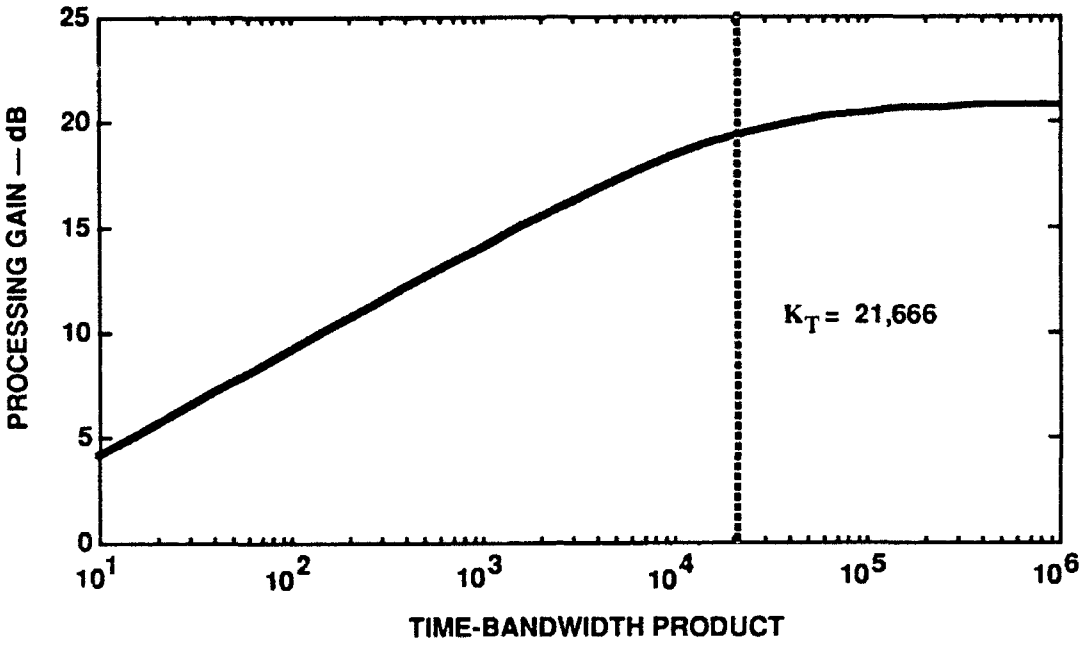

FIGURE 5.1
PROCESSING GAIN FOR THE FM WAVE BURST, AS A FUNCTION OF TIME-BANDWIDTH PRODUCT, FOR A CONSTANT CUTOFF VALUE $K_T = 21{,}666$

downward to K_∞.) Thus, as T and the time-bandwidth product go up, the cutoff value K_T will move downward, finally coming to rest at the value K_∞ as given by Eq. (5.136).

In most circumstances that can be imagined (barring flutter with extremely intense low frequency components and very large Q), the value of K_T will have settled out at K_∞ long before the time-bandwidth product rises to meet it. It follows that Fig. 5.1 can be used as a prototype plot of the dependence of processing gain upon time-bandwidth product, for an FM wave burst, putting the dashed line (and knee) at K_∞ as computed by Eq. (5.136). More importantly, it follows that

$$\left[\textbf{Proc. Gain}\right]_{max} \cong 5 \log_{10} K_\infty - 0.88\,\text{dB} . \qquad (5.137)$$

Figure 5.2 plots this approximate upper limit as a function of flutter magnitude, as expressed by the root mean square equivalent observer velocity, for values of $Q = 3$ and $Q = 10$. The flutter strength shown in the figure spans a range from 0.01 cm/s to 100 cm/s, which covers the flutter environments likely to be encountered in practice. The lower limit of 0.01 cm/s is representative of medium-induced flutter in a quiet environment, as suggested by the results of Section 4, and the upper limit of 100 cm/s represents a flutter due to platform meander that has a root mean square value of 70.7 cm/s in the direction of sonar interrogation. (Recall from Section 3.2.2 that variance contributed to equivalent observer velocity is twice that of the sonar platform velocity.) This is a rather extreme amount of platform meandering, enough to cover most conceivable scenarios.

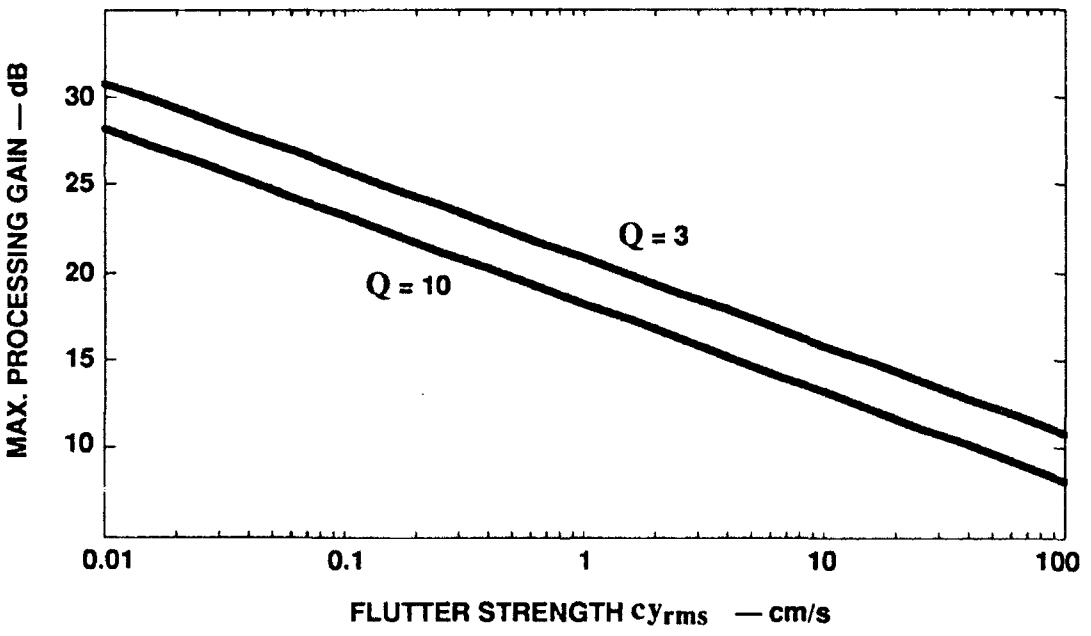

FIGURE 5.2
APPROXIMATE MAXIMUM PROCESSING GAIN AS A FUNCTION OF FLUTTER STRENGTH, FOR THE FM WAVE BURST

5.14 SECTION SUMMARY

The mathematical developments of this section are not simple (especially Section 5.12), but they have led to some simple results. For example, it was determined that the shape of the fluttered and compressed pulse tends to mimic the shape of the probability density function of the flutter process $y(t)$. An equivalent statement is that it must mimic the shape of the probability density function the equivalent observer velocity $cy(t)$.

The formulas and graphs that were developed should have practical value for predicting the benefit that can be gained by application of a pulse-compression filter. An example will illustrate: Suppose a sonar has a center frequency (f_0) of 200 kHz, a bandwidth (Δf) of 50 kHz, and a transmitted waveform duration (T) of 1 s. In the absence of flutter the pulse compression (i.e., replica correlation) filter will yield a processing gain of 22.6 dB, according to Eq. (5.132). However, suppose the sonar platform is moving and has a random meander (or, in the case of a Doppler compensated sonar, suppose that there are residual micro-navigational errors), to the extent that the equivalent observer velocity of the flutter exhibits a sample standard deviation of 2 cm/s during the 1 s duration of the waveform. Then the pulse compression filter will only yield a processing gain of 18.3 dB, according to Eq. (5.132).

Finally, the most important result developed in this section is so subtle that it is easily overlooked: When flutter is introduced, it does not destroy the energy of the compressed pulse $p(t)$ in the case of an FM wave burst, nor does it scatter its energy throughout the entire duration of $p(t)$ (which is an interval of length $2T$). Instead, the flutter merely *elongates* the central pulse, to a degree that is proportional to the strength of the flutter (in particular, to the strength of $y(t)$).

It is really not so surprising that the pulse energy is preserved, since that is merely a consequence of the fact that $x_{rep}(t)$ is a CAFS waveform. For such a waveform the replica correlation filter is a bandpass filter with unity gain (albeit with a special phase response), which must preserve the energy of the received signal. (Energy could be lost if the flutter were so severe that it splattered the

input spectrum beyond the bandpass limits, but that is as an extreme, pathological circumstance.) More surprising is the fact that all of the energy of the compressed pulse remains clustered at the center, with merely an elongation due to the flutter. This is a property that *seems to be unique* to the FM waveform (including waveforms with very FM-like behavior, i.e., waveforms having slow, steady variation in frequency).

The subject of FM waveform transmissions is addressed again in later sections of this report. Results of computer simulations are described in Section 7, and Section 8 provides a handy review of the theory (including some simple results that are extend the developments of this section).

6. EFFECT OF FLUTTER ON A HOPCODE BURST

It will be recalled that for an arbitrary transmitted waveform the fluttered and compressed pulse is

$$\tilde{p}(t) = \int_{-\infty}^{+\infty} x^{*}_{rep}(\tau - t)\, \tilde{x}_{rep}(\tau)\, d\tau \quad , \tag{6.1}$$

where

$$\tilde{x}_{rep}(t) = x_{rep}\big(t + \varepsilon(t)\big) \, . \tag{6.2}$$

(The formula for $\tilde{p}(t)$ in Eq. (6.1) was obtained from Eq. (5.2) by substituting $\lambda = \tau - t$.) In this section the effect of flutter will be explored for the case in which $x_{rep}(t)$ is a frequency hop-encoded waveform, which includes the stepped-linear FM wave burst as a special case.

(If the reader has already been overburdened by the mathematical complexities of Section 5, he or she may wish to scan the developments of this section superficially, and then read Sections 6.6 - 6.8.)

6.1 THE HOPCODE WAVEFORM

The formula

$$x_{rep}(t) = \frac{N}{T}\, e^{j2\pi f_0 t} \sum_{n=-N'}^{N'} x_n(t) \, , \tag{6.3}$$

where $N = 2N' - 1$, describes a continuous phase, frequency-hopped waveform, in which $x_n(t)$ the nth "chip" is actually a tone burst of duration T/N, defined as

$$x_n(t) = \Pi\left(\frac{t-t_n}{T/N}\right) e^{j2\pi f_n t} , \tag{6.4}$$

where t_n defines the center point of the nth chip,

$$t_n = \frac{T}{N} n , \tag{6.5}$$

and f_n defines its baseband frequency:

$$f_n = \frac{N}{T} \Omega(n) , \tag{6.6}$$

for $n = -N', \cdots -1, 0, 1, \cdots, N'$, and

T = duration of entire waveform,
N = $2N'-1$ = number of chips (an odd integer),
f_0 = center frequency, and
$\Omega(n)$ = an arbitrary mapping of the integers $\{-N', \cdots -1, 0, 1, \cdots, N'\}$ onto themselves.

The assumption that the waveform contains an odd number of chips is made for mathematical convenience, with little loss in generality. The integer mapping $\Omega(n)$ is the "code" of the hopcode waveform. If this mapping is the trivial one $\Omega(n) = n$, then $x_{rcp}(t)$ will simply be a stepwise-linear FM wave burst. In general, however, $\Omega(n)$ is used to scramble the order of frequencies.

As a result of the switching function $\Pi(\cdot)$ in Eq. (6.4), the nth chip in the summation of Eq. (6.3) is zero outside of the interval of duration T/N, bounded by the points

$$t = t_n \pm \frac{T}{2N} . \tag{6.7}$$

The chip intervals are contiguous, without overlap. Upon substitution of the interval boundary values of Eq. (6.7) and the frequencies of Eq. (6.6) into the

definition of $x_n(t)$ given in Eq. (6.4), one can easily verify that the phase of each $x_n(t)$ is zero on those boundaries; thus, the aggregate waveform $x_{rep}(t)$ has continuous phase. The frequency of the nth chip, including the effect of the carrier, is

$$F_n = f_0 + f_n . \tag{6.8}$$

Since $\Omega(n)$ maps a sequence of integers onto itself, it follows that the tonal frequencies blanket a total frequency range of $[(N-1)N/T]$ Hz. However, each chip is a tone burst of duration T/N, whose bandwidth is on the order of N/T Hz. As a result, the highest and lowest frequency chips at the ends of the spectrum should each contribute an additional half-bandwidth equal to $0.5 \times N/T$ Hz, so the waveform actually blankets a total frequency range of

$$\Delta f = \frac{N^2}{T} . \tag{6.9}$$

If N is large, then the spectrum of $x(t)$ will be quite flat over this band, so $B_e \cong \Delta f$ and the time-bandwidth product is

$$B_e T \cong \Delta f T = N^2 . \tag{6.10}$$

The factor $N/T = \sqrt{\Delta f / T}$ that appears as a scaling factor in Eq. (6.3) thus makes $x(t)$ a normalized CAFS signal, in conformance with Eq. (2.27).

6.2 THE FLUTTERED AND COMPRESSED PULSE

Combining the replica correlation and flutter effect formulas of Eqs. (6.1) and (6.2), one obtains

$$\tilde{p}(t) = \int_{-\infty}^{+\infty} x^*_{rep}(\tau - t)\, x_{rep}\big(\tau + \varepsilon(\tau)\big)\, d\tau . \tag{6.11}$$

After substituting the chip summation formula of Eq. (6.3) for x_{rep}, rearranging terms, noting that $N^2/T^2 = \Delta f/T$, and interchanging the order of summation and integration, one obtains

$$\tilde{p}(t) = \frac{\Delta f}{T} e^{j2\pi f_0 t} \sum_{m=-N'}^{N'} \sum_{n=-N'}^{N'} \tilde{p}_{mn}(t), \tag{6.12}$$

where $\tilde{p}_{mn}(t)$ is defined as

$$\tilde{p}_{mn}(t) = \int_{-\infty}^{+\infty} x_m^*(\tau - t)\, x_n(\tau + \varepsilon(\tau))\, e^{j2\pi f_0 \varepsilon(\tau)}\, d\tau . \tag{6.13}$$

This equation can be expanded by using the definition of x_n from Eq. (6.4), giving

$$\tilde{p}_{mn}(t) = e^{j2\pi f_m t} \int_{-\infty}^{+\infty} \Pi\left(\frac{\tau - t - t_m}{T/N}\right) \Pi\left(\frac{\tau + \varepsilon(\tau) - t_n}{T/N}\right) e^{-j2\pi f_{mn}\tau}\, e^{j2\pi F_n \varepsilon(\tau)}\, d\tau, \tag{6.14}$$

in which F_n is as defined in Eq. (6.8), and f_{mn} is defined as

$$f_{mn} = f_m - f_n . \tag{6.15}$$

The formula for $\tilde{p}_{mn}(t)$ will be simplified in six steps. The first step is to change the dummy-variable of integration to $\lambda = \tau - t_n$, giving

$$\tilde{p}_{mn}(t) = e^{-j2\pi f_{mn} t_n}\, e^{j2\pi f_m t} \times \int_{-\infty}^{+\infty} \Pi\left(\frac{\lambda - t + t_n - t_m}{T/N}\right) \Pi\left(\frac{\lambda + \varepsilon_n(\lambda)}{T/N}\right) e^{j2\pi F_n \varepsilon_n(\lambda)}\, e^{-j2\pi f_{mn}\lambda}\, d\lambda , \tag{6.16}$$

where $\varepsilon_n(\cdot)$ is a shifted version of the flutter process $\varepsilon(\cdot)$, defined as

$$\varepsilon_n(t) = \varepsilon(t + t_n) . \tag{6.17}$$

The second step is to shift the independent variable from t to $t - t_m + t_n$, i.e., to convert the formula for $\tilde{p}_{mn}(t)$ into a formula for $\tilde{p}_{mn}(t - t_m + t_n)$. Before doing so, however, one can deduce from the definitions of t_n, f_n, and f_{mn} in Eqs. (6.5), (6.6), and (6.15) that the quantity $f_{mn}t_n$ must take an integer value (remembering that N is an odd integer), and it follows that the first exponential factor preceding the integral in Eq. (6.16) has unit value, and can be dropped. Thus,

$$\tilde{p}_{mn}(t - t_m + t_n) = e^{j2\pi f_m(t - t_m + t_n)} \times$$

$$\int_{-\infty}^{+\infty} \Pi\left(\frac{\lambda - t}{T/N}\right) \Pi\left(\frac{\lambda + \varepsilon_n(\lambda)}{T/N}\right) e^{j2\pi F_n \varepsilon_n(\lambda)} e^{-j2\pi f_{mn}\lambda} \, d\lambda . \tag{6.18}$$

(The integral now looks a lot like that of Eq. (5.13) of Section 5, but a slightly different analysis technique will be used here.)

The third step in simplifying the formula for $\tilde{p}_{mn}(t)$ is based upon the idea that the $\Pi(\cdot)$ functions merely cause the integration limits to collapse to finite values, and if the $\varepsilon_n(\lambda)$ term in the second $\Pi(\cdot)$ were set to zero the effect would be to shift one or both of the collapsed integration limits by an amount that could not exceed ε_{max}, defined as

$$\varepsilon_{max} = \max_{|t| \le T/2} |\varepsilon(t)| . \tag{6.19}$$

Furthermore, since the integrand has unit magnitude the value of the integral would only be perturbed by an amount $2\varepsilon_{max}\eta$, where the complex number η has, at most, unit magnitude. (The 2 accounts for the possibility that both limits of integration could be perturbed.) Thus, the $\varepsilon_n(\lambda)$ term in the second $\Pi(\cdot)$ function of Eq. (6.18) can be set to zero if a correction term $2\varepsilon_{max}\eta$ is added:

$$\tilde{p}_{mn}(t - t_m + t_n) = e^{j2\pi f_m(t - t_m + t_n)} \times$$

$$\left\{ 2\varepsilon_{max}\eta + \int_{-\infty}^{+\infty} \Pi\left(\frac{\lambda - t}{T/N}\right) \Pi\left(\frac{\lambda}{T/N}\right) e^{j2\pi F_n \varepsilon_n(\lambda)} e^{-j2\pi f_{mn}\lambda} \, d\lambda \right\}, \qquad (6.20)$$

where η is some complex number (which we shall never bother to compute) that satisfies $|\eta| \leq 1$. The number η can depend upon m and n, and it is also a function of t; however, it could be expressed as a function of $t - t_m + t_n$. It is also convenient to absorb the leading exponential factor into the definition of η (which does not alter its magnitude). Thus, we define

$$\eta_{mn}(t - t_m + t_n) = e^{j2\pi f_m(t - t_m + t_n)} \eta, \qquad (6.21)$$

so that Eq. (6.20) becomes

$$\tilde{p}_{mn}(t - t_m + t_n) = 2\varepsilon_{max}\eta_{mn}(t - t_m + t_n) + e^{j2\pi f_m(t - t_m + t_n)} \times$$

$$\int_{-\infty}^{+\infty} \Pi\left(\frac{\lambda - t}{T/N}\right) \Pi\left(\frac{\lambda}{T/N}\right) e^{j2\pi F_n \varepsilon_n(\lambda)} e^{-j2\pi f_{mn}\lambda} \, d\lambda, \qquad (6.22)$$

where the function $\eta_{mn}(\cdot)$ obeys $|\eta_{mn}(\cdot)| \leq 1$. (It is important to remember that $\eta_{mn}(\cdot)$ merely accounts for the deletion of the $\varepsilon_n(\lambda)$ term in the second $\Pi(\cdot)$ function).

The fourth step is to assume that the flutter process $\varepsilon(t)$ changes slowly enough during a single chip's duration that it can be approximated by a fixed value (which can be different for each chip). This assumption automatically applies to $\varepsilon_n(t)$ as well, since it is just a shifted version of $\varepsilon(t)$, and permits the following approximation to be made under the integral:

$$e^{j2\pi F_n \varepsilon_n(\lambda)} \cong e^{j2\pi F_n \varepsilon_n(0)} = e^{j2\pi F_n \varepsilon(t_n)}, \qquad (6.23)$$

where the last equality follows from the definition of ε_n in Eq. (6.17).

Before this approximation is used, it is worthwhile to take a closer look at how slowly varying $\varepsilon(t)$ must be. For the approximation to be valid, the phasor on the left-hand side of Eq. (6.23) must stay relatively constant during the chip interval T/N, and this means that the angle $2\pi F_n \varepsilon_n(\lambda)$ must not change more than about 0.3 rad. If, indeed, $\varepsilon(t)$ changes very slowly then its net change during the chip interval can be estimated as the product of its derivative, $y(t)$, and the chip interval T/N. (Recall from Section 3 that $y(t)=\dot{\varepsilon}(t)$ is the normalized frequency deviation of the flutter.) Since $\varepsilon_n(\lambda) = \varepsilon(\lambda + t_n)$ by definition, so that the derivative of $\varepsilon_n(\lambda)$ at the center of the chip interval is $y(t_n)$, it follows that the angular change would be well approximated by $2\pi F_n y(t_n) T/N$. Thus, our assumption requires that

$$2\pi F_n y(t_n) T/N \leq 0.3 \text{ rad} \tag{6.24}$$

be approximately satisfied, which means that the equivalent observer velocity of the flutter (see Section 3.1.3) must satisfy the approximate limit

$$c\,y(t_n) \leq c\,\frac{0.3 \text{ rad}}{2\pi F_n}\,\frac{N}{T} \cong \frac{7500 \text{ cm/s}}{N}\,\frac{\Delta f}{F_n} . \tag{6.25}$$

(The fact that $\Delta f\, T = N^2$ was exploited in the last step.) For example, with a time-bandwidth product of 10,000 in a sonar whose bandwidth is about one third of its center frequency f_0 (around which the chip frequencies F_n are packed), the equivalent observer velocity can range up to about 25 cm/s without violating the upper limit expressed in Eq. (6.25).

We can now put the approximated value of Eq. (6.23) into the integral formula of Eq. (6.22) and factor it out of the integral, giving

$$\tilde{p}_{mn}(t - t_m + t_n) = 2\varepsilon_{max}\,\eta_{mn}(t - t_m + t_n)$$

$$+ e^{j2\pi f_m (t - t_m + t_n)}\, e^{j2\pi F_n \varepsilon(t_n)} \int_{-\infty}^{+\infty} \Pi\left(\frac{\lambda - t}{T/N}\right) \Pi\left(\frac{\lambda}{T/N}\right) e^{-j2\pi f_{mn}\lambda}\, d\lambda \quad . \tag{6.26}$$

The fifth step in simplifying the formula for $\tilde{p}_{mn}(t)$ is to evaluate the integral. It is the same as the integral of Eq. (5.15) with T/N substituted for T and f_{mn} substituted for f_t, and it can be deduced from Eq. (5.19) that the integral is given by

$$\int_{-\infty}^{+\infty} \cdots d\lambda \;=\; \Pi\left(\frac{t}{2T/N}\right)\left(\frac{T}{N}-|t|\right)\operatorname{sinc}\left[\left(\frac{T}{N}-|t|\right)f_{mn}\right]e^{-j\pi f_{mn}t}\,. \qquad (6.27)$$

From the definitions of f_{mn} and f_n in Eqs. (6.15) and (6.6), respectively, it follows that

$$f_{mn} \;=\; [\,\Omega(m)-\Omega(n)\,]\frac{N}{T}\,, \qquad (6.28)$$

and, with minor algebraic manipulation and use of $\Lambda(\cdot)$, the integral reduces to

$$\int_{-\infty}^{+\infty} \cdots d\lambda \;=\; \frac{T}{N}\Lambda\left(\frac{t}{T/N}\right)\operatorname{sinc}\left\{[\,\Omega(m)-\Omega(n)\,]\Lambda\left(\frac{t}{T/N}\right)\right\}e^{-j\pi f_{mn}t}\,. \qquad (6.29)$$

The sixth step is to substitute this formula into the expression for $\tilde{p}_{mn}(t-t_m+t_n)$ that was obtained in Eq. (6.26) and then undo the variable shift that was done previously, by substituting $(t-t_n+t_m)$ for t. This gives the result

$$\tilde{p}_{mn}(t) \;=\; 2\varepsilon_{max}\,\eta_{mn}(t) \;+\; e^{j2\pi f_m t}\,e^{j2\pi F_n \varepsilon(t_n)}\;\times$$

$$\frac{T}{N}\Lambda\left(\frac{t-t_n+t_m}{T/N}\right)\operatorname{sinc}\left\{[\,\Omega(m)-\Omega(n)\,]\Lambda\left(\frac{t-t_n+t_m}{T/N}\right)\right\}\exp[\,-j\pi f_{mn}(t-t_n+t_m)]\,. \qquad (6.30)$$

However, from the definition of t_n in Eq. (6.5) one can determine that

$$-t_n+t_m \;=\; -(n-m)\frac{T}{N}\,, \qquad (6.31)$$

and from the expression for f_{mn} in Eq. (6.28) one then has

$$\exp\left[-j\pi f_{mn}(t-t_n+t_m)\right] \;=\; (-1)_{mn}\, e^{-j\pi f_{mn}t}, \tag{6.32}$$

where $(-1)_{mn}$ is defined as

$$(-1)_{mn} \;=\; (-1)^{\left[\Omega(m)-\Omega(n)\right](m-n)}. \tag{6.33}$$

This simplifies the expression for $\tilde{p}_{mn}(t)$ in Eq. (6.30) to

$$\tilde{p}_{mn}(t) \;=\; 2\varepsilon_{max}\,\eta_{mn}(t) \;+\; (-1)_{mn}\, e^{j2\pi \bar{f}_{mn}t}\; e^{j2\pi F_n \varepsilon(t_n)} \;\times$$

$$\frac{T}{N}\,\Lambda\!\left(\frac{t-(n-m)T/N}{T/N}\right)\mathrm{sinc}\left\{\left[\,\Omega(m)-\Omega(n)\,\right]\Lambda\!\left(\frac{t-(n-m)T/N}{T/N}\right)\right\}, \tag{6.34}$$

where $\bar{f}_{mn}$ is the average of the baseband frequencies of the mth and nth chips:

$$\bar{f}_{mn} \;=\; \frac{f_m + f_n}{2}. \tag{6.35}$$

The six-step simplification of the formula for $\tilde{p}_{mn}(t)$ is now complete.

6.3 DIAMONDS IN THE NO-FLUTTER CASE

In the absence of flutter the formula for $\tilde{p}(t)$ in Eq. (6.12) reverts to

$$p(t) \;=\; \frac{\Delta f}{T}\, e^{j2\pi f_0 t} \sum_{m=-N'}^{N'} \sum_{n=-N'}^{N'} p_{mn}(t), \tag{6.36}$$

and, setting $\varepsilon(\cdot) = 0$ in the earlier formula for $\tilde{p}_{mn}(t)$ of Eq. (6.30), one obtains

$$p_{mn}(t) \;=\; (-1)_{mn}\, e^{j2\pi \bar{f}_{mn}t} \;\times$$

$$\frac{T}{N}\,\Lambda\!\left(\frac{t-(n-m)T/N}{T/N}\right)\mathrm{sinc}\left\{\left[\,\Omega(m)-\Omega(n)\,\right]\Lambda\!\left(\frac{t-(n-m)T/N}{T/N}\right)\right\}. \tag{6.37}$$

The double summation of the N×N array $\{p_{mn}(t)\}$ in Eq. (6.36) can also be done along diagonals:

$$\sum_{m=-N'}^{N'} \sum_{n=-N'}^{N'} p_{mn}(t) = \sum_{k=-(N-1)}^{+(N-1)} D_k(t) , \tag{6.38}$$

where $D_k(t)$ is the sum of terms along the kth diagonal.

$$D_k(t) = \sum_{\substack{m,n: \\ n-m=k}} p_{mn}(t) . \tag{6.39}$$

Notice that the subscript k ranges over a larger range of positive and negative values than m and n (because an N×N array has $2N-1$ diagonals), and the D_k's do not all have the same number of terms. For example, D_0 is the sum of the N terms along the main diagonal of the p_{mn} array, whereas D_{N-1} consists only of the upper-right element $p_{1N'}(t)$. In general, the k^{th} diagonal has $N-|k|$ elements.

A picture may help to clarify the nature of this diagonal summation. It can be seen in the definition of Eq. (6.13) that $\tilde{p}_{mn}(t)$, or $p_{mn}(t)$ in the unfluttered case, is the result of correlating the nth chip of the echo pulse with the mth chip of the replica. The results of these chip-to-chip crosscorrelations are depicted in Fig. 6.1 for a 9-chip waveform. Each of the cells represents one of the 81 terms $p_{mn}(t)$. (The hand-drawn waveforms are only intended to be suggestive of the complex-valued functions that would actually result in the case of a stepped FM wave, and should not be taken too seriously.)

A component $D_k(t)$ is formed by adding up those elements $p_{mn}(t)$ for which $n-m=k$, i.e., the elements that align vertically in Fig. 6.1. For example, $D_0(t)$ is obtained by adding the elements that lie along the vertical midline of Fig. 6.1, which are the self-correlations of the nine chips.

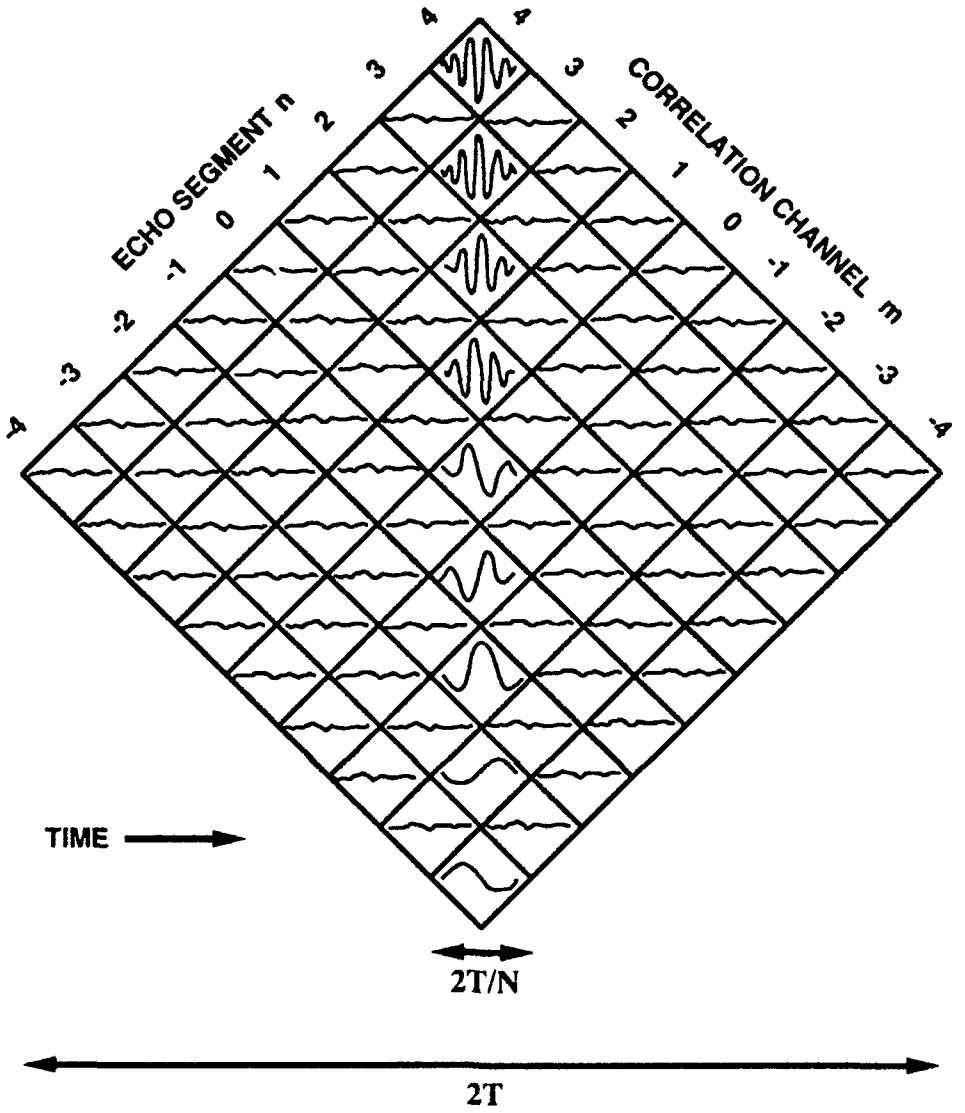

FIGURE 6.1

GRAPHIC REPRESENTATION OF THE $p_{mn}(t)$'s SHOWING THEIR TIMING RELATIONSHIP AND ALIGNMENT PRIOR TO VERTICAL (DIAGONAL) SUMMATION, FOR N = 9

From the no-flutter formula for $p_{mn}(t)$ in Eq. (6.37) it follows that

$$D_k(t) = \frac{T}{N}\Lambda\left(\frac{t-kT/N}{T/N}\right)\times$$

$$\sum_{\substack{m,n:\\ n-m=k}} (-1)_{mn}\, e^{j2\pi \bar{f}_{mn} t}\, \mathrm{sinc}\left\{\left[\,\Omega(m)-\Omega(n)\,\right]\Lambda\left(\frac{t-kT/N}{T/N}\right)\right\}. \qquad (6.40)$$

Since the summation contains $N-|k|$ terms, each of which has at most unit magnitude, it follows that

$$|D_k(t)| \le (N-|k|)\frac{T}{N}\,\Lambda\left(\frac{t-kT/N}{T/N}\right). \qquad (6.41)$$

From this it is clear that each $D_k(t)$ is only nonzero within an interval of duration $2T/N$ centered at $t=kT/N$; indeed, it is contained entirely by *a diamond* shaped envelope of duration $2T/N$ centered at $t=kT/N$. The peak-to-peak amplitude of that bounding envelope is $(1-|k/N|)2T$. (However, it turns out that $D_k(t)$ stays well within its bounding envelope most of the time.)

Because of this diamond shaped nature of the bounding envelopes, the $D_k(t)$'s will be referred to as *diamonds*. Since the diamonds $D_k(t)$ are of duration $2T/N$ but are spaced apart by T/N, there is some degree of overlap: Each time instant t is covered by exactly two of the diamonds. The size of these diamonds can be inferred from Fig. 6.1. The 81 small 45°-rotated squares that make up the figure can be regarded as the bounding envelopes of the $p_{mn}(t)$ terms. When vertical strings of these are added, the overall bounding envelopes form 17 overlapping diamonds.

These 17 overlapping diamonds are as shown in Fig. 6.2. Specifically, the tall diamond shaped figures depicted in Fig. 6.2 are the bounding envelopes that appear in the right side of Eq. (6.41). They are shown as white for even k, and shaded for odd k, with the white diamonds in front. However, the diamonds actually overlap in an additive fashion.

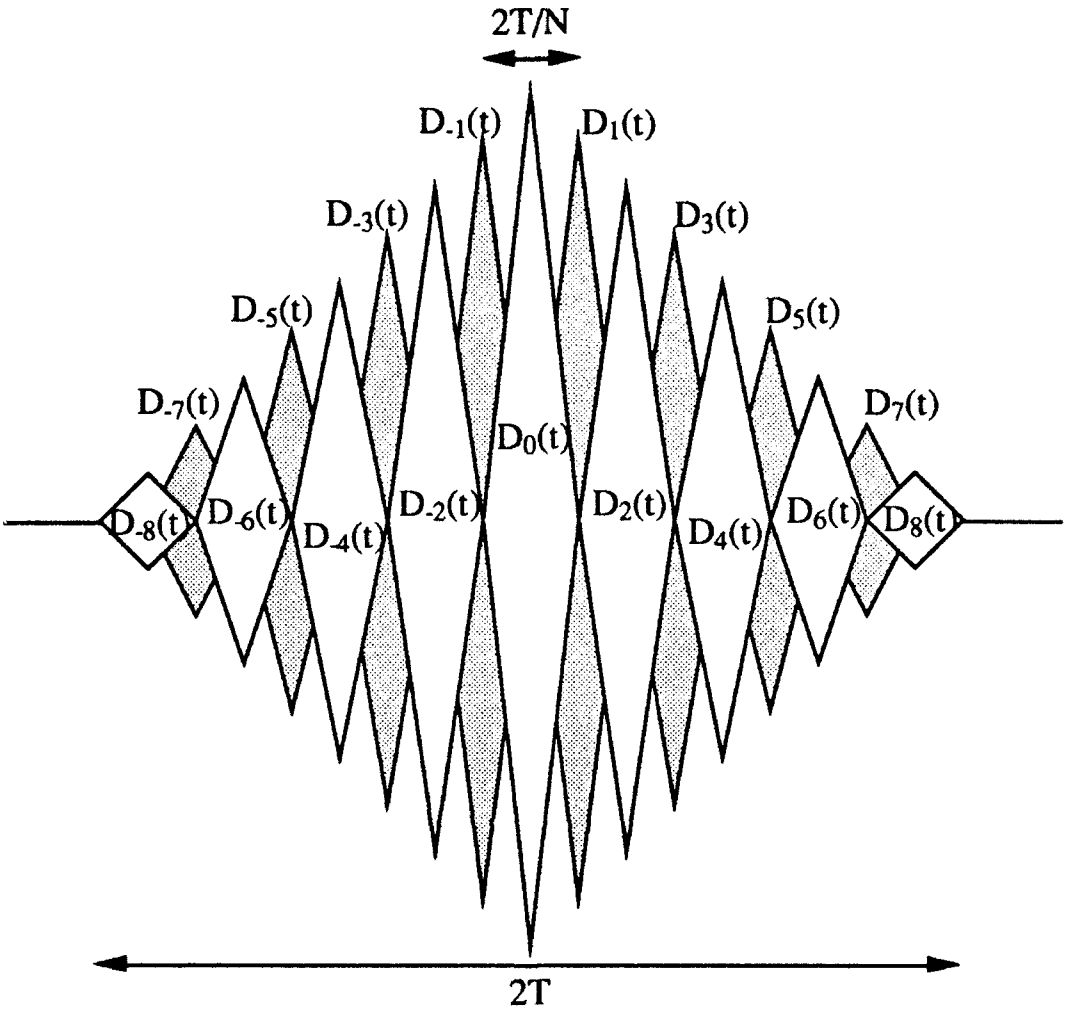

FIGURE 6.2
PATTERN OF 17 OVERLAPPING DIAMONDS FOR N = 9

Since the diagonal summation formula of Eq. (6.38) is merely a rearrangement of the square array summation formula for p(`` of Eq. (6.36), the D_k's must sum to give p(t):

$$p(t) = \frac{\Delta f}{T} e^{j2\pi f_0 t} \sum_{k=-(N-1)}^{+(N-1)} D_k(t) \ . \tag{6.42}$$

Thus, the compressed pulse p(t) may be considered to be a sum of $2N-1$ *diamonds* $D_k(t)$, each of width $2T/N$, that partially overlap to give a total duration of $2T$, whereas the original signal $x_{rep}(t)$ was a sum of N contiguous, non-overlapping rectangular *chips* $x_n(t)$ of duration T/N that gave a total duration of T.

In contrast to the constant power nature of $x_{rep}(t)$, however, the pulse p(t) has its energy concentrated at the center. The central diamond, $D_0(t)$, which contains the chip self-correlations, is obtained by setting $k = 0$ in the formula for $D_k(t)$ of Eq. (6.40) and performing the summation over the main diagonal, i.e., over terms satisfying $m = n$. This makes the argument of sinc(·) equal to zero and forces $(-1)_{mn} = 1$ (using its definition in Eq. (6.33)). The result is

$$D_0(t) = \frac{T}{N} \Lambda\left(\frac{t}{T/N}\right) \sum_{n=-N'}^{N'} e^{j2\pi f_n t} \ . \tag{6.43}$$

It will be recalled from their definition in Eq. (6.6) that the f_n's are given by

$$f_n = \frac{N}{T} \Omega(n) \ , \tag{6.44}$$

where the hop "code" $\Omega(n)$ reorders the integers into scrambled order. However, in the summation of Eq. (6.43) it does not really matter what order one uses for the integers, and this means that

$$\sum_{n=-N'}^{N'} e^{j2\pi f_n t} = \sum_{n=-N'}^{N'} \exp\left(j2\pi \frac{N}{T} nt\right) \ . \tag{6.45}$$

This summation is then immediately recognizable as a truncated Fourier series of $\delta(t)$ over the interval $|t| \le 2T/N$, and it invites the use of a well-known trigonometric identity (see §19.39 of Spiegel (1968)), giving

$$\sum_{n=-N'}^{N'} \exp\left(j2\pi \frac{N}{T} nt\right) = \frac{\sin[\pi(N^2/T)t]}{\sin[\pi(N/T)t]} = N \frac{\mathrm{sinc}[\Delta f t]}{\mathrm{sinc}[(N/T)t]} , \qquad (6.46)$$

where the last formula has been simplified by using the fact that $N^2 = \Delta f T$. The formula can be substituted into the summation formula for $D_0(t)$, i.e., into Eq. (6.43), to give

$$D_0(t) = T \Lambda\left(\frac{t}{T/N}\right) \frac{\mathrm{sinc}(\Delta f t)}{\mathrm{sinc}[(N/T)t]} . \qquad (6.47)$$

It is clear (see Eq. (6.46)) that the numerator's $\mathrm{sinc}(\cdot)$ is of much shorter duration than the denominator's $\mathrm{sinc}(\cdot)$, and the effective duration of $D_0(t)$ is therefore approximately equal to that of $\mathrm{sinc}(\Delta f t)$, which is $1.5/\Delta f$ (see Eq. 2.11)). Actually, however, the ratio of $\mathrm{sinc}(\cdot)$ functions in Eq. (6.47) is periodic with period T/N. (This can be verified most easily in the ratio of sine functions in the middle of Eq. (6.46).) Thus, the central spike of the numerator's $\mathrm{sinc}(\cdot)$ function is repeated at $t = \pm T/N$, i.e., at the ends of the diamond. However, the $\Lambda(\cdot)$ function multiplier in $D_0(t)$, as expressed in Eq. (6.47), goes to zero at the ends of the diamond, and kills these two extraneous spikes; only the central spike survives.

Furthermore,

$$D_0(t) \cong T \, \mathrm{sinc}(\Delta f t) \qquad (6.48)$$

if the effective duration is enough smaller than T/N that the $\Lambda(\cdot)$ function and the denominator's $\mathrm{sinc}(\cdot)$ function both have nearly unit value. Simple algebra, using $N^2 = \Delta f T$, shows that the condition $1.5/\Delta f << T/N$ is equivalent to

$$\Delta f T >> (1.5)^2 , \qquad (6.49)$$

which is easily met. Thus, the formula for the central diamond $D_0(t)$ given in Eq. (6.48) is a pretty good approximation.

In fact, when that approximation is put into the summation formula for the compressed pulse p(t), i.e., into Eq. (6.42), it gives a contribution

$$[p(t)]_{0^{th}\,\text{diamond}} = \frac{\Delta f}{T} e^{j2\pi f_0 t} D_0(t) \cong \Delta f\ \text{sinc}(\Delta f\, t)\, e^{j2\pi f_0 t}\ , \quad (6.50)$$

which coincides with the ideal, theoretical form of the compressed pulse for a large time-bandwidth product, CAFS waveform of bandwidth Δf (see Eq. (2.29)). There is nothing left for the other diamonds to contribute. Indeed, they are constructed from the off-diagonal terms of the p_{mn} array, which consist of crosscorrelations of the chip waveforms (all of different frequency), so they should be vanishingly small anyway. They do contribute a small amount of "ripple" that lasts for the full duration (2T), sometimes known as *self-noise.*

6.4 FLUTTERED DIAMONDS

When the effect of flutter is put back into the problem, its effect upon $\tilde{p}_{mn}(t)$ (as given in Eq. (6.34)) occurs in two steps: (1) A factor $e^{j2\pi F_n \varepsilon(t_n)}$ is applied, and (2) a quantity $2\varepsilon_{max}\,\eta_{mn}(t)$ is added. When the $\tilde{p}_{mn}(t)$ array is summed in Eq. (6.12) to give the fluttered and compressed pulse $\tilde{p}(t)$, the result can be restated as

$$\tilde{p}(t) = \tilde{p}_\eta(t) + \frac{\Delta f}{T} e^{j2\pi f_0 t} \sum_{m=-N'}^{N'} \sum_{n=-N'}^{N'} p_{mn}^{(\varepsilon)}(t)\ , \quad (6.51)$$

where $\tilde{p}_\eta(t)$ is defined as

$$\tilde{p}_\eta(t) = \frac{\Delta f}{T} e^{j2\pi f_0 t} \left[2\varepsilon_{max} \sum_{m=-N'}^{N'} \sum_{n=-N'}^{N'} \eta_{mn}(t) \right], \quad (6.52)$$

and $p_{mn}^{(\varepsilon)}(t)$ is defined as

$$p_{mn}^{(\varepsilon)}(t) \;=\; (-1)_{mn}\, e^{j2\pi \bar{f}_{mn} t}\; e^{j2\pi F_n \epsilon(t_n)} \;\times$$

$$\frac{T}{N}\Lambda\!\left(\frac{t-(n-m)T/N}{T/N}\right)\mathrm{sinc}\left\{\left[\,\Omega(m)-\Omega(n)\,\right]\Lambda\!\left(\frac{t-(n-m)T/N}{T/N}\right)\right\} . \qquad (6.53)$$

The latter quantity, $p_{mn}^{(\varepsilon)}(t)$, is the important one. It is the same as the $p_{mn}(t)$ of the no-flutter case, except that the phase-deviating effect of the flutter has been included. The $\widetilde{p}_{\eta}(t)$ term, which is an artifact introduced when a convenient simplifying approximation was made, will later be shown to be relatively insignificant.

The procedure now is to mimic what was done in Eqs. (6.38)-(6.47) for the no-flutter case. Since the method has already been described, the descriptions given here are rather terse:

The double summation of the N×N array $\left\{p_{mn}^{(\varepsilon)}(t)\right\}$, as given in Eq. (6.51), can be done along diagonals,

$$\sum_{m=-N'}^{N'}\sum_{n=-N'}^{N'} p_{mn}^{(\varepsilon)}(t) \;=\; \sum_{k=-(N-1)}^{+(N-1)} \widetilde{D}_k(t)\ , \qquad (6.54)$$

where the *fluttered diamond* $\widetilde{D}_k(t)$ is the sum of terms along the kth diagonal.

$$\widetilde{D}_k(t) \;=\; \sum_{\substack{m,n:\\ n-m=k}} p_{mn}^{(\varepsilon)}(t)\ . \qquad (6.55)$$

From the formula for $p_{mn}^{(\varepsilon)}(t)$ in Eq. (6.53) it then follows that

$$\widetilde{D}_k(t) \;=\; \frac{T}{N}\Lambda\!\left(\frac{t-kT/N}{T/N}\right)\times$$

$$\sum_{\substack{m,n:\\ n-m=k}} (-1)_{mn}\, e^{j2\pi F_n \epsilon(t_n)}\, e^{j2\pi \bar{f}_{mn} t}\,\mathrm{sinc}\left\{\left[\,\Omega(m)-\Omega(n)\,\right]\Lambda\!\left(\frac{t-kT/N}{T/N}\right)\right\} . \qquad (6.56)$$

Even in the presence of flutter, the diamond-envelope bounding formula of Eq. (6.41) applies; i.e.,

$$|\tilde{D}_k(t)| \leq (N-|k|)\frac{T}{N}\,\Lambda\left(\frac{t-kT/N}{T/N}\right), \tag{6.57}$$

and the diamonds $\tilde{D}_k(t)$ have the same locations and bounding envelopes as they did in the no-flutter case. Figures 6.1 and 6.2 thus remain applicable when flutter is present. From the formula for $\tilde{p}(t)$ given in Eq. (6.51) and the summation-by-diagonals representation of Eq. (6.54), it follows that

$$\tilde{p}(t) = \tilde{p}_\eta(t) + \frac{\Delta f}{T} e^{j2\pi f_0 t} \sum_{k=-(N-1)}^{+(N-1)} \tilde{D}_k(t) \quad . \tag{6.58}$$

As in the no-flutter case, the central diamond, $\tilde{D}_0(t)$, is obtained by setting $k = 0$ in the $\tilde{D}_k(t)$ formula of Eq. (6.56) and performing the summation over the main diagonal. The result can be expressed as

$$\tilde{D}_0(t) = \frac{T}{N}\Lambda\left(\frac{t}{T/N}\right)B(t) \ , \tag{6.59}$$

where $B(t)$ is defined as

$$B(t) = \sum_{n=-N'}^{N'} e^{j2\pi F_n \epsilon(t_n)}\, e^{j2\pi f_n t} \quad . \tag{6.60}$$

Again, it will be recalled from their definition in Eq. (6.6) that the f_n's are given by

$$f_n = \frac{N}{T}\Omega(n) \ , \tag{6.61}$$

where the hop "code" $\Omega(n)$ reorders the integers into scrambled order. However, in this flutter-perturbed case we shall have to be more careful in changing the order of summation. In particular, we change the variable of summation to $m = \Omega(n)$, which ranges over the same limits as n, and gives $f_n = (N/T)m$. This change of summation variables, as applied to the definition

of $B(t)$ in Eq. (6.60), gives

$$B(t) = \sum_{m=-N'}^{N'} e^{j\Theta_m} \exp\left[j2\pi\left(\frac{N}{T}\right)m\,t\right], \tag{6.62}$$

where $\{\Theta_m\}$ is the same as the sequence $\{2\pi F_n \varepsilon(t_n)\}$ but in inverse scrambled order:

$$\Theta_m = \{2\pi F_n \varepsilon(t_n)\}_{n=\Omega^{-1}(m)}, \tag{6.63}$$

where $\Omega^{-1}(\cdot)$ denotes the inverse mapping of the hopcode. It should be noted that the sequence $\{2\pi F_n \varepsilon(t_n)\}$ represents the instantaneous phase deviation of the received waveform, measured at the centers of the chips, and sampled throughout the entire duration T of the hopcode waveform. Thus, $\{\Theta_m\}$ is a very thoroughly mixed up version of the original sequence of phase deviation samples.

The summation in Eq. (6.62) is a finite Fourier series in which the Fourier coefficients are the set $\{e^{j\Theta_m}\}$. Thus, its average power is

$$\langle |B(t)|^2 \rangle = \sum_{m=-N'}^{N'} |e^{j\Theta_m}|^2 = N. \tag{6.64}$$

If the flutter is sufficiently strong that the phase deviation varies over a range of at least 2π in the duration T of the hopcode waveform, then $\{\Theta_m\}$ will be a sequence of uniform amplitude but totally random phase. (This assumes that the hop "code" $\Omega(n)$ is a random sequence.) It does not matter whether the flutter-induced phase deviations change rapidly or slowly, the inverse scrambling will thoroughly "whiten" the sequence. This means that the waveform $B(t)$ will have its energy rather uniformly distributed over time.

This is a different result from the no-flutter case. In fact, the no-flutter case can be gotten by setting the elements of the sequence $\{\Theta_m\}$ to zero in the $B(t)$ formula of Eq. (6.62), and using the trigonometric identity from Eq. (6.46):

$$[B(t)]_{\text{no flutter}} = N\frac{\text{sinc}[\Delta f\, t]}{\text{sinc}[(N/T)t]}. \qquad (6.65)$$

Thus, for the no-flutter case the energy of $B(t)$ is concentrated at the center in an effective duration $1.5/\Delta f$. The total energy in the central pulse of Eq. (6.65) is then $N^2/\Delta f$, and that gives a total energy in the central diamond $D_0(t)$, accounting for linear multiplication by T/N in Eq. (6.59), of $T^2/\Delta f$.

Let us see how this compares with the energy in the central diamond $\tilde{D}_0(t)$ for the flutter-included case. Assuming the power of $B(t)$ is approximately constant and equal to the value N given in Eq. (6.65), the only time-varying effect is due to the factor $\Lambda[t/(T/N)]$ that is applied in Eq. (6.59). It has a mean square value of $1/3$ over the diamond's duration of $2T/N$, so the total energy of $\tilde{D}_0(t)$, accounting for the scalar factor T/N in Eq. (6.59), is

$$[\tilde{D}_0(t)]_{\text{energy}} = N \times 1/3 \times 2T/N \times (T/N)^2 = \tfrac{2}{3}T^2/\Delta f \qquad (6.66)$$

(using $N^2 = \Delta f T$), which is two-thirds as much energy as in the no-flutter case.

However, the loss of central pulse energy is not nearly as serious as the fact that the energy is smeared all over the central diamond, and this will happen even with a modest amount of flutter. Indeed, the effective duration of this diamond pulse (using the result following Eq. (2.9)) is approximately $(10T)/(9N)$. This is larger than the no-flutter compressed pulse duration by a factor that can be computed as

$$\frac{(10T)/(9N)}{1.5/\Delta f} \approx \frac{20}{27}\sqrt{T\Delta f}\ . \qquad (6.67)$$

As in the no-flutter case, the other diamonds are constructed from the off-diagonal terms of the p_{mn} array, which consist of crosscorrelations of the individual chip waveforms (which are all of different frequency). They will still contribute some "ripple" that lasts for the full duration ($2T$), but their contributions should not be enlarged by the phase perturbations that are induced by the flutter. However, an exception to this statement will occur if the flutter is so

strong that the pure tone spectral spreading bandwidth $B_{\tilde{f}_0}$, discussed in Section 3.1.6, is on the order of the chip bandwidth, i.e., on the order of $1.5N/T$. In this case the crosscorrelations can be enhanced by frequency "leakage" caused by the flutter-induced Doppler spreading.

For completeness, we must acknowledge that there is an additional contribution in the form of the term $\tilde{p}_\eta(t)$ defined in Eq. (6.52). It was defined in terms of a double summation of terms $\eta_{mn}(t)$, each having no more than unit magnitude, that were originally defined through Eq. (6.22). Because of that definition, each $\eta_{mn}(t)$ has (approximately) the same "activity window" as $\tilde{p}_{mn}(t)$; i.e., it is zero except (approximately) when t falls within a window of duration $2T/N$ centered at $t=(n-m)T/N$ (see Eq. (6.34)). Thus, one can do the double-summation of $\eta_{mn}(t)$'s in Eq. (6.52) by diagonals just as was done for $\tilde{p}_{mn}(t)$. The result is that at the location of each diamond $\tilde{D}_k(t)$ there is also a contribution from diagonally summed $\eta_{mn}(t)$ terms. Since each diagonal has at most N elements, the summed contribution of $\eta_{mn}(t)$ terms for any diamond could at most have magnitude N (since $|\eta_{mn}(t)| \le 1$ by definition), and that could only occur at the central diamond (with extraordinary coherence in the summation).

This upper limit magnitude N, after multiplying by the factor $2\varepsilon_{max}$ that appears in Eq. (6.52), can be compared with the magnitude of the central diamond $\tilde{D}_0(t)$. However, it is easier to express that comparison in terms of energy: The energy of $\tilde{D}_0(t)$ was determined in Eq. (6.66) to be $(2/3)(T^2/\Delta f)$. If the competing contribution due to $\eta_{mn}(t)$ has, at most, magnitude $2N\varepsilon_{max}$, then its total energy over the $2T/N$ duration of the central diamond can be no greater than $(2N\varepsilon_{max})^2 \times 2T/N$. The ratio of this upper limit of energy to the energy of $\tilde{D}_0(t)$ is therefore

$$\frac{(2N\varepsilon_{max})^2 \times 2T/N}{\frac{2}{3}(T^2/\Delta f)} = \frac{4}{3}\left[\frac{\varepsilon_{max}}{T}(T\Delta f)^{0.75}\right]^2, \qquad (6.68)$$

which will be insignificant if

$$\varepsilon_{max} << \frac{\sqrt{3}\,T}{2\,(T\Delta f)^{0.75}}. \tag{6.69}$$

This condition (which is a very conservative one) will usually be met, so that the contribution of the $\eta_{mn}(t)$ terms remains negligible. For example, with a time-bandwidth product of 1000 and a waveform duration T of 1 s, Eq. (6.69) requires that the maximum time axis perturbation be less that 4.9 ms.

6.5 THE SPECIAL CASE OF STEPPED-LINEAR FM

If the hop "code" is the trivial one $\Omega(n)=n$, then the waveform is a stepped-linear FM wave burst, and the flutter effect is much less damaging. In that case the sequence $\{\Theta_m\}$ of Eq. (6.63) is the same as the sequence $\{2\pi F_m \varepsilon(t_m)\}$ without any scrambling. This means that the Fourier series in Eq. (6.62) is

$$B(t) = \sum_{m=-N'}^{N'} e^{j2\pi F_m \varepsilon(t_m)} \exp\left[j2\pi\left(\frac{N}{T}\right)m\,t\right]. \tag{6.70}$$

However, the instantaneous phase shift due to the flutter is

$$\phi(t) = 2\pi\,\varepsilon(t)\times\left\{\begin{matrix}\text{instantaneous frequency}\\ \text{of waveform}\end{matrix}\right\}, \tag{6.71}$$

where the instantaneous frequency at time t_m is F_m (see definition in Eq. (6.8)). The result is

$$B(t) = \sum_{m=-N'}^{N'} e^{j\phi(t_m)} \exp\left[j2\pi\left(\frac{N}{T}\right)m\,t\right]. \tag{6.72}$$

From the definition of t_n in Eq. (6.5) we see that

$$m = \frac{N}{T}\,t_m\ . \tag{6.73}$$

When this is used in place of m in the series for B(t) of Eq. (6.72) the result can be expressed as

$$B(t) = \left\{ \sum_{m=-N'}^{N'} e^{j\phi(t_m)} \exp[-j2\pi f t_m] \right\}_{f \to -\Delta f \frac{L}{T}} \quad (6.74)$$

If it is assumed that the flutter process $\varepsilon(t)$, which produces the instantaneous phase ϕ in accordance with Eq. (6.71), varies slowly enough that it does not change very much during the chip interval T/N (which is also the spacing between sample points $\{t_m\}$), then the summation of Eq. (6.74) approximates an integral:

$$B(t) \cong \frac{1}{T} \left\{ \int_{-\infty}^{+\infty} \Pi\left(\frac{t}{T}\right) e^{j\phi(t)} \exp[-j2\pi f t]\, dt \right\}_{f \to -\Delta f \frac{L}{T}} . \quad (6.75)$$

This result, which can be used to estimate the duration of the central, compressed pulse (since it produces the central diamond $\tilde{D}_0(t)$ through Eq. (6.59)), is identical to the integral that was encountered in Section 5 (see Eq. (5.61), for example). This should not be surprising, since a stepped-linear FM wave burst closely approximates a continuous, linear FM wave burst if the number of chips is large.

There is no need to pursue the stepped-FM case any further, since the results of Section 5 apply. However, the behavior of the stepped-FM case makes it easier to understand why a random hopcode waveform is more susceptible to flutter. It will be recalled from Section 5 that the elongation of the fluttered and compressed pulse in the linear FM case depended upon the size of $y(t)=\dot{\varepsilon}(t)$, the normalized instantaneous frequency deviation of the flutter (see Eq. (5.107) for example). Thus, in the linear-FM case the magnitude of the time axis perturbation $\varepsilon(t)$ can actually be quite large without causing much pulse elongation, so long as it varies slowly enough that its derivative remains small.

On the other hand, when a random hopcode is used the $\varepsilon(t)$ values are effectively time scrambled during the replica correlation process, insofar as the

central diamond $\tilde{D}_0(t)$ is concerned. This can be seen, for example, in Eqs. (6.62) and (6.63), which can be interpreted as representing $\tilde{D}_0(t)$ (through Eq. (6.59) in terms of an equivalent stepped-linear FM hopcode, but at the cost of time scrambling the phase deviations. One may then conclude that, since $\varepsilon(t)$ is replaced by a time scrambled version of itself, its derivative (which would play the role of $y(t)$ in the "equivalent" linear FM case) then exhibits very large magnitudes even though the original $\varepsilon(t)$ might have been slowly varying.

This interpretation is in accord with the results of Section 6.3 for the random hopcode case, where it was found that a modest amount of flutter would smear the central pulse over an interval of duration $2T/N$, no matter how slowly $\varepsilon(t)$ varied, i.e., no matter how small $y(t)$ was (assuming, of course, that $\varepsilon(t)$ did cover a span of 2π radians during the waveform duration T). In effect, the use of a random hopcode reorders and prewhitens the flutter process $\varepsilon(t)$, whether we like it or not.

6.6 PROCESSING GAIN FOR A RANDOM HOPCODE

In the absence of flutter, the pulse compression (i.e., replica correlation) filter reduces the sonar pulse duration from T to $1.5/\Delta f$, since the hopcode signal is always a CAFS waveform. Thus, the processing gain yielded by the replica correlation process is (see Section 2.3.4)

$$\textbf{Proc. Gain} \cong 5\log_{10}\left(\frac{\Delta f T}{1.5}\right) = 5\log_{10}(\Delta f T) - 0.9\,\text{dB}\,. \qquad (6.76)$$

However, when flutter $\varepsilon(t)$ is present in sufficient strength to deviate the phase by at least a few cycles during the duration (T) of the sonar waveform, then (for a random hopcode) the results of Section 6.3 will apply: The energy of the pulse will be smeared over the central diamond, which has an effective duration of $(10/9)(T/N)$. The processing gain will drop to

$$\textbf{Proc. Gain} \cong 5\log_{10}\left(\frac{T}{\frac{10}{9}\frac{T}{N}}\right) = 2.5\log_{10}(\Delta f T) - 0.2\,\text{dB}\,, \qquad (6.77)$$

where, to get the last step, use has been made of the fact that $N = \sqrt{\Delta f T}$.

To those accustomed to computing gain (in decibels) as $10\log_{10}(K)$ where K represents a ratio of powers, energies, or durations, it is already hard to accept the $5\log_{10}(K)$ formula that accounts for the false alarm rate characteristics of an energy detector (see Section 2.3.4). When the formula degenerates to $2.5\log_{10}(K)$, it adds insult to injury. As if that were not enough, one should also take into account the fact that the pulse energy in the central diamond is diminished by a factor of 2/3 as reported in Eq. (6.66). Since this reduction is against the direct competition of noise power, it degrades the processing gain by $10\log_{10}(2/3) = -1.8$ dB, so Eq. (6.77) should be corrected to

$$\textbf{Proc. Gain} \cong 2.5\log_{10}(T\Delta f) - 2.0\,\text{dB}. \tag{6.78}$$

6.7 RANDOM HOPCODE IN STRONG FLUTTER

There is an even greater degradation if the flutter process, $y(t)=\dot{\varepsilon}(t)$, becomes strong enough to spread the spectra of the chips outside their normal boundaries. To take this rigorously into account, one would have to go all the way back to the integral formula for $\tilde{p}_{mn}(t - t_m + t_n)$ in Eq. (6.22), and avoid making the stepwise-constant $\varepsilon(t)$ approximation of Eq. (6.22). The resulting difficulties in carrying out the analysis would be quite burdensome. There is a another approach that gives a crude estimate of the degradation. It is based upon a sequence of logical conclusions, as follows.

In Section 3.1.6 it was shown that a pure tone at frequency f_0 would be subjected to spectral broadening due to the flutter, producing a bandwidth that was given in Eq. (3.40) as

$$B_{\tilde{f}_0} \cong 2\sqrt{3}\, y_{rms}\, f_0 \tag{6.79}$$

for a flutter process $y(t)=\dot{\varepsilon}(t)$ whose point statistics described a uniform distribution. (Very nearly the same result was obtained for the cases of Gaussian and sinusoidal flutter.) It is reasonable to conclude that the

bandwidth of the nth chip, at frequency F_n, will be spread to

$$\tilde{B}_n \cong 2\sqrt{3}\, y_\sigma^{(T/N)} F_n k \,, \tag{6.80}$$

provided this bandwidth is significantly greater than the *unfluttered* bandwidth of the chip, which is

$$B_n = 1.5N/T \tag{6.81}$$

by Eq. (2.6) (since each chip is actually a tone burst of duration T/N).

The rationale for this conclusion is as follows: If the flutter spreads the spectrum of a pure tone at frequency F_n into a bandwidth $\tilde{B}_n$, then it ought to do the same thing to any narrowband signal centered at F_n. By "narrowband" we mean that its original bandwidth was significantly less than $\tilde{B}_n$. The nth chip meets this definition of a narrowband signal if its original bandwidth B_n is significantly less than $\tilde{B}_n$.

The substitution of the sample standard deviation over the chip interval T/N, $y_\sigma^{(T/N)}$, in place of y_{rms} in going from Eq. (6.79) to Eq. (6.80) was done for the same reason that $y_\sigma^{(T)}$ was substituted for y_{rms} in going from Eq. (5.92) to Eq. (5.106). (An independent sample of length T/N is taken for each chip.)

Although Eq. (6.80) gives the correct bandwidth for the fluttered chip only when it is significantly greater than its unfluttered bandwidth $1.5N/T$, one can correct that defect by approximating

$$\tilde{B}_n \cong B_n + 2\sqrt{3}\, y_\sigma^{(T/N)} F_n \,. \tag{6.82}$$

Having defended and improved the formula for the bandwidth of a fluttered chip, we can now proceed with the strong flutter analysis.

When the replica correlation process is done, the central diamond $\tilde{D}_0(t)$ (which contains the fluttered and compressed pulse) consists of the summed

diagonal elements of the $\tilde{p}_{mn}(t)$ array; i.e., it consists of summed contributions of each chip correlated with a fluttered version of itself. Each individual correlation may be regarded as a replica correlation filtering process for the chip. Any spectral energy of the fluttered chip that falls outside the spectral width of the unfluttered (replica) chip will be lost, and the energy loss factor will be approximately given by

$$\frac{\tilde{B}_n}{B_n} \cong 1 + \frac{2\sqrt{3}\, y_\sigma^{(T/N)} F_n}{1.5N/T} . \tag{6.83}$$

Since the chip frequencies F_n are packed around the center frequency f_0, it does not violate the approximation very much to replace F_n by f_0 in this equation. Thus, each contributing chip-replica correlation loses approximately the same amount of energy, that loss being given by

$$\textbf{energy loss}_{dB} \cong 10\log_{10}\left[1 + \frac{2\sqrt{3}}{1.5} y_\sigma^{(T/N)} \frac{f_0 T}{N}\right] . \tag{6.84}$$

As far as the contribution to the central diamond is concerned, energy that is lost from one correlation does not "spill" into one of the others, because the chips do not arrive at the same time. Thus, all of the contributions to the energy of the central diamond $\tilde{D}_0(t)$ are diminished (approximately) by the amount given in the formula, so the energy of the fluttered and compressed pulse is diminished by that same amount, which means that the processing gain formula of Eq. (6.78) must be corrected to

$$\textbf{Proc. Gain} \cong 2.5\log_{10}(T\Delta f) - 2.4\,dB$$

$$-10\log_{10}\left[1 + 2.3\sqrt{\Delta f T}\left(\frac{f_0}{\Delta f}\right) y_\sigma^{(T/N)}\right] , \tag{6.85}$$

to allow for strong flutter. (The fact that $N^2 = \Delta f T$ has been used to simplify the result.)

6.8 SECTION SUMMARY

In the absence of flutter, a random hopcode waveform performs just as well as any other CAFS waveform, such as a linear FM wave burst (insofar as the basic issues of this report are concerned). However, if there is enough flutter to cause phase deviations that accumulate through a few cycles of phase error during the interval of the waveform, then the energy of the compressed pulse will be spread to a duration roughly equal to the chip interval (actually $2T/N$), and about one-third of the energy will be lost, although it must be preserved as "grass" noise that is distributed throughout the $2T$ interval.

Especially in the presence of slow flutter (where $\varepsilon(t)$ is significant but $y(t)$ is small), the spreading will be significantly less for a linear FM wave burst than for a random hopcode. (Pulse spreading in the case of a linear FM wave burst occurs only when the magnitude of $y(t)=\dot{\varepsilon}(t)$ becomes significant.)

If the flutter becomes strong, then the fluttered and compressed pulse of the linear FM wave burst will continue to elongate, with no loss in energy. The behavior for the random hopcode waveform is quite different: The duration of the central pulse never becomes any larger than $2T/N$ as the flutter increases. Although this might seem to be an advantage, the price one pays for this advantage is that the *energy* of this fixed width pulse diminishes rapidly when the flutter becomes stronger (i.e., when it becomes strong enough to spread the chip spectra significantly).

Indeed, once the flutter is strong enough to randomize the phases of the Fourier coefficients of the $B(t)$ series of Eq. (6.62), then the central diamond exhibits the same behavior regardless of whether the hopcode has a random or stepped-linear FM form. However, for a random hopcode the *non-central* diamonds are all mixed up, and have roughly comparable energies. For a stepped-linear FM hopcode, the total energy remains clustered around the center (as described in Section 5).

Perhaps it will be helpful to the reader if the progressive effect of increasing flutter upon the compressed pulse is restated, in the simplest terms,

for each type of hopcode waveform (for simplicity, we assume $y(t)$ has a uniform distribution).

Pulse A: Stepped-linear FM hopcode Starting at $1/\Delta f$, the duration of $\tilde{p}(t)$ increases as its amplitude diminishes, keeping a constant energy. Eventually it becomes wide enough that it exhibits an approximately flat-topped shape. As the flutter gets stronger, the duration is given approximately by the formula of Eq. (5.108), i.e.,

$$\mathbf{dur} \;\cong\; \left(\frac{T}{\Delta f}\right)\left(\, 2\times\sqrt{3}\; y_{\mathrm{rms}}^{(T)}\, f_0 \,\right) . \tag{6.86}$$

Pulse B: Random hopcode Starting at $1/\Delta f$, the duration first increases faster than for pulse A, but stops increasing when it reaches a width of $2T/N$, at which point it has lost one-third of its original energy. From that point onward it keeps a constant width, but diminishes in energy and amplitude. The energy that is gradually bled away from the central pulse is redistributed all over the domain (which is a triangular window of duration $2T$), in the form of "self-noise". The amplitude of pulse B eventually begins to track that of pulse A, but as both amplitudes diminish, pulse A retains its energy by elongating, whereas pulse B has to sacrifice its energy because it refuses to elongate. Soon pulse B becomes lost in its own "self-noise".

It is interesting to note that in radar (and communications) applications the use of a random hopcode is often done with no hope of ever compressing the pulse to less than a chip width; indeed, noncoherent processing is often applied, so that one concedes at the outset that the processing gain will only be $2.5\log_{10}(T\Delta f) - 2.4\,\mathrm{dB}$. (When that is done, there is little penalty involved with dispersing the chips over a larger time interval to make a frequency-hopped, time-hopped waveform, if desired.)

There is one final comment to be made before proceeding to the computer simulation example: One should avoid the conclusion that a random hopcode can ever do better, in general, than an FM wave burst. Although the formula (i.e., $2.5\log_{10}(T\Delta f) - 2.4\,\mathrm{dB}$) seems to imply that the processing gain

for the random hopcode can increase without bound, in contrast to the FM wave case of Section 5, this is only an illusion created by the approximations. In particular, note that the summary discussion above for pulse B did not include the "energy loss" adjustment of Section 6.7, and Eq. (6.85). For a fixed center frequency f_0 and bandwidth Δf, the time-bandwidth product ΔfT can only increase in proportion to the duration T, and the chip duration T/N must then go up as $\sqrt{\Delta fT}$ since $\Delta fT = N^2$ by Eq. (6.10). As the (pure tone) chips increase in duration their bandwidths become very narrow, and it becomes increasingly likely that the flutter will spread their spectra outside the chip band limits. Thus, any amount of flutter will eventually display the attributes of "strong flutter" as referred to in Section 6.7 if the waveform duration T is long enough, and the processing gain will be limited.

7. COMPUTER SIMULATION EXAMPLE

For purposes of illustration, an example of flutter is studied in this section for a hopcode waveform of the type analyzed in Section 6. It also approximates the FM wave burst of Section 5 when an ordered sequence of chip frequencies is used instead of a random sequence.

7.1 GENERAL SPECIFICATIONS OF THE EXAMPLE PROBLEM

The following example is selected:

Sonar center frequency: $f_0 = 200$ kHz

Sonar bandwidth: $\Delta f = 50$ kHz

Waveform types: Stepped-linear FM hopcode
Random hopcode

Waveform durations:

$T = 505.62$ ms	$T = 52.02$ ms	$T = 4.5$ ms
159 chips	51 chips	15 chips
(chip = 3.18 ms)	(chip = 1.02 ms)	(chip = 0.3 ms)
$T\Delta f = 25{,}281$	$T\Delta f = 2{,}601$	$T\Delta f = 225$

Flutter strength: $cy_{rms} =$ 0.5, 2, 5, 20, and 100 cm/s

Flutter type: Periodic parabolic cusps
Period $T_\varepsilon = 325$ ms
(flutter frequency fundamental $f_\varepsilon = 1/T_\varepsilon = 3.077$ Hz)

7.2 THE FLUTTER $\varepsilon(t)$

The flutter is defined in terms of the perturbation of the time axis $\varepsilon(t)$, as follows:

$$\varepsilon(t) = \left\{ \begin{array}{l} \sqrt{3}\, y_{rms} \left[\frac{T_\varepsilon}{12} - \frac{t^2}{T_\varepsilon} \right] \quad \text{for } |t| \le \frac{T_\varepsilon}{2}, \\ \\ \text{repeated with period } T_\varepsilon \text{ for } |t| > \frac{T_\varepsilon}{2}. \end{array} \right\} \tag{7.1}$$

Figure 7.1 displays $\varepsilon(t)$ for the case where the equivalent observer velocity cy_{rms} is set to 5 cm/s:

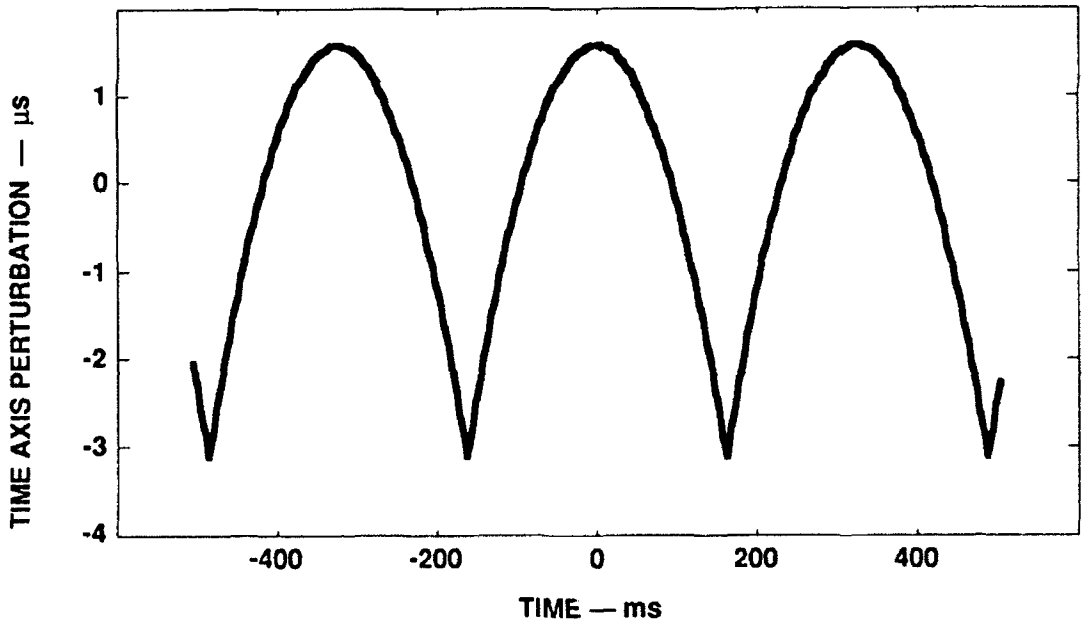

FIGURE 7.1
TIME AXIS PERTURBATION $\varepsilon(t)$ OF EXAMPLE, FOR AN EQUIVALENT OBSERVER VELOCITY cy_{rms} = 5 cm/s

The normalized frequency deviation of the flutter, $y(t) = \dot{\varepsilon}(t)$, is

$$y(t) = \begin{cases} -\sqrt{3}\, y_{rms} \left[\dfrac{t}{\frac{1}{2} T_\varepsilon} \right] & \text{for } |t| \le \dfrac{T_\varepsilon}{2}, \\ \text{repeats with period } T_\varepsilon \text{ for } |t| > \dfrac{T_\varepsilon}{2}. \end{cases} \tag{7.2}$$

The equivalent observer velocity $cy(t)$ is plotted in Fig. 7.2 for the case where the equivalent observer velocity cy_{rms} is set to 5 cm/s (assuming c = 1500 m/s):

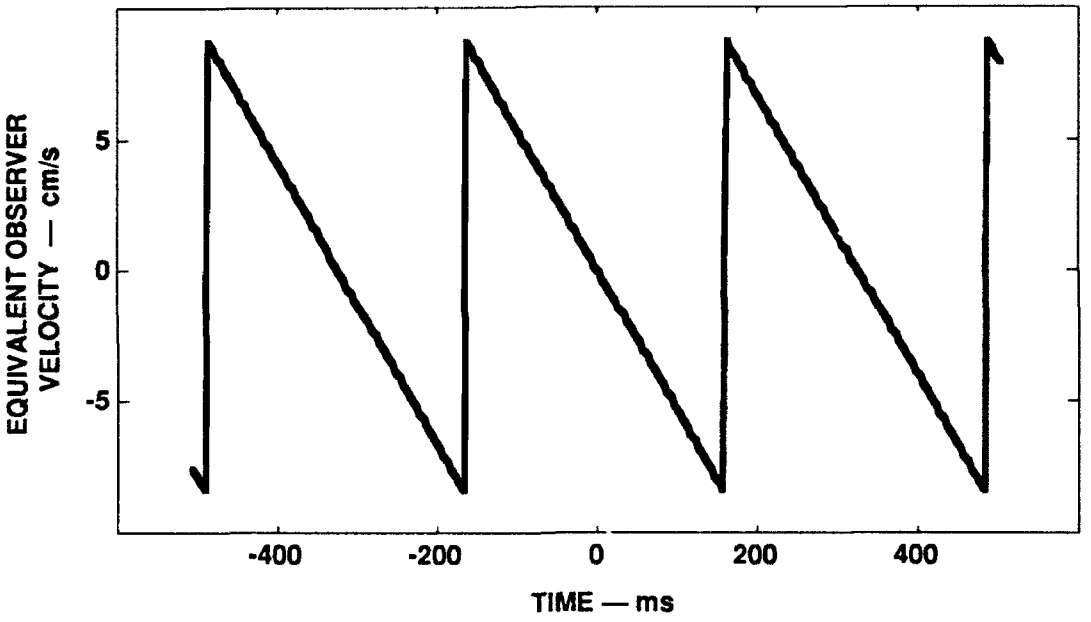

FIGURE 7.2
EQUIVALENT OBSERVER VELOCITY $cy(t)$ OF EXAMPLE, FOR cy_{rms} = 5 cm/s

Two things are evident from this plot of $cy(t)$. (1) Over the long term, the normalized frequency deviation $y(t)$ is uniformly distributed over its range, and (2) because of its simple sawtooth waveform, $y(t)$ can be readily expressed in terms of a Fourier series (Tuma, 1979):

$$y(t) = \sqrt{12}\, y_{rms} \sum_{n=1}^{\infty} \frac{(-1)^n}{n\pi} \sin(2\pi n f_\varepsilon t), \qquad (7.3)$$

where f_ε is the flutter's fundamental frequency, i.e., $f_\varepsilon = 1/T_\varepsilon$, which for the example is 3.077 Hz. It follows that the power spectrum of $y(t)$ is

$$S_y(f) = \frac{12\, y_{rms}^2}{\pi^2} \sum_{n=1}^{\infty} n^{-2} \left[\delta(f - n f_\varepsilon) + \delta(f + n f_\varepsilon) \right]. \qquad (7.4)$$

Since the impulses vanish except where $f = \pm n f_\varepsilon$, this formula remains valid if $(f/f_\varepsilon)^{-2}$ is substituted for n^{-2}:

$$S_y(f) = \left(\frac{12\, f_\varepsilon^2\, y_{rms}^2}{\pi^2} \right) f^{-2} \sum_{n=1}^{\infty} \left[\delta(f - n f_\varepsilon) + \delta(f + n f_\varepsilon) \right]. \qquad (7.5)$$

This formula shows how the periodic nature of $y(t)$ gives rise to a line spectrum rather than a smooth spectrum as might be the case for a random process. However, a more significant aspect of this formula is that $S_y(f)$ rolls off like f^{-2}, which means that $S_\varepsilon(f)$ rolls off like f^{-4}, since $S_y(f) = (2\pi f)^2 S_\varepsilon(f)$. Thus, the flutter process of our example, although deterministic and periodic, has a spectral rolloff that is similar to those of the measured flutter processes that were presented in Section 4.

The reader may wonder why a deterministic, periodic, non-random flutter was chosen for the computer simulation example. The advantages are as follows.

(1) Being deterministic, it can be replicated easily by other investigators.

(2) For the durations listed in the example specifications of Section 7.1, the "window" of the sonar waveform is at most 505.62 ms. That is only enough time for about one and one half cycles of $\varepsilon(t)$ anyway, which is not enough time for the replica correlation process to "see" whether $\varepsilon(t)$ is truly periodic, or merely

quasi-periodic with enough long-term randomness to smooth its spectrum. To put it another way, the windowing effect of the transmitted sonar waveform duration smears the effective spectrum of $\varepsilon(t)$ through sidelobe leakage, so that it no longer has a line spectrum anyway.

(3) The time varying nature of $\varepsilon(t)$ depicted in Fig 7.1, with its fundamental frequency of approximately 3 Hz, is not entirely unreasonable as an example of the possible effects of platform motion. Such a motion might result from turbulence-induced nonlinear oscillations of the sonar unit as it is pulled or pushed through the water. Indeed, the plot of $\varepsilon(t)$ looks rather like a full-wave rectified sine wave, rich in harmonic structure, and suggestive of simple harmonic motion that has been subjected to some kind of nonlinear conversion. Nevertheless, the fact that $\varepsilon(t)$ does *not* consist of exactly sinusoidal pieces (the pieces are parabolic arcs, not sinusoidal arcs) means that $\varepsilon(t)$ never looks exactly like a simple, single frequency sinusoid no matter how short the window.

(4) As mentioned above, the power spectral density $S_\varepsilon(f)$ rolls off like f^{-4}, *which is generally consistent* with the flutter spectra described in Section 4.

(5) This $\varepsilon(t)$ gives a very simple $y(t)$, which has a simple long-term distribution (specifically, a uniform distribution).

(6) Being described by a simple formula, the $\varepsilon(t)$ of Fig. 7.1 can be easily computed for any discrete sampling rate that is chosen for numerical computation. Thus, if one wants to double the sampling rate, the same $\varepsilon(t)$ can be used; a deterministic $\varepsilon(t)$ is not sample-rate dependent in the way that a random noise sequence generally is, nor does it display the artificial characteristic of being perfectly bandlimited.

Figures 7.1 and 7.2 describe the flutter process for the condition cy_{rms} = 5 cm/s; however, $\varepsilon(t)$ and $y(t)$ need only to be scaled by 0.1, 0.4, 4, and 20 to give the other specified flutter strengths of 0.5, 2, 20, and 100 cm/s.

7.3 EFFECT FOR A VERY LARGE TIME-BANDWIDTH PRODUCT

For the case of relatively weak flutter, cy_{rms} = 0.5 cm/s, Fig. 7.3 depicts the magnitude of the fluttered and compressed pulse for the longest duration of slightly over a half-second (T = 505.62 ms), for which the time-bandwidth product is 25,281. The upper part of the plot is for the stepped-linear FM case, and the lower part (plotted upside down) is for a random sequence of chip frequencies. The pulse magnitudes have been normalized to have exactly unit value in the absence of flutter. In effect, Fig. 7.3 depicts the no-flutter case since the flutter is so weak that both pulses have nearly full (unit) amplitude.

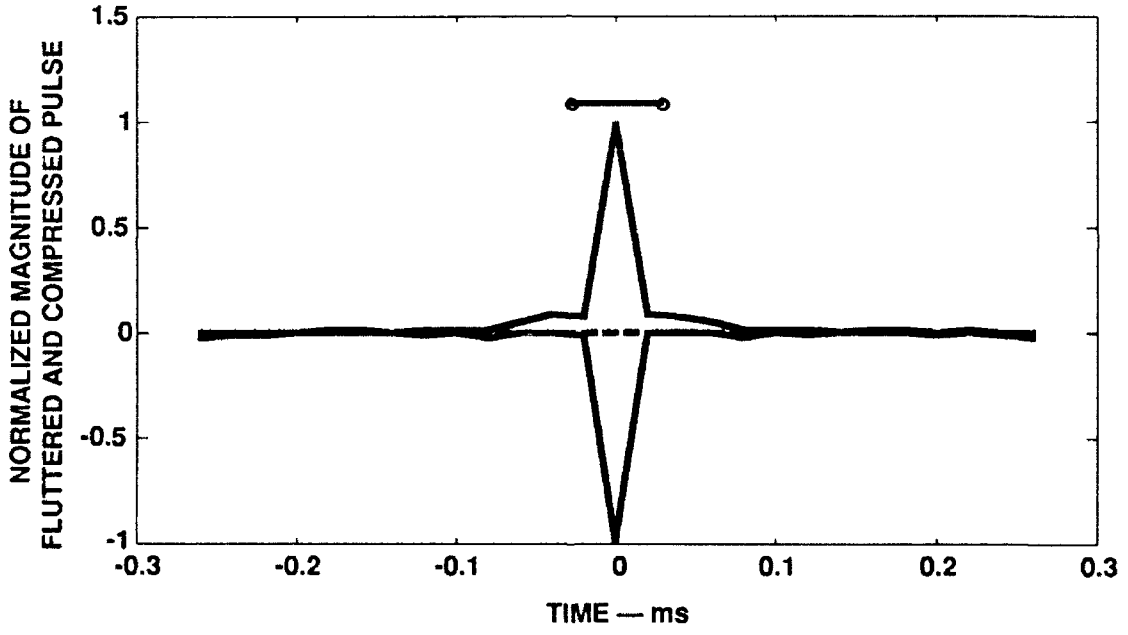

FIGURE 7.3
FLUTTERED AND COMPRESSED PULSE FOR cy_{rms} = 0.5 cm/s, FOR 505.62 ms TRANSMISSION, 50 kHz BANDWIDTH LINEAR FM (UPPER) AND RANDOM HOPCODE (LOWER)

The "dumbbell" symbol at the top of the plot indicates the duration predicted by Eq. (5.108) for the FM pulse, i.e.,

$$\mathbf{dur}\left(\left|\tilde{p}_1(t)\right|\right)_{\substack{\text{smoothed,}\\ \text{single pulse}}} \cong \left(\frac{1.5}{\Delta f}\right)\left[1+\left(Tf_0\right)\left(\frac{cy_\sigma^{(T)}}{650\ \text{m/s}}\right)\right]. \tag{7.6}$$

The formula appears to predict the correct duration for this case. However, it should be noted that the plot resolution is limited by a numerical sampling rate of 50 kHz (= Δf) for the sake of computational feasibility. This means that the sampling period is 0.02 ms, which is half the base length of the pulses shown in Fig. 7.3. (It is for this reason, and not because of the "diamond theory" of Section 6, that the pulses in Fig. 7.3 appear to have perfectly triangular shapes.)

The parameter $y_\sigma^{(T)}$ that appears in Eq. (7.6) deserves some elaboration. It will be recalled from the discussion following Eq. (5.106) that $y_\sigma^{(T)}$ refers to "the sample standard deviation, i.e., the root mean square average of the flutter process $y(t)$ during the specific interval $|t| \le T/2$ after subtracting the mean value over that same interval". That discussion also pointed out that $y_\sigma^{(\infty)} = y_{rms}$. Thus, although Fig. 7.3 specifically assumes cy_{rms} = 0.5 cm/s, this does not necessarily imply that $cy_\sigma^{(T)}$ = 0.5 cm/s. In fact, for the duration T = 505.62 ms it turns out that $cy_\sigma^{(T)} \approx$ 0.554 cm/s, which is higher than cy_{rms} by a factor of 1.1086. The reason is that the duration T = 505.62 ms is enough to encompass slightly more than one full sawtooth of Fig. 7.2, with the result that it includes a few extra samples of the $y(t)$ curve near its peaks. Thus, as viewed through the sonar transmission's "window", the value of $y(t)$ is not exactly uniformly distributed; it has an increased likelihood of being near its minima and maxima. This makes $y_\sigma^{(T)}$ slightly larger than y_{rms} and, therefore, makes $cy_\sigma^{(T)}$ slightly larger than cy_{rms}.

When the flutter strength is increased from cy_{rms} = 0.5 cm/s to the larger value cy_{rms} = 2 cm/s, while keeping the duration of the sonar transmission at T = 505.62 ms, the effect of flutter becomes more visible, as shown in Fig. 7.4.

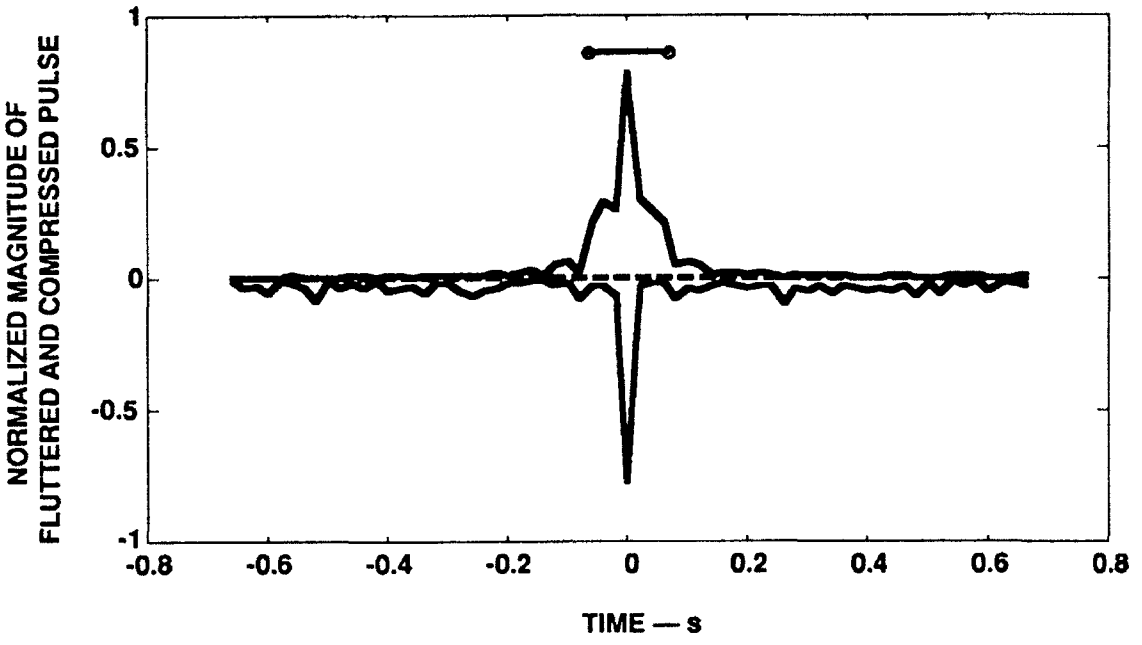

FIGURE 7.4
FLUTTERED AND COMPRESSED PULSE FOR cy_{rms} = 2 cm/s, FOR 505.62 ms TRANSMISSION, 50 kHz BANDWIDTH LINEAR FM (UPPER) AND RANDOM HOPCODE (LOWER)

For the stepped-linear FM case the fluttered and compressed pulse has been elongated to about four times its unfluttered duration. The predicted duration from the formula of Eq. (7.6), as indicated by the "dumbell" symbol, agrees with the visible duration. (With cy_{rms} = 2 cm/s, the value of $cy_{\sigma}^{(T)}$ is still larger by the factor 1.1086, i.e., $cy_{\sigma}^{(T)}$ = 2.217 cm/s.) Since the pulse compression filter uses a normalized CAFS waveform as its replica, the pulse energy has to be preserved; this means that the root mean square amplitude has to drop to about one-half of its original (unit) value. The plot is roughly consistent with this prediction.

For the random hopcode the effect is different. There is a central pulse (upside down in the plot) whose duration is still the same as for the unfluttered case, but its amplitude has been reduced to a level that is roughly comparable

to that of the upper plot (i.e., of the stepped-linear FM case). This means that energy of the central pulse must have diminished.

Figure 7.5 shows the result of increasing the flutter strength to cy_{rms} = 5 cm/s (for which $cy_{\sigma}^{(T)}$ = 5.543 cm/s):

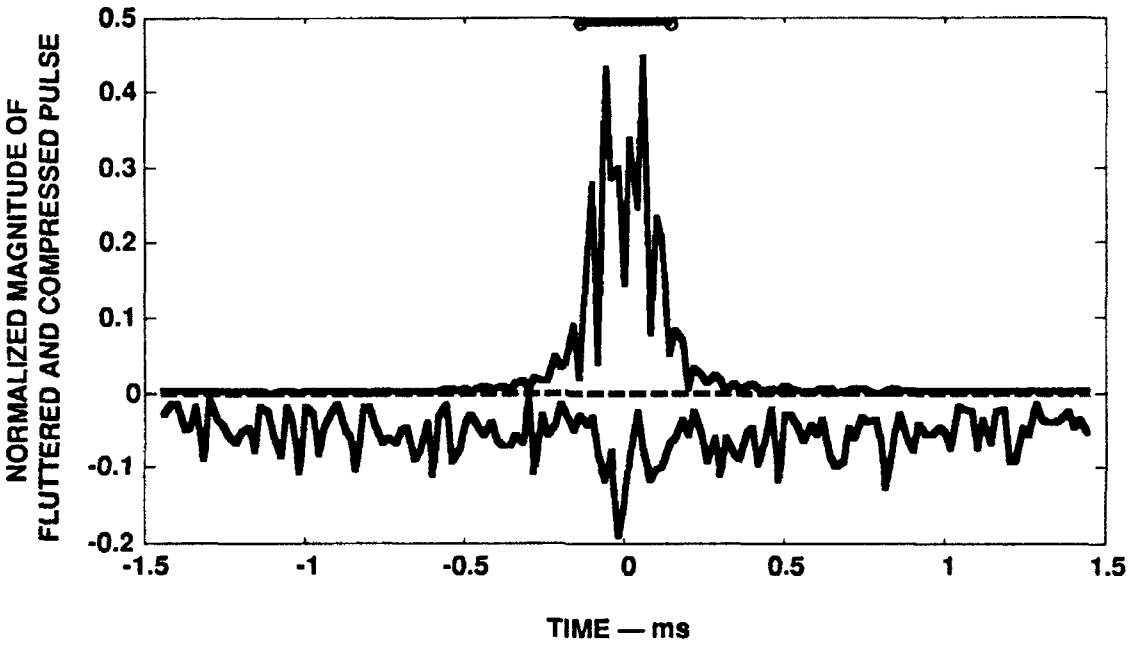

FIGURE 7.5
FLUTTERED AND COMPRESSED PULSE FOR cy_{rms} = 5 cm/s, FOR 505.62 ms TRANSMISSION, 50 kHz BANDWIDTH LINEAR FM (UPPER) AND RANDOM HOPCODE (LOWER)

The pulse duration formula (as depicted by the "dumbell") continues to give the correct answer for the FM pulse. Furthermore, the pulse energy is confined to the central zone as the theory of Section 5 predicted. The pulse is elongated by a factor of about 9.6 relative to its unfluttered length, implying (by energy conservation) that the average amplitude must be divided by $\sqrt{9.6}$, which gives the value $1/\sqrt{9.6}$ = 0.323. This is in visible agreement with the plot.

For the case of the random hopcode, the central pulse (shown upside down) retains its short duration, but loses so much energy that it almost disappears in the "self-noise" that is caused by energy leakage into the central diamond. (It will be recalled from Section 6.8 that the energy in the random hopcode case is distributed in a diamond pattern whose span is twice the chip duration, i.e., 2 X 3.18 ms = 6.36 ms. If the plotting boundaries of Fig. 7.5 permitted the entire 6.28 ms span of the central diamond to be seen, the triangular pattern of "self-noise" energy would be visible.

Figure 7.6 shows the effect of increasing the flutter strength to 20 cm/s (for which $cy_{\sigma}^{(T)}$ = 22.17 cm/s). The FM pulse duration formula still works and the central diamond pattern of the random hopcode pulse is now clearly evident.

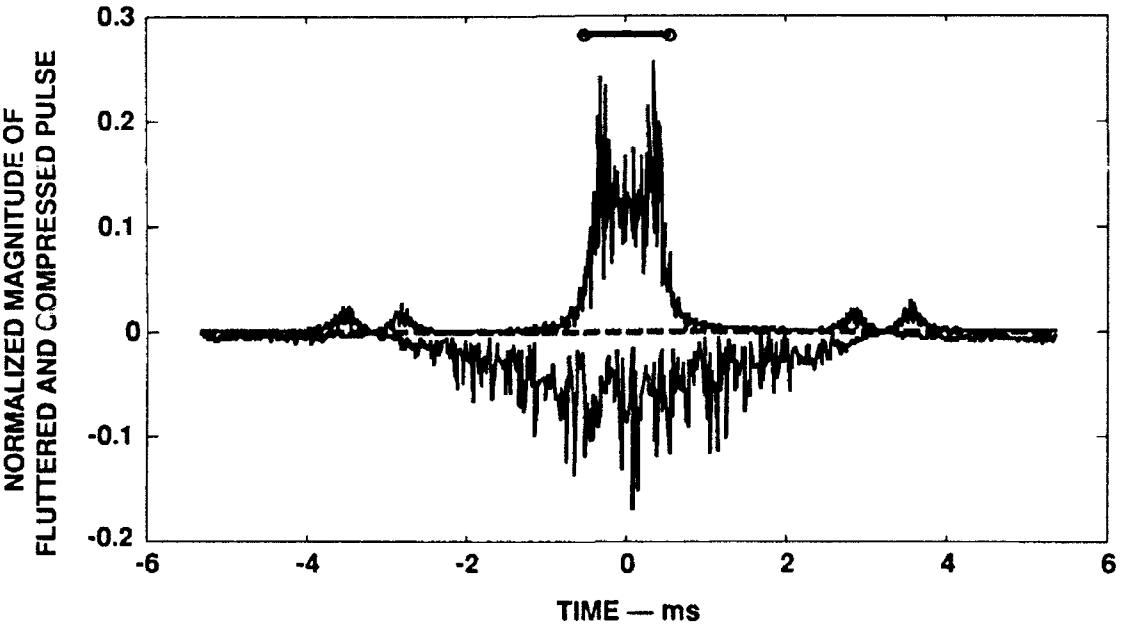

FIGURE 7.6
FLUTTERED AND COMPRESSED PULSE FOR cy_{rms} = 20 cm/s, FOR 505.62 ms TRANSMISSION, 50 kHz BANDWIDTH LINEAR FM (UPPER) AND RANDOM HOPCODE (LOWER)

Figures 7.4, 7.5, and 7.6 confirm much of the theory developed in Sections 5 and 6 for predicting the pulse distortion due to flutter. However, the

plots have also revealed an aspect of behavior not obvious from the formulas: A central pulse often persists, with the original unfluttered duration but weakened in amplitude, until it is obscured by the energy that has leaked to the surrounding interval. Actually this behavior is consistent with the narrowband versus wideband modulation theory that was discussed in the pure tone spectral spreading discussion of Section 3.1.6. It will be recalled from that discussion that very weak flutter merely adds a pair of sidebands to a pure tone transmission, and only reduces the pure tone's amplitude to the extent needed to supply energy to the sidebands. The central tone remains until the flutter becomes strong enough to produce one or more cycles of phase shift. It is only after this strength of flutter is reached that one can express the fluttered spectrum in terms of the probability distribution of the normalized frequency deviation $y(t)$ (such as was done in Eq. (3.31), for example, which was actually an application of Woodward's Theorem; see Blachman and McAlpine, 1969).

However, our computer simulation example uses a stepped-linear FM waveform or a random hopcode waveform, not a pure tone. Nevertheless, Section 5 has established that for a linear FM wave burst the shape of the fluttered and compressed pulse, as viewed in the time domain, matches the shape of the *spectrum* of the flutter-induced phase deviation process. Furthermore, that phase deviation spectrum is not much different from what it would be for a pure tone transmission (assuming the FM wave burst has modest bandwidth). Thus, the fluttered and compressed pulse should display a central "carrier" pulse plus "sidebands" until the flutter-induced phase deviation exceeds one full cycle (2π radians). For the random hopcode the situation is similar, except that the flutter process is effectively time scrambled (see discussion at the end of Section 6.5). The time scrambling spreads out the sideband spectra of the phase deviation process, but the "carrier" pulse plus "sidebands" interpretation still applies for the case of weak flutter.

Figure 7.4 best illustrates this behavior. Since it assumes $cy_{rms} = 2$ cm/s, the plot of $\varepsilon(t)$ in Fig. 7.1 has to be scaled by 0.4, whereupon it is seen that $\varepsilon(t)$ swings between approximate limits of -1.2 and $+0.6$ μs. A rough estimate of the flutter-induced phase deviation can be obtained by multiplying $\varepsilon(t)$ by f_0 and 360°, where f_0 is the center frequency (200 kHz for our example). This implies

a phase deviation swinging between approximate limits of –86° and +43°, which is enough to weaken, but not destroy, the central "carrier" pulse. Indeed, Fig. 7.4 clearly shows the central pulse, only slightly attenuated, for both the stepped-linear FM waveform (upper) and random hopcode (lower, upside down).

However, in Fig. 7.5 the flutter strength is cy_{rms} = 5 cm/s, so that the $\varepsilon(t)$ plot of Fig. 7.1 is correct as it stands, swinging between limits of –3 and +1.5 μs, and giving a phase deviation that swings between approximate limits of –216° and +108°. This is almost a full cycle of phase deviation, which is enough to severely attenuate the central pulse. In fact, the bottom plot of Fig. 7.5 shows that the central pulse has been attenuated to less than 20% of its unfluttered amplitude. In the upper plot (for the stepped-FM) a central pulse of comparable size may be present, but the closely packed concentration of sidebands has obscured it. In Fig. 7.6, for which the flutter strength has been further quadrupled (causing the phase deviation to swing between approximate limits of –864° and +432°), the phase deviation is sufficient to be characterized as wideband FM, so that no true central pulse remains.

Finally, it should be noted that the "energy loss" formula of Eq. (6.84) does not apply to our computer simulation example, because the flutter was not strong enough, even at cy_{rms} = 20 cm/s, to spread the chip spectra beyond their band limits. Thus, as Fig. 7.6 shows, the pulse energy remained within the central diamond. It would have required a very large magnitude of flutter to spread the chip bandwidths significantly beyond their limits, and it was not considered appropriate to do so in our example. If the center frequency chosen for our example had been much higher, Eq. (6.84) might have had an effect at lower, and more realistic, levels of flutter.

7.4 EFFECT OF SHORTENING THE PULSE DURATION

With Fig. 7.6 as the starting point, and keeping the flutter strength at cy_{rms} = 20 cm/s, it is interesting to see what happens when the sonar waveform pulse duration is shortened from 505.62 ms to 52.02 ms, while keeping the bandwidth at 50 kHz. This means that the time-bandwidth product is reduced

from 25,281 to 2601. (Note that each of these time-bandwidth products is the perfect square of an odd integer, as required by our formula for the hopcode waveform that is given in Section 6.1 Within that requirement, these values are the closest approximations to a 10:1 geometric progression.) Figure 7.7 shows the fluttered and compressed pulse magnitudes for this shorter duration.

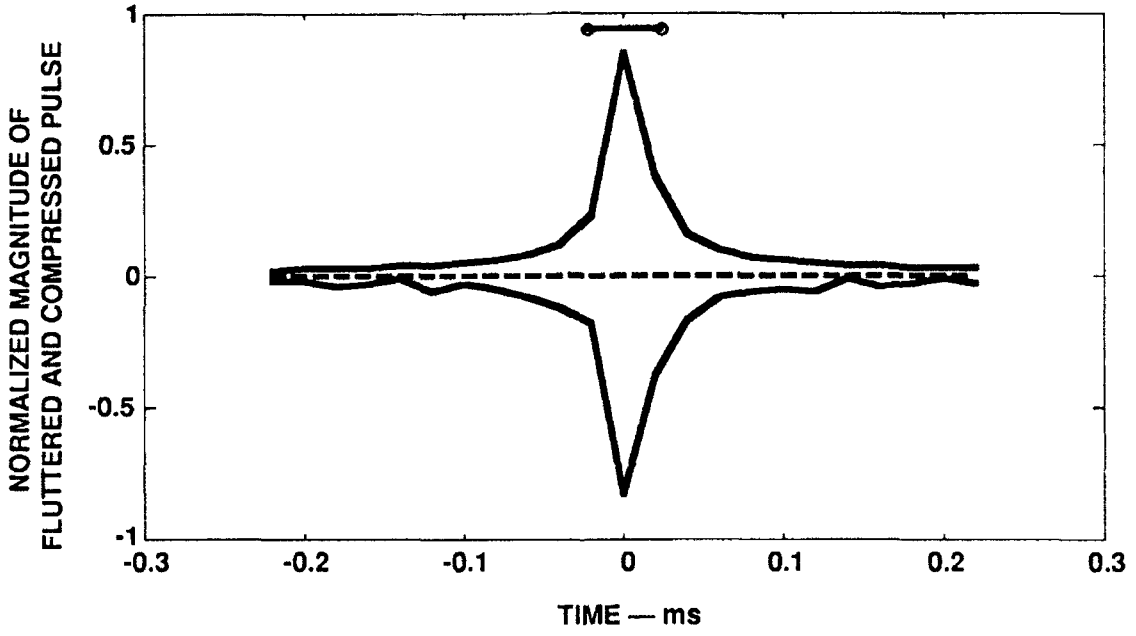

FIGURE 7.7
FLUTTERED AND COMPRESSED PULSE FOR cy_{rms} = 20 cm/s, FOR 52.02 ms TRANSMISSION, 50 kHz BANDWIDTH LINEAR FM (UPPER) AND RANDOM HOPCODE (LOWER)

As indicated by the dumbbell (for the stepped-linear FM case), the duration formula of Eq. (7.6) continues to give the correct answer. The compressed pulse shows only a 1.5X elongation due to flutter, as compared to the 35X for Fig. 7.6, even though the flutter is the same. This happens because $cy_{\sigma}^{(T)}$ drops to 3.20 cm/s for the 52.02 ms window. This dramatic reduction occurs because, as shown in Fig. 7.1, $\varepsilon(t)$ has a broad plateau at the origin, which is precisely where the sonar waveform is centered. When the duration T

was 5[illegible]2 ms, it encompassed one positive-valued plateau and two negative-valued cusps of $\varepsilon(t)$. However, now that the duration has been reduced to $T = 52.02$ ms it encompasses only the central plateau, where $\varepsilon(t)$ is virtually constant. In fact, when the $y(t)$ plot of Fig. 7.2 is viewed through this 52.02 ms window, the very small values of $y(t)$ that are seen there span only about 16% of the full range of $y(t)$. Thus $cy_{\sigma}^{(T)}$ is only about 16% of cy_{rms}, i.e., it is only 3.20 cm/s.

Figure 7.8 shows what happens when the flutter $\varepsilon(t)$ of Fig. 7.1 is shifted by one-half the flutter period T_{ε}, so that the 52.02 ms duration T of the sonar waveform captures a cusp of $\varepsilon(t)$ instead of a plateau.

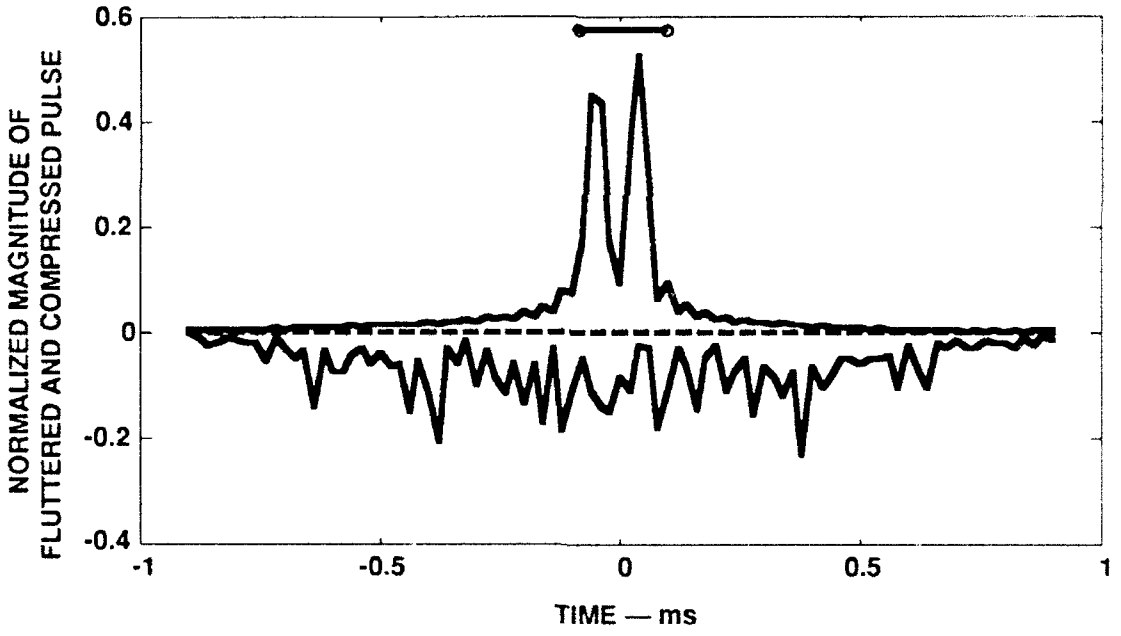

FIGURE 7.8
FLUTTERED AND COMPRESSED PULSE FOR cy_{rms} = 20 cm/s, FOR 52.02 ms TRANSMISSION, 50 kHz BANDWIDTH LINEAR FM (UPPER) AND RANDOM HOPCODE (LOWER) WITH THE FLUTTER SHIFTED TO CAPTURE A CUSP OF $\varepsilon(t)$

Now $cy_{\sigma}^{(T)}$ is 31.9 cm/s which is 160% of cy_{rms}, not 16%. Since the 52.02 ms duration straddles a cusp of $\varepsilon(t)$, it straddles a pair of maxima and minima of $y(t)$, which explains why $cy_{\sigma}^{(T)}$ is so large. It also explains why the (upper) FM pulse of Fig. 7.8 has two distinct peaks: As viewed within the 52.02 ms window, $y(t)$ appears to be bimodally distributed, with peaks in its probability distribution at the maximum and minimum values of $y(t)$. Thus the fluttered and compressed pulse, which mimics the probability distribution of $y(t)$ (using the results of Section 5 for the FM waveform; see Eq. (5.105)), must show the same bimodal behavior.

It is noteworthy that the (dumbbell) duration formula of Eq. (7.6) continues to give the correct result for the (upper) FM wave in Fig. 7.8, even for this seemingly pathological "cusp" case. The fluttered and compressed duration in Fig. 7.8 increases to about 4X what it was in Fig. 7.7, merely because the sonar waveform caught the flutter $\varepsilon(t)$ at an inopportune time, when the equivalent observer velocity $cy(t)$ was undergoing a dramatic sign reversal at a cusp of $\varepsilon(t)$. It is also interesting that no central peak is visible, either in the upper (FM) case or the (lower) random hopcode case. Apparently the bimodal distribution of $y(t)$, which can be characterized as upward Doppler shift followed immediately by downward Doppler shift, kills the central "carrier" pulse rather efficiently.

Figure 7.9 shows what happens when the sonar waveform duration is shortened to 4.5 ms, but the flutter strength is increased to the rather extreme value of cy_{rms} = 100 cm/s. For this figure, $\varepsilon(t)$ is shifted back to its original position, so that a plateau is captured rather than a cusp. The duration formula (dumbbell) still works; however, it should be noted that for this case the flutter does not elongate the pulse significantly. Although the the root mean square flutter strength is cy_{rms} = 100 cm/s over the long term, the windowed value is only $cy_{\sigma}^{(T)}$ = 3.20 cm/s, because of the very short duration and the fact that $\varepsilon(t)$ is caught in a broad plateau.

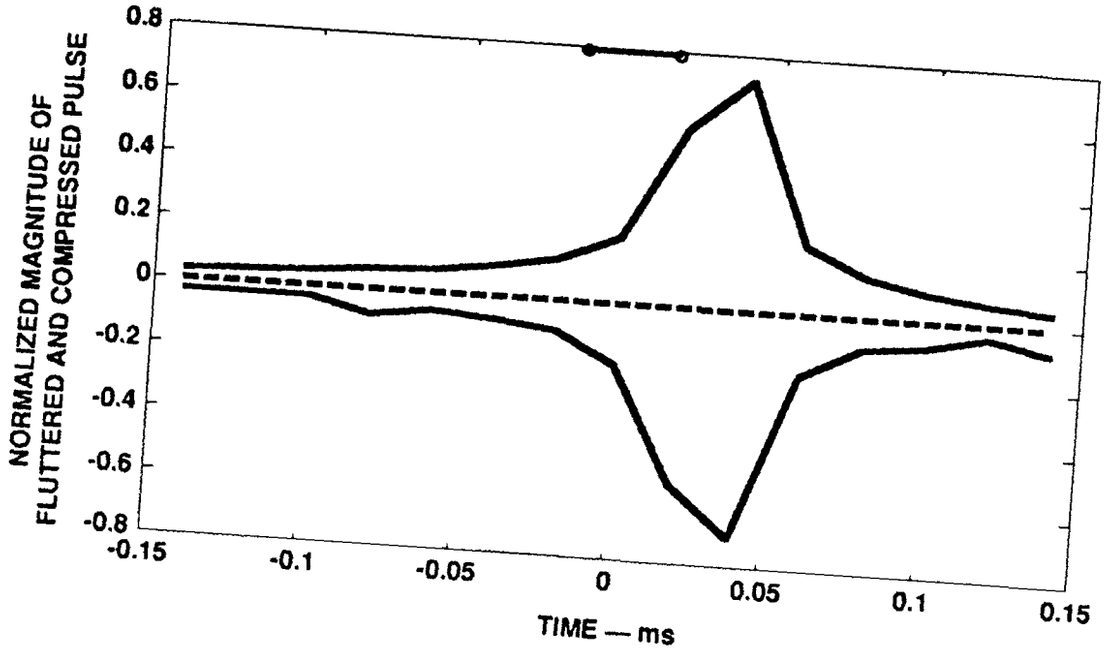

FIGURE 7.9
FLUTTERED AND COMPRESSED PULSE FOR cy_{rms} = 100 cm/s, FOR 4.5 ms TRANSMISSION, 50 kHz BANDWIDTH LINEAR FM (UPPER) AND RANDOM HOPCODE (LOWER)

Notice that the pulse has been delayed by about one-third of a millisecond. The reason is that the very brief sonar waveform samples only the central portion of the $\varepsilon(t)$ plot of Fig. 7.1 (which must be scaled by 20X to account for the fact that cy_{rms} = 100 cm/s instead of 5 cm/s). Thus, the time axis perturbation $\varepsilon(t)$ is approximately equal to 20 X 1.5 μs = 0.035 ms during the 4.5 ms duration of the sonar waveform, which agrees with what is seen in Fig. 7.8.

Figure 7.10 shows what happens when $\varepsilon(t)$ is time shifted so that a cusp, instead of a plateau, is captured by the 4.5 ms duration. In this case the flutter-induced pulse elongation is greater because $cy_{\sigma}^{(T)}$ = 172 cm/s.

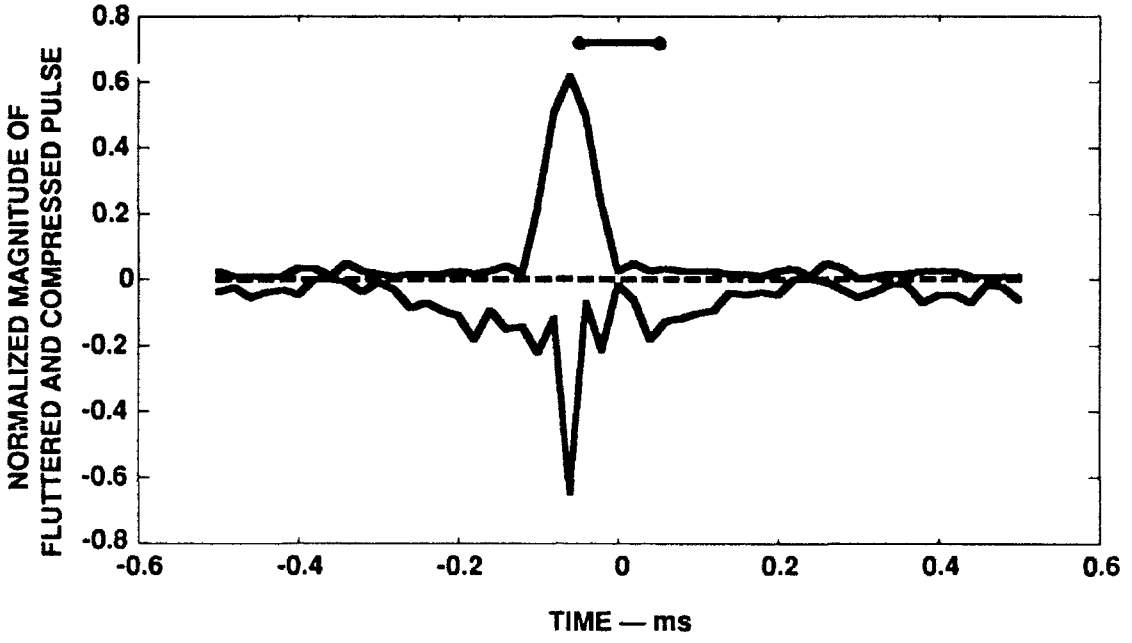

FIGURE 7.10
FLUTTERED AND COMPRESSED PULSE FOR cy_{rms} = 100 cm/s, FOR 4.5 ms TRANSMISSION, 50 kHz BANDWIDTH LINEAR FM (UPPER) AND RANDOM HOPCODE (LOWER) WITH THE FLUTTER SHIFTED TO CAPTURE A CUSP OF $\varepsilon(t)$

Despite the extremely large value of $cy_{\sigma}^{(T)}$, the pulse is only elongated 3.4X due to the flutter, in the FM case. Although $y(t)$ has a bimodal distribution (since a cusp of $\varepsilon(t)$ is captured), the flutter is simply not strong enough to kill the central "carrier" pulse, which appears with approximately the same amplitude in both the FM (upper) and random hopcode (lower) case. In contrast to Fig. 7.9, the peaks are shifted to the *left* because a negative cusp of $\varepsilon(t)$ is captured, rather than a positive plateau.

7.5 SECTION SUMMARY

The computer simulation studies of this section are in confirmation of the theoretical results of Sections 5 and 6. The pulse elongation formula of

Eq. (7.6) for the stepped-linear FM case, which appeared originally as Eq. (5.108) for the continuous linear FM wave burst, has been shown to be an accurate predictor in a variety of circumstances, with no failures having been discovered. In particular, the incorporation of $y_{\sigma}^{(T)}$ (first introduced in Eqs. (5.105) and (5.106)) into the formula in place of y_{rms} was shown to be not only valid, but essential. The studies also clarify the behavior of the central, narrow pulse in the case of weak flutter, for which the theory had been rather sketchy.

The computer simulation also helps to answer the question of whether a random hopcode can ever perform better than an FM wave burst in the presence of flutter. The answer, it appears, is a qualified "no". To the casual observer, Fig. 7.4 might suggest otherwise, since the compressed pulse of the random hopcode (the lower plot, upside down) gives a pulse that is uncontaminated by nearby sidelobes. In fact, the random hopcode might possibly be better for distinguishing a weak target at almost the same range as a strong target, and it might permit more precise estimates of target range. However, assuming that detection of targets in noise is the prime consideration, the concentration of sidelobe energy around the main pulse (in the FM case) can only help, not hinder, the receiver detection performance.

8. FINAL RESULTS AND CONCLUSIONS

Due to the mathematical complexity of this report, it seems wise to restate the principal results in a more streamlined way, even at the risk of being repetitious. The summary presented below does contain some new mathematical developments, but the general intent is to provide a "short story" version of the report. For more details the reader is referred to the main body of the report. In some instances, such as in Sections 8.3 and 8.6-8.8, the previous results are brought together in a new way with the benefit of hindsight.

8.1 BASIC CONCEPTS

Flutter is defined as a rapidly fluctuating perturbation in the time axis of the sonar echo, such as might be caused either by propagational instabilities in the medium, by sonar platform vibration or, perhaps, by target motion. This distortion can impair the performance of a high resolution sonar that is designed to do pulse compression filtering in cases where the transmitted pulse waveform has a long duration. For some object detection applications, long duration waveforms may be desirable. (In the context of this report, a high resolution sonar is assumed to operate at a range of 10-1000 m and at a frequency in the range 25-500 kHz.)

As set forth in Sections 1 and 2, *the goal of flutter analysis is to determine how much reduction there will be in the processing gain of the sonar's pulse compression filter*, in typical flutter environments. The processing gain can be calculated by the approximate formula

$$\textbf{Proc. Gain} \;\cong\; 5\log_{10}\left[\frac{T}{T_{pc}}\right], \tag{8.1}$$

where T and T_{pc} denote the effective pulse duration before and after pulse compression (where "pulse" means the sonar echo of an ideal point target, in this context). As discussed in Sections 2.3.4 and 2.7, this formula only measures the insertion gain of the pulse compression filter; furthermore, a

multiplier value of 4 rather than 5 would give a better approximation. (The value 5 was selected to conform with tradition.)

The pre-compression pulse duration, T, is the same as the duration of the transmitted sonar pulse. Time-bandwidth product theory tells us that the post-compression pulse duration, T_{pc}, cannot be smaller that the ideal value $1.5/B_e$, where B_e is the effective bandwidth of the sonar pulse. If the flutter merely elongates the compressed pulse, then it is appropriate to express the performance deficit as a reduction in processing gain, relative to the ideal case.

$$\textbf{Flutter Loss} \cong -\left[5\log_{10}\left(\frac{T}{T_{pc}}\right) - 5\log_{10}\left(\frac{T}{1.5/B_e}\right)\right]$$

$$= 5\log_{10}\left[\frac{T_{pc}}{1.5/B_e}\right]. \qquad (8.2)$$

8.2 HOW TO QUANTIFY FLUTTER

Several ways to quantify flutter have been introduced in Section 3. Flutter is defined mathematically in terms of the perturbation $\varepsilon(t)$ of the time-axis variable or, equivalently, in terms of its derivative $y(t) = \dot{\varepsilon}(t)$. Thus, $\varepsilon(t)$ is expressed in units of time, but $y(t)$ is dimensionless. Non-fluctuating components of $\varepsilon(t)$ are irrelevant, since any component that is constant during the transmit/receive period produces only a trivial time displacement, and any linearly time varying component produces a steady Doppler effect. (Presumably the sonar can compensate for steady Doppler effects, by using a bank of Doppler channels if necessary.) It follows that the flutter will have no significant effect unless $y(t)$ fluctuates. This fluctuation can be characterized in terms of its standard deviation, denoted y_{rms}.

Unfortunately y_{rms} does not adequately predict the corruptive effect of flutter, since it reveals nothing about the rate of fluctuation. For example, if $y(t)$ fluctuates so slowly that it remains essentially constant during the transmitted pulse duration, then there will be no significant spreading of the compressed pulse no matter how large y_{rms} is over the long term. A more useful measure is

$y_\sigma^{(T)}$, the sample standard deviation of $y(t)$ within the duration T of the sonar transmission. (The notation $y_\sigma^{(T)}$ has been introduced in Section 5.11, in the context of analyzing flutter effects upon a linear FM pulse.) The number $y_\sigma^{(T)}$ measures the net amplitude of flutter components that are rapid enough to do significant damage during the transmitted pulse duration T. One would have to measure $y_\sigma^{(T)}$ experimentally for several different values of T in order to make a general assessment of a particular flutter environment.

A more scientific way to assess a particular flutter environment is to do a spectral analysis of the time axis perturbation $\varepsilon(t)$ or its derivative $y(t)$. If the flutter is a stationary random process it can be characterized by a power spectral density $S_\varepsilon(f)$ or, equivalently, $S_y(f) = (2\pi f)^2 S_\varepsilon(f)$. Either spectrum can be measured experimentally. Dependence of the flutter's spectral characteristics upon other parameters, such as temperature gradients, sonar depth, sonar platform speed, or turbulence in the medium, can also be studied.

If the power spectral density $S_y(f)$ is known, one can predict the size of $y_\sigma^{(T)}$ by computing the square root of $E(\tilde{y}^2)$, where $\tilde{y}$ is the result of subtracting the running average from $y(t)$, i.e.,

$$\tilde{y}(t) = y(t) - \frac{1}{T}\int_{t-T/2}^{t+T/2} y(t)\, dt \,. \tag{8.3}$$

This equation implies that the quantity $\tilde{y}(t)$ is produced from $y(t)$ by a linear, time-invariant transformation whose impulse response is $\delta(t) - T^{-1}\Pi(t/T)$. The Fourier transform, $1 - \mathrm{sinc}(Tf)$, is the system transfer function that describes this transformation in the frequency domain. It follows that $y_\sigma^{(T)}$ can be estimated as

$$y_\sigma^{(T)} \overset{\text{est.}}{=} \sqrt{E(\tilde{y}^2)} = \left[\int_{-\infty}^{+\infty} [1 - \mathrm{sinc}(Tf)]^2 S_y(f)\, df\right]^{\frac{1}{2}} , \tag{8.4}$$

which provides a handy formula for computing typical values of $y_\sigma^{(T)}$ for arbitrary duration T of the transmitted pulse, in terms of the flutter spectral density $S_y(f)$.

Although the spectra $S_\varepsilon(f)$ and $S_y(f)$, together with the overall amplitude y_{rms} and the more specific amplitude $y_\sigma^{(T)}$, are all very effective measures of the flutter environment, it is often useful to describe the flutter in terms that are more readily visualized. For example, it is helpful to have a graphical depiction of the flutter as a function of time, because it allows one to imagine the dynamic processes that could have caused the flutter. The most easily understood visual representation of flutter would be plot of the time axis perturbation $\varepsilon(t)$. But the amplitude of $\varepsilon(t)$ is not a very good indicator of the potential for sonar impairment, without taking account of the spectral distribution. The variable $y(t)$ would be a better choice in that respect, especially since one can visually ignore oscillations whose periods are much longer than hypothetical durations of sonar transmissions. The value of $y(t)$ also has a tangible meaning: It indicates the percentage deviation in the instantaneous frequency of a pure tone.

However, the dimensionless nature of $y(t)$ makes it too abstract. A compromise is to plot $cy(t)$, where c is the speed of sound. The distinction between $y(t)$ and $cy(t)$ is just matter of scale, but $cy(t)$ has a physical meaning that is easier to visualize. As discussed in Section 3.1.3, $cy(t)$ is the *equivalent observer velocity*, representing a hypothetical motion of the sonar platform (at the time of reception) that could have been responsible for the flutter. Because of this attractive feature, $cy(t)$ has been used frequently in the main body of the report, for computations as well as for illustrating flutter dynamics.

8.3 HOW TO PROBE THE FLUTTER ENVIRONMENT

It might seem that a steady, pure tone transmission could be used as a probe signal to study the spectral characteristics of the flutter environment. Flutter does, in fact, spread the tone's line spectrum into a power spectrum of characteristic shape and width. Unfortunately, according to the results of Section 3.1.6, that spectral shape mimics the shape of the probability density of $y(t)$, not its power spectral density. For example, if the flutter fluctuations exhibit Gaussian statistics, as will likely occur over the long term, then the tone's line

spectrum will be broadened into a Gaussian shape. (This linkage between broadened spectral shape and the probability density of $y(t)$ will apply if the flutter is strong enough to produce phase deviations of substantially more than a radian. Flutter that produces only a small phase distortion does not pose much of a threat to pulse compression filtering.)

Although the shape of the pure tone's broadened spectrum is too predictable to provide much useful information, its width is somewhat revealing. According to Eq. (3.47), the spectral width $B_{\tilde{f}_0}$ obeys the simple law

$$B_{\tilde{f}_0} \cong 2\times\left\{\sqrt{2}, \sqrt{3}, \text{or } \sqrt{\pi}\right\} y_{rms} f_0 , \tag{8.5}$$

where $\sqrt{2}, \sqrt{3}, \text{or} \sqrt{\pi}$ is selected depending upon whether the flutter is sinusoidal, uniformly distributed, or Gaussian. The parameter f_0 is the center frequency of the transmitted pure tone. Thus, the value of y_{rms} can be deduced from the pure tone's measured spectral width. However, as noted above, the value of y_{rms} is not very useful without additional information as to the spectral characteristics of the flutter.

There is another drawback to using steady tone transmissions to probe the flutter environment. Multipath effects are likely to cause wave interference, thereby putting kinks into the flutter-broadened spectrum. Indeed, it is to be expected that multipath will have a devastating effect when steady tone transmission experiments are performed in any environment that resembles the typical operating scenario of a high resolution sonar.

The story is different for pure tone *bursts*, however. If a tone burst is brief enough, multipath effects can be gated out. The received tone burst is then

$$x(t) = A\ \Pi\left(\frac{t+\varepsilon(t)}{T}\right) e^{j2\pi f_0[t+\varepsilon(t)]}, \tag{8.6}$$

which can be carrier-demodulated and fed into a phase detector to get the instantaneous phase deviation $\phi(t)=2\pi f_0\varepsilon(t)$, from which $\varepsilon(t)$ may be computed directly, while the tone burst lasts. However, in order to get an accurate representation of $\varepsilon(t)$ the signal must strongly dominate the noise, to a

much greater extent than is required for normal sonar applications. There are a number of ways to achieve high signal-to-noise ratios in a controlled experiment. The best way is to use a one-way transmission path, by putting either a transmitter or a receiver at the target location. The flutter amplitude will then be cut in half, but that is easy enough to compensate for in the analysis.

It will usually be necessary to limit the duration of the experimental tone burst to no more than one or two milliseconds to avoid multipath interference, and then to allow many hundreds of milliseconds to elapse before transmitting another tone burst of the same frequency. At best, such a procedure provides a series of extremely brief glimpses of the flutter process. This is not adequate to determine $S_\varepsilon(f)$ over the most relevant ranges of flutter frequency. This limitation can be overcome by using a very rapid sequence of pure tone bursts of many different frequencies, almost contiguous in time, but with sufficiently large guard bands between the frequencies that they can be easily separated by spectral filters at the receiver (or by a computer if the received signals are recorded for laboratory analysis). With this frequency hopping method, it should be possible to track the flutter-induced phase variations almost continuously, without danger of multipath interference.

It is also be possible to use long duration FM sweeps as flutter probing signals. In this case pulse compression filtering (i.e., replica correlation) can be used to isolate the desired signal from spurious contributions due to multipath. One can then take the Fourier transform of the compressed wave $\tilde{p}(t)$, after masking it with a suitable window to exclude the effects of multipath, and compare the result to the similarly windowed Fourier transform of the ideal, unfluttered, compressed waveform $p(t)$. The computed phase difference then represents the phase deviation induced by the flutter, as a function of frequency. This frequency dependence can then be converted to a time dependence, using the original FM sweep's defining formula (which expresses its instantaneous frequency as a linear function of time). Thus, one can compute the instantaneous phase deviation $\phi(t)$ due to flutter, as it evolves over the entire duration of the FM sweep. It is then a simple matter to solve for $\varepsilon(t)$ in the quadratic formula

$$\phi(t) \;=\; 2\pi\left[f_0 + \frac{t}{T}\Delta f + \frac{\varepsilon(t)}{2T}\Delta f\right]\varepsilon(t)\,. \tag{8.7}$$

(See Eq. (5.9)). A phase-unwrapping algorithm must first be applied to $\phi(t)$, but that should pose no problem if the signal level strongly dominates the noise, which it will in a controlled experiment using a one-way transmission path. This FM sweep method is roughly equivalent to the aforementioned frequency hopping method if the frequency hops are done in a linear sequence. However, the FM sweep method is probably more efficient.

Assuming that a long duration FM sweep has been transmitted, one might suppose that the flutter spectrum could be estimated directly from the envelope of the fluttered and compressed pulse $\tilde{p}(t)$, since, according to the results of Section 5.8,

$$\left|\tilde{p}(t)\right|^2 \;\cong\; \left| \underset{\tau\to f}{\mathcal{F.T.}}\left\{ \Pi\left[\frac{\tau}{T}\right] e^{j\phi(\tau)} \right\} \right|^2_{f\to -\Delta f\frac{t}{T}}\,, \tag{8.8}$$

where T and Δf denote the duration and sweep width of the original FM sweep. This seems to provide a tailor-made picture of the flutter spectrum, through a simple linear transformation of the independent variable (see Sections 5.8-5.9 for details). However, since the effect of $\varepsilon(t)$ is felt in the exponent $\phi(t)$, this method will not yield an estimate of $S_\varepsilon(f)$ or $S_y(f)$. In fact, according to the results of Section 5.9, $\left|\tilde{p}(t)\right|^2$ will merely take the shape of the probability density of $y(t)$, as sampled within the duration of the FM sweep. This might be of use in determining the value of the parameter $y_\sigma^{(T)}$, but it is not as illuminating as direct spectral analysis of $\varepsilon(t)$.

Based upon the foregoing discussion, there are nine steps to successful experimental evaluation of a given flutter environment, all of which are important:

(1) Ensure that the signal-to-noise ratio is very high, by using a one-way transmission path. (Put a receiver or transmitter at the target position.)

(2) Transmit continually (if not continuously) in order to sample the relevant flutter frequencies without aliasing.

(3) Use frequency diversity to avoid multipath interference. Use either a long duration FM sweep or a rapid-fire sequence of frequency-hopped tone bursts having discrete, well spaced frequencies. In both cases the instantaneous frequency of the transmitted signal serves as an identity tag to indicate exact time of transmission.

(4) Use a carefully designed test geometry, combined with linear signal processing at the receiver, to eliminate multipath interference. For the FM sweep transmission use a pulse compression filter (i.e., a replica correlator) to shift the multipath effects away from the pulse center. For the frequency hopping method use a bank of spectral filters to isolate the tone bursts, thereby eliminating multipath interference.

(5) Determine the flutter-induced phase shift at each frequency. For the FM case, compute a centrally windowed Fourier transform of the pulse-compressed signal, and then compute its phase for each frequency. For the frequency-hopped case, simply detect the phases at the outputs of the filter bank.

(6) Express the flutter-induced phase shift as a function time, $\phi(t)$, by using the time/frequency tagging formula of the original transmission. (In the FM case, a simple linear formula relates time and frequency.)

(7) Apply a phase unwrapping algorithm to $\phi(t)$. Also, subtract any systematic phase deviations that might have been artificially introduced by the measuring system. (These systematic phase deviations can be identified by applying an electronically simulated test signal that represents the ideal, unfluttered version of the received signal.)

(8) Compute $\varepsilon(t)$ from $\phi(t)$. For the FM case, solve Eq. (8.7) for $\varepsilon(t)$. For the frequency-hopped case, $\varepsilon(t) = \phi(t)/[2\pi f_0(t)]$, where $f_0(t)$ denotes the frequency of the tone burst that was arriving at time t.

(9) Compute an estimate of the flutter power spectral density $S_\varepsilon(f)$, or $S_y(f)$.

In any such study it would be crucial to measure and record sonar platform motions (including vibration) very carefully, as well as target motions, where applicable. Obviously, one should also measure and record as many relevant environmental and oceanographic parameters as possible, in order to develop models for prediction of flutter effects in real sonar environments.

8.4 PRIOR STUDIES OF FLUTTER IN THE PROPAGATION MEDIUM

To our knowledge, neither the FM sweep method nor the frequency hopping method have ever been used in an experiment to assess flutter in a high resolution sonar environment. Although acoustic telemetry experiments have been performed with frequency-hopped transmissions, no published works were encountered that permitted a scientific assessment of flutter caused by propagational fluctuations, at the typical ranges of high resolution sonar.

The single frequency tone burst method has been used in many experiments, to assess fluctuations encountered in ocean sound propagation. Although amplitude fluctuations have received more attention, phase fluctuations (due to flutter) have been studied in many of these experiments. However, due to the large intervals between successive tone bursts (to avoid contamination by multipath and other problems), none of these experiments has achieved a sampling rate high enough to assess the flutter environment properly for high resolution sonar applications, without upward extrapolation to flutter frequencies of relevance to pulse compression.

As noted in the review of prior experimental studies given in Section 4, Ewart *et al.* used tone bursts separated by 15.7 s, Christoff *et al.* used a 1.0 s separation, Bartels used a 1 min separation (in a lake environment), and

Kennedy used a 6 min separation between tone bursts. The study of Farmer *et al.* used a binary phase encoded sequence that permitted a somewhat longer tone burst duration (25.4 ms) to be used, while still guarding against multipath effects (see Section 4.3 for the details). The transmissions were repeated five times per second, giving the shortest period (200 ms) between bursts of any of the reported studies. Even at that highest rate, the sampling rate is inadequate for our purposes.

The study of Gough and Hayes used a linear FM transmission of 0.8 s duration, repeated continuously, giving an effective period between measurements of 0.8 s. At first glance, their probing technique might seem to be equivalent to the FM probing method described above in Section 8.3. However, the study of Gough and Hayes was unique among those reported in the respect that a passive sonar target was used, with a two-way (echo-ranging) propagation path. As a result, the noise effects (especially bottom reverberation) were rather substantial. The signal certainly did not dominate the noise to the extent desired for use of the Fourier transform technique of Section 8.3.

In all of these studies the investigators apparently assumed that the phase varied so slowly that relatively long gaps could be tolerated between the phase measurements. This is unfortunate. In assessing the effect of flutter on a large time-bandwidth sonar pulse of 1 s duration (for example) it would be desirable to know $S_\varepsilon(f)$ or $S_y(f)$ up to flutter frequencies of at least 100 Hz. In the reported studies, however, the low sampling rates caused the contributions of relevant flutter frequencies to be aliased. When the phase was sampled only once every 20 s. for example, all flutter frequencies higher than 0.025 Hz were aliased.

Admittedly, in some of the studies (that of Bartels in particular) the flutter varied so slowly that flutter contributions at frequencies higher than 0.1 Hz were inconsequential; i.e., they produced too small a phase deviation to have any effect upon pulse compression filtering. Nevertheless, it would be desirable to know the shape and rolloff characteristics of $S_\varepsilon(f)$ in order to project the results to more severe phase deviations that might be encountered at higher sonar

operating frequencies or longer ranges.

Wherever it was possible to extract and digitize phase data from a published paper or report of the studies reported in Section 4, an estimate of $S_\varepsilon(f)$ was made and plotted by the present author. (Since Ewart had already plotted an estimate of $S_\varepsilon(f)$, with different notation and units, his results merely needed to be digitized and replotted with different scales.) None of these computed spectra provided values of $S_\varepsilon(f)$ at flutter frequencies higher than a few hundred millihertz, and most were limited to much lower frequencies. Nevertheless, a simple formula for $S_\varepsilon(f)$ was developed, representing a rough consensus of the reported studies with extrapolation to the higher frequencies of interest. Its inverse-cubic frequency dependence was originally derived as an approximation to Ewart's data. The formula, first expressed in Eq. (4.5), is repeated here for convenience.

$$S_\varepsilon(f) \equiv \left(\frac{2 \times R_{son}}{17.2\ km}\right) |f|^{-3} \times 10^{-13} , \qquad (8.9)$$

where R_{son} represents the sonar range, measured in kilometers. (NOTE: Remember that the variable f represents flutter frequency, not transmitted frequency.)

This formula has a number of shortcomings. It is a crude approximation that fails to take environmental factors into account (it ignores water depth, turbulent mixing rates, density inhomogeneities, etc.). It is based upon a rather simplistic upward extrapolation to the higher flutter frequencies, using measurements made at a much lower sampling rate. It fails to diminish rapidly enough at high frequencies (Section 3.1.4 says $S_\varepsilon(f)$ has to decay faster than f^{-3} as $f \to \infty$), and it blows up too fast at the origin (Section 3.3 says it must not grow as fast as f^{-3} as $f \to 0$). Range dependence was artificially appended, based upon a heuristic argument that was known to have limitations.

Despite these faults, it is about as good as one can do with the published experimental data. We hope that it is correct within a couple of orders of magnitude, over the most relevant range of flutter frequencies (0.01 Hz to

100 Hz). The formula can be multiplied by $(2\pi f)^2$ to give

$$S_y(f) \cong \left(\frac{10^{-12}\,R_{son}}{6.84\ km}\right)|f|^{-1}, \tag{8.10}$$

which, when substituted into Eq. (8.4), provides a formula for estimating the value of $y_\sigma^{(T)}$,

$$y_\sigma^{(T)} \overset{est.}{\cong} \sqrt{E(\tilde{y}^2)} \cong \left[\left(\frac{10^{-12}\,R_{son}}{6.84\ km}\right)\int_{-\infty}^{+\infty}[1-\mathrm{sinc}(Tf)]^2|f|^{-1}\,df\right]^{\frac{1}{2}}. \tag{8.11}$$

The integral fails to converge at the limits $\pm\infty$, because of the too-slow decay of our spectral approximation at high flutter frequencies. In practice, there must exist some frequency f_{max} above which $S_\varepsilon(f)$ decays faster than f^{-3}, and, equivalently, $S_y(f)$ decays faster than f^{-1}. The limits of integration in Eq. (8.11) can then be collapsed to $\pm f_{max}$, as an approximation. When this is done, and the variable of integration is changed to $x = Tf_{max}$, the result is

$$y_\sigma^{(T)} \overset{est.}{\cong} \left[\left(\frac{10^{-12}\,R_{son}}{6.84\ km}\right)\int_{-Tf_{max}}^{+Tf_{max}}\frac{[1-\mathrm{sinc}(x)]^2}{|x|}\,dx\right]^{\frac{1}{2}}. \tag{8.12}$$

Using numerical integration, one can easily verify that the integral goes rapidly to zero as Tf_{max} drops below 0.61, and for $Tf_{max} > 0.61$ it is well approximated by the simple algebraic formula $[1 + 4.65\log_{10}(Tf_{max})]$, which goes to zero at $Tf_{max} = 0.61$, i.e., at $T = 0.61/f_{max}$. Thus,

$$y_\sigma^{(T)} \overset{est.}{\cong} \sqrt{1 + 4.65\log_{10}(Tf_{max})}\sqrt{\frac{R_{son}}{6.84\ km}}\times 10^{-6} \tag{8.13}$$

except when the term under the first radical is negative, in which case $y_\sigma^{(T)} \cong 0$.

This says that the relevant flutter amplitude $y_\sigma^{(T)}$ is essentially zero for a transmitted pulse of such short duration that none of the significant flutter

oscillations can complete 61% of a full cycle. This seems quite reasonable. Moreover, Eq. (8.13) implies that the effective flutter amplitude is proportional to $\sqrt{\log_{10} T}$ for pulses of substantially larger duration. A weakness of the formula is its dependence upon the somewhat mysterious quantity f_{max} (i.e., the highest strong flutter frequency), whose value can only be guessed at. Luckily the formula is rather insensitive to f_{max}. For example, assuming a desired sonar pulse duration of 1 s, the leading radical in Eq. (8.13) increases only by a factor of 3.87 as f_{max} varies from 1 Hz to 1000 Hz.

Beyond providing a generic formula for $S_\varepsilon(f)$, and the resultant formula for $y_\sigma^{(T)}$ that was just derived, the review of experimental studies (of Section 4) has provided some other interesting results of a general nature. For one thing, propagational instabilities in the ocean medium never seem to produce a time axis perturbation $\varepsilon(t)$ that exceeds a few milliseconds (except for gross, long range, long term effects due to movement of refracted paths). Furthermore, the equivalent observer velocity, $cy(t)$, rarely exceeds a few millimeters per second. The amplitude of $cy(t)$ becomes even smaller when one ignores the very low frequency components that are unlikely to affect performance of high resolution sonars. It is also noteworthy that the flutter spectrum, $S_\varepsilon(f)$, never seems to show a very complex structure (although Ewart was able to discern tidal effects). This means that simple ν^{th}-power approximations should be adequate for the more extensive studies that might done in the future, assuming that one or more breakpoints are put into the approximation. (No breakpoint was used in the crude formula of Eq. (8.9), however, unless one regards f_{max} as a breakpoint.)

It should be mentioned that the referenced experimental studies never mentioned the word "flutter". Instead, they addressed phase and amplitude fluctuation of transmitted signals. We ignored their amplitude fluctuation data and divided their published phase fluctuation data by $2\pi f_0$ to get the time axis perturbation $\varepsilon(t)$, where f_0 denotes the stated frequency of transmission. (One of the experimenters, Ewart, had already converted his data to a time deviation $\varepsilon(t)$, but he still referred to it as "phase".)

Finally, it should be acknowledged that there is a large body of

theoretical literature on propagation through inhomogeneous media. It was of little help in assessing flutter induced by propagational instabilities. The theoretical results were just too complex, arcane, assumption-dependent, and inflexible to permit statistical prediction of perturbations in the time axis. It might be said that one good experimental study would be worth a score of theoretical papers, especially as regards high resolution sonar operation at short range. (Others may disagree.)

8.5 FLUTTER DUE TO SONAR PLATFORM MOTIONS

In view of the rather low levels of flutter reported in the experimental studies, it appears likely that motions of the sonar platform will cause more flutter than propagational instabilities in the ocean medium. (This assertion is discussed more fully in Section 4.9.) This is especially true if the platform is a cable-towed or free-swimming body of low inertia. Such a platform may undergo oscillatory motions due to turbulence effects. Even on more massive foundations, elasticity of mountings may contribute to platform vibration at high speeds.

Using plate vibration theory, it has been argued in Section 3.2.3 that any contributions to $S_\varepsilon(f)$ that are due to elastic platform vibration will roll off approximately as f^{-7} at high flutter frequencies. However, it has also been argued that rigid body motions due to "white" turbulent forces will produce components that roll off as f^{-4}. One thus concludes that contributions to $S_\varepsilon(f)$ that are due to sonar platform motion will probably roll off at least as fast as contributions due to propagational instabilities. However, at lower frequencies the platform motional spectra are certain to exhibit irregularities, due to resonance effects.

Unfortunately, no applicable data were available to assess typical platform motional amplitudes or spectra under actual operating conditions. A few measured spectra of sonar platform vibration were discovered, but their frequency range was too high to be applicable. (This is a bit ironic; the studies of propagational instabilities were confined to flutter frequencies that were too *low* to be applicable.) None of the environmental studies reported in Section 4

produced platform motion spectra, since they used fixed-position transducers to avoid any such effects.

8.6 EFFECT OF FLUTTER ON AN FM WAVE BURST: RESULTS

A very extensive theoretical development has been done in Section 5 for the case in which the sonar uses a linear FM wave burst as its transmitted pulse. It turns out that the flutter has a very simple effect. The compressed pulse continues to retain its energy in a closely packed configuration, but becomes more elongated. Not surprisingly, the elongation increases with the flutter amplitude. According to Eqs. (5.105) and (5.130), if the flutter is strong enough to produce wideband phase modulation then the power envelope of the fluttered and compressed pulse is given approximately by

$$|\tilde{p}(t)|^2 \cong \bar{\rho}_y^{(T)}\left(-\frac{\Delta f}{T f_0}\, t\right) \times \left[\frac{(\Delta f)^2}{T f_0}\right] I_\varepsilon(t), \tag{8.14}$$

where Δf, T, and f_0 are the sweep width, duration, and center frequency of the FM wave burst that was transmitted. The window function $I_\varepsilon(t)$ is of little consequence; it takes unit value over the entire domain of the compressed pulse. The probability density function $\rho_y^{(T)}(\cdot)$ merely describes the probability distribution of values of the flutter $y(t)$ that are captured within the duration T of the transmitted wave. (The bar over $\rho_y^{(T)}(\cdot)$ in this approximate formula just indicates that a slightly "smeared" version of $\rho_y^{(T)}(\cdot)$ is to be used; see Eq. (5.72) for the details.)

The shape of the compressed pulse's power envelope thus mimics the probability distribution of the flutter $y(t)$, but only for the limited sample that is seen within the duration of the transmitted wave. If the flutter has Gaussian statistics and T is large, then the power envelope of the compressed pulse will have a Gaussian shape. However, if the transmitted wave is so brief that $y(t)$ can be approximated by a straight line within the interval T, then $\bar{\rho}_y^{(T)}(\cdot)$ will describe a uniform distribution, and the energy of the compressed pulse will be approximately uniformly distributed along the time axis for as long as it lasts. In any case, the energy of the compressed pulse will remain constant, irrespective

of the flutter amplitude (because the integral of Eq. (8.14) is always equal to Δf).

It follows that the duration of the fluttered and compressed pulse is determined by the flutter's sample standard deviation $y_\sigma^{(T)}$. According to Eq. (5.131), the duration of the fluttered and compressed pulse is

$$T_{pc} \cong \left(\frac{1.5}{\Delta f}\right)\left[1 + (Tf_0)\left(\frac{c\, y_\sigma^{(T)}}{650 \text{ m/s}}\right)\right], \tag{8.15}$$

where c denotes the speed of sound. This expression can be substituted for T_{pc} in Eq. (8.1) to get the processing gain of the pulse compression filter,

$$\textbf{Proc. Gain} \cong 5 \log_{10}\left[\frac{(T\Delta f)K_T}{(T\Delta f) + K_T}\right] - 0.88 \text{ dB}, \tag{8.16}$$

where the definition of K_T is given in Eqs. (5.134) - (5.135), restated here for convenience,

$$K_T = \left(\frac{\Delta f}{f_0}\right) \times \left[\frac{650 \text{ m/s}}{c\, y_\sigma^{(T)}}\right]. \tag{8.17}$$

The parameter K_T is a very important measure of the flutter's effect. If the time-bandwidth product $T\Delta f$ is much smaller than, or much larger than, the critical value K_T, then the processing gain formula of Eq. (8.16) simplifies to

$$\textbf{Proc. Gain} \cong \begin{cases} g(T\Delta f) & \text{for } T\Delta f << K_T \\ g(K_T) & \text{for } T\Delta f >> K_T \end{cases}, \tag{8.18}$$

where the processing gain function $g(\cdot)$ is defined as

$$g(\alpha) \stackrel{\text{def.}}{=} 5 \log_{10}\alpha - 0.88 \text{ dB}. \tag{8.19}$$

This suggests a simplified version of the approximate gain formula,

$$\textbf{Proc. Gain} \;\cong\; \min\left\{\, g(T\Delta f),\, g(K_T) \,\right\}\,,$$

$$= \; g\left(\min\left\{\, T\Delta f,\, K_T \,\right\}\right). \qquad (8.20)$$

[NOTE: This processing gain formula will always give a slightly larger result than Eq. (8.16). However, the discrepancy between the two formulas will never exceed 1.5 dB, and will only get that large when $T\Delta f \cong K_T$. These assertions can be proven by use of the algebraic identity

$$\log(\min\{a,b\}) - \log(2) \;\le\; \log\left[ab/(a+b)\right] \;\le\; \log(\min\{a,b\}), \qquad (8.21)$$

which holds for all positive a and b, and for any base of logarithms.]

The simplified formula of Eq. (8.20) shows that K_T acts as a ceiling on usable time-bandwidth product, insofar as the processing gain of the pulse compression filter is concerned. As a result, there is also a ceiling on the processing gain itself. That ceiling is $g(K_T)$. To illustrate, let us predict the ceilings for a sonar whose "Q" is 10 (i.e., $f_0/\Delta f = 10$), in four flutter environments where the flutter has equivalent observer velocities given by $c\,y_\sigma^{(T)} = 0.01$, 0.1, 1, and 10 cm/s. For these four cases, Eq. (8.17) gives the usable time-bandwidth product ceilings as $K_T = 6.5 \times 10^5$, 6.5×10^4, 6500, and 650. The corresponding gain ceilings are $g(K_T) = 28.2$, 23.2, 18.2, and 13.2 dB.

One important use of the processing gain formula of Eq. (8.20) is to determine the effect of increasing the transmitted pulse duration T, in a specific operating environment. The answer is simple: The processing gain increases 5 dB for each decade factor of T, until it reaches the gain ceiling. A slight complication is that the gain ceiling $g(K_T)$ is a moving target, due to the T–dependence of K_T. Regardless, the ceiling is reached when $g(T\Delta f) = g(K_T)$, i.e., when the time-bandwidth product reaches the critical value K_T. Using the definition of K_T given in Eq. (8.17), it follows that the gain ceiling will be reached when the equation

$$T = \left(\frac{1}{f_0}\right) \times \left[\frac{650 \text{ m/s}}{c\, y_\sigma^{(T)}}\right] \tag{8.22}$$

is satisfied. Although T appears on both sides, the equation is very simple to solve by iteration. (A good starting guess is $T = 1$ s.)

The iteration converges quickly because of the very mild dependence of $y_\sigma^{(T)}$ upon T. An example will illustrate: We assume a high resolution sonar operating at a range of $R_{son} = 300$ m, with a center frequency of $f_0 = 200$ kHz. In the absence of any real environmental data, we use the generic formula of Eq. (8.13) to predict the flutter amplitude $y_\sigma^{(T)}$ attributable to propagational instabilities, for which we assume that $f_{max} = 100$ Hz. (Our example fails to take account of platform motion, which has been alleged to be a more serious source of flutter than the propagation medium.) The iteration proceeds as follows: After selecting a starting value of $T = 1$ s, we use Eqs. (8.13) and (8.22) to calculate the next iterated value $T = 3.22$ s, and then repeat the process to get $T = 2.91$ s. Convergence is declared at the next value, $T = 2.93$ s.

In practice, one ought to use $y_\sigma^{(T)}$ data that are appropriate to the actual flutter environment, if such data are available. This might entail the use of the integral formula of Eq. (8.4), if the data are in the form of flutter spectral measurements. As discussed in Section 5.14, the parameter $y_\sigma^{(T)}$ increases with T (maybe not monotonically) until it reaches its long term limit, $y_\sigma^{(\infty)} = y_{rms}$. In moderate flutter environments this limit will likely be approached before T gets large enough to satisfy Eq. (8.22). If so, the processing gain ceiling is just $g(K_\infty)$, where K_∞ is the result of setting $y_\sigma^{(T)} = y_{rms}$ in Eq. (8.17).

The T that satisfies Eq. (8.22) might be termed the *maximum flutter-safe interval*, denoted T_{max}. This parameter makes it possible to describe the effect of flutter in a very concise way: For a pulse compression sonar that transmits an FM wave of duration $T < T_{max}$, flutter will have little or no effect upon pulse compression. Contrarily, if $T > T_{max}$ then the processing gain of the pulse compression filter will already have hit the gain ceiling, and will be limited to what it would have been for $T = T_{max}$. Note that T_{max} depends only upon the

flutter environment and sonar center frequency, not upon the sonar's transmitted bandwidth, or any other sonar parameters. In the example just described the maximum flutter-safe interval was T_{max} = 2.93 s. With a transmitted bandwidth of Δf = 50 kHz, for instance, the processing gain ceiling would have been $g(K_T) = g(T_{max}\Delta f) = 23.8$ dB.

[NOTE: Using computer simulation with FM wave signals, Bartels (1989) demonstrated that vibration-induced flutter would elongate the compressed pulse, giving it a characteristic shape and a duration that was roughly proportional to the root mean square vibration amplitude. This result inspired the theoretical work done by the present author, leading to the T_{pc} formula of Eq. (8.15) with y_{rms} in place of $y_{\sigma}^{(T)}$. In the process of carrying out more extensive computer simulations of the type presented in Section 7, it was determined that y_{rms} was an inadequate descriptor of flutter. This led to the definition of $y_{\sigma}^{(T)}$, and to the various other results presented in this report.]

8.7 FM WAVE CASE WITH A NON-ADAPTIVE DETECTOR WINDOW

When the sonar uses an FM wave burst as its transmitted waveform, the results of the previous section can be correctly applied *only* if the detector readjusts its integration window to match T_{pc}, the duration of the fluttered and compressed pulse. To accommodate different flutter environments the detector would have to adapt its integration window to match T_{pc}. Indeed, it would have to be equipped with some means for sensing the flutter environment (including platform motion) before adapting to it. This adaptive behavior requires a degree of sophistication that may be hard to achieve in many circumstances. For that reason it is of interest to examine the case where the sonar uses an integration window of fixed duration T_{det}.

Suppose T_{det} is designed with a somewhat elongated pulse duration in mind, based upon a presumed "worst case" flutter scenario, with the corresponding value of processing gain computed by Eq. (8.1) with T_{det} substituted for T_{pc}. If the flutter turns out to be weaker, so that the compressed pulse duration T_{pc} is actually smaller than T_{det}, will the processing gain be degraded? The answer is "no." The detection performance will be just as good

with a shorter pulse. All of its energy will still be captured within the window, so that the probability of detection (and false alarm rate) will be the same as if the pulse duration had been as large as anticipated.

This means that the processing gain of the pulse compression filter, to the extent that it is exploited, is given by the approximate formula

$$\textbf{Exploited Proc. Gain} \cong 5 \log_{10}\left[\frac{T}{T_{det}}\right], \tag{8.23}$$

for $T_{det} > T_{pc}$. Theoretically the pulse compression filter has the larger value of processing gain expressed by Eq. (8.1), but some of it has been sacrificed by the use of too long an integration window. There are two compensations for that sacrifice. (1) The detector window does not have to be adaptive, and (2) the detection performance is stabilized with respect to variations in flutter amplitude, so long as it remains weak enough that $T_{det} > T_{pc}$.

The flutter might turn out to be *stronger* than anticipated, so that the actual compressed pulse duration T_{pc} is larger than T_{det}. Will the processing gain be degraded if that happens? The answer is "yes", because some of the pulse energy will spill outside the detector's integration window. Only a fraction of the pulse's energy will be captured, that fraction being equal to

$$k \overset{\text{def.}}{=} \frac{T_{det}}{T_{pc}} \tag{8.24}$$

when $T_{det} < T_{pc}$. One might therefore suppose that the effect would be to subtract $10 \log_{10}(k^{-1})$ from the processing gain formula of Eq. (8.23). However, the spillover loss is not quite that large because there are some extra opportunities for detection as the integration window slides along the elongated pulse. Indeed, the number of "distinct" opportunities for detection is k^{-1}, so the required probability of detection for each opportunity is only $\left[1 - (1 - Q_d)^k\right]$, where Q_d is the overall probability of detection. Therefore, using the results of Section 2.7, it is a straightforward algebraic exercise to work out the spillover loss in dB. The result is

$$\textbf{Spillover} \;=\; 10\log_{10}\left[\frac{\lambda\left(\left[1-(1-Q_d)^k\right],FAR,B_e,T_{det}\right)}{k\times\lambda\left(Q_d,FAR,B_e,T_{det}\right)}\right], \qquad (8.25)$$

when $T_{det} < T_{pc}$, where $\lambda(\cdot)$ denotes the function defined in Eq. (2.35) and k is as defined in Eq. (8.24).

It is possible to find a simple approximation for this rather complicated formula, in the same manner that was used to attack the somewhat similar formula of Eq. (2.36). The approach is to consider a representative example, and then generalize. The example will be the same one that was used in Section 2.7, with a slight alteration. Thus, it is assumed that the sonar uses a transmitted pulse of effective bandwidth B_e = 60 kHz and duration T = 500 ms, giving a time-bandwidth product of 30,000. The desired false alarm rate is specified as FAR = 0.02/s, and the desired detection probability is Q_d = 0.8. Under ideal circumstances, the pulse compression filter should compress the duration to $1.5/B_e$ = 0.025 ms. Here is the alteration: It has been decided to use a fixed integration window ten times that long, to accommodate a possible elongation due to flutter. Thus, T_{det} = 0.25 ms.

The next step is to compute the spillover loss for a set of imperfectly compressed pulse durations T_{pc} that exceed this value of T_{det}. In particular, we choose to perform the computation for T_{pc} = 0.75, 2.5, 7.5, and 25 ms. Such durations might be expected for cases of increasingly severe flutter amplitude (very severe!). According to Eq. (8.24), the corresponding captured-energy fractions are k = 0.33, 0.1, 0.033, and 0.01. By using the computational routine outlined in Section 2.7 to compute the λ function, one can then compute the spillover loss by Eq. (8.25). The resulting values of spillover loss are, respectively, 3.39, 7.22, 10.87, and 14.84 dB.

These values are well approximated by the simple formula

$$\textbf{Spillover} \;\cong\; 7.2\log_{10}\left(k^{-1}\right) \;=\; 7.2\log_{10}\left[\frac{T_{pc}}{T_{det}}\right], \qquad (8.26)$$

which is somewhat smaller than our original guess of $10\log_{10}(k^{-1})$.

This completes the derivation of an approximate formula for spillover loss. It turns out that the approximation holds fairly well when the sonar parameters are varied over a wide range of realistic values for high resolution sonar applications. (The same assertion was made in defense of Eq. (2.37), which was derived in a similar fashion.) The spillover loss must be subtracted from the *processing gain formula of* Eq. (8.23) when the detector's integration window is too short; i.e.,

$$\textbf{Exploited Proc. Gain} \cong 5\log_{10}\left[\frac{T}{T_{det}}\right] - 7.2\log_{10}\left[\frac{T_{pc}}{T_{det}}\right], \quad (8.27)$$

for $T_{det} < T_{pc}$.

8.8 EFFECT OF FLUTTER ON A HOPCODE BURST: RESULTS

As defined in Eq. (6.3), a hopcode burst is of the form

$$x(t) = \left[\frac{N}{T}\sum_{n=-N'}^{N'} x_n(t)\right] e^{j2\pi f_0 t}, \quad (8.28)$$

consisting of N "chips", packed end to end with continuous phase, with each chip being a tone burst of duration T/N,

$$x_n(t) = \Pi\left(\frac{t-t_n}{T/N}\right) e^{j2\pi f_n t}. \quad (8.29)$$

The following definitions apply:

T = duration of entire hopcode wave burst,
f_0 = center frequency,
N = $2N'-1$ = number of chips (an odd integer),

t_n = nT/N = center point of the nth chip,
f_n = $\Omega(n)\,N/T$ = baseband frequency of the nth chip,
Δf = N^2/T = total band occupancy, and
$\Omega(n)$ = an arbitrary mapping of the integers $\{-N', \cdots -1, 0, 1, \cdots, N'\}$ onto themselves.

The integer mapping $\Omega(n)$ is the "code" of the hopcode waveform, which is normally selected to scramble the order of frequencies. If N is large, then the spectrum of $x(t)$ will be quite flat over a band of frequencies centered at f_0, with bandwidth $B_e \cong \Delta f = N^2/T$, so that the time-bandwidth product is

$$T\Delta f = N^2. \tag{8.30}$$

The trivial code $\Omega(n) = n$ gives a stepwise-linear FM wave burst that is a good approximation to a simple linear FM wave burst. In fact, during preparation of the computer simulation studies for Section 7 it was determined that a stepwise-linear FM wave burst could be substituted for a true linear FM wave without significant error in the results. Thus, for the non-scrambled mapping $\Omega(n) = n$ it may be assumed that all of the previous results for FM waves are applicable to the prediction of flutter effects, including the pulse elongation and processing gain formulas of the previous section.

The results are quite different when $\Omega(n)$ is a random mapping of the integers that scrambles the frequency order. That case must be explained in an entirely different way. It is best to begin by reflecting upon the general nature of the pulse compression filter. All of the signal types considered in this report are constant amplitude, flat spectrum (CAFS) signals; consequently, the pulse compression filter (i.e., replica correlator) can be regarded as a bandpass filter that has a constant gain across its passband. The only thing that makes it different from an ordinary bandpass filter is its phase response. Ideally, its phase response is supposed to cancel out the phases of the various frequency components of the incoming waveform (which is assumed to be a sonar echo from an ideal point target), leaving a sum of in-phase frequency components that add up to form a pulse of duration $1.5/B_e = 1.5T/N^2$. For purposes of our

analysis, this pulse will be called the *narrow pulse*.

However, if there is a severe, random discrepancy in the phase response of the pulse compression filter, such as might be caused by very strong flutter, then the pulse compression filter will actually stretch out the pulse, rather than compress it. The output will look like a random noise burst that spreads over a time interval of width $2T$, but it will have a triangular envelope. (This happens because the output is the convolution of the input and impulse response, both of which are CAFS waveforms of duration T that occupy the same band but with a random phase relationship.) This triangular noise burst will be referred to as the *fat diamond*. Because of its triangular shape, the effective duration is 5/9 of the interval width (see Eq. (2.6), i.e., the effective duration is $1.11T$.

If the flutter is moderate, but not too strong, it will apply random phase factors to the individual chips of the hopcode burst, but without producing enough Doppler effect to shift the frequencies of the chips beyond their natural borders. Under these circumstances, it has been established in Section 6.4 that the output pulse energy will be distributed mainly within a *central diamond* that is spread over a time interval of width $2T/N$. This central diamond is a kind of time-compressed version of the fat diamond described above, with the same kind of triangular shape. Thus, the central diamond has the appearance of a noise burst with a diamond-shaped envelope. Its effective duration is $1.11T/N$, which is 5/9 of $2T/N$.

One can get a pictorial view of these diamond-shaped envelopes by referring to Fig. 6.2. The central diamond is the one in the middle, labeled $D_0(t)$. The fat diamond is the full aggregation of all of the diamonds shown in the figure. (The "other" diamonds, labeled $D_n(t)$, are of interest only in the theoretical development of Section 6.) The central pulse is not shown in the figure.

As the flutter amplitude increases from negligible to moderate to very strong, the fluttered and compressed pulse undergoes a metamorphosis, changing from a narrow pulse of duration $1.5T/N^2$, to a central diamond of width $2T/N$, to a fat diamond of width $2T$. This change is gradual, but it is not

achieved by time-stretching as one might expect. Instead, energy is mysteriously transferred from one structure to the next. Here is the way it works: In the absence of flutter, the narrow pulse stands alone. As flutter is introduced, the narrow pulse diminishes in amplitude without getting any wider. The missing energy reappears in the central diamond, which begins to look like a carpet of sprouting grass that grows in amplitude as the narrow pulse relinquishes its energy. Eventually, the narrow pulse shrinks to invisibility. Then, as the flutter is increased further, the central diamond starts to lose its energy to the fat diamond, by a similar process.

Section 6.7 addresses the loss of energy from the central diamond to the fat diamond, as a function of the flutter amplitude. However, Eq. (6.85) shows that no significant energy will be lost to the fat diamond unless there is an extraordinarily large combination of flutter amplitude, system "Q" (i.e., $f_0/\Delta f$), and time-bandwidth product. (This conclusion was also borne out by the computer simulations of Section 7.) Thus, the transfer of energy from the narrow pulse to the central diamond is more important. The fat diamond can usually be ignored completely.

Unfortunately, there is no formal theoretical result that quantifies the narrow pulse's amplitude loss as a function of flutter amplitude. There are a couple of informal results, however. The first informal result predicts that a substantial portion of the energy in the narrow pulse will be lost to the central diamond when the value of flutter amplitude $y_{\sigma}^{(T)}$ gets as large as $(f_0 T)^{-1}$.

[The "derivation" is as follows: Since the formation of the narrow pulse is dependent upon a coherent summation of equal contributions from the chips, the process will fail if there are random phase deviations in those contributions (in fact, this is what creates the central diamond). The phase deviation is approximately $2\pi f_0 \varepsilon(t)$, since the tone burst (chip) frequencies are centered around f_0. If $\varepsilon(t)$ deviates over a span of at least f_0^{-1} during the transmission duration T, so that the phase deviation $2\pi f_0 \varepsilon(t)$ varies over a span of 2π or more, then it is likely that the phase deviations of the chips will constitute a very random set, especially in view of the time-scrambling nature of the random hopcode. However, for $\varepsilon(t)$ to deviate over a span of f_0^{-1} in time T, its derivative

y(t) would be of the order of f_0^{-1}/T within the interval T, i.e., $y_\sigma^{(T)} \cong (f_0 T)^{-1}$.]

It is interesting to note that the condition $y_\sigma^{(T)} \cong (f_0 T)^{-1}$ may also be expressed as

$$T \cong \left(\frac{1}{f_0}\right) \times \left[\frac{1}{y_\sigma^{(T)}}\right] \cong 2.3 \times \left(\frac{1}{f_0}\right) \times \left[\frac{650 \text{ m/s}}{c y_\sigma^{(T)}}\right], \qquad (8.31)$$

which, except for the factor 2.3, is the same as the defining equation for T_{max}, the maximum flutter-safe interval for *linear FM* transmissions (see Eq. (8.22) and subsequent text). Since $y_\sigma^{(T)}$ depends so weakly upon T, it follows that the solution of Eq. (8.31) is about $2.3T_{max}$. The conclusion is that T_{max} is just as important a parameter for the random hopcode as it was for the linear FM case. In the linear FM case the flutter begins to have a significant pulse elongation effect when T reaches the critical value T_{max}, whereas, in the random hopcode case the flutter will have have seriously diminished the energy of the narrow pulse (without elongating it) by the time T reaches $2.3T_{max}$.

The second informal result is based upon the observation that the amplitude of the narrow pulse in the random hopcode case is roughly the same as the amplitude of the elongated pulse in the stepped-FM case; i.e., the power of the fluttered and compressed pulse is the same in those two cases, even though the energy may be quite different. This observation is mainly empirical, based upon computer simulations, but some heuristic theoretical explanations have been offered (Brudner *et al.*, 1990). Thus, although the power is the same in the two cases, for the hopcode case the narrow pulse's duration remains fixed as its energy diminishes whereas, in the stepped-FM case, the pulse energy remains fixed as its duration increases in accordance with Eq. (8.15). Since energy is the product of power and duration, it follows that the energy lost in the narrow pulse due to flutter is in inverse proportion to the formula of Eq. (8.15). Thus, in dB, the energy loss of the narrow pulse is

$$\textbf{energy loss}_{dB} \cong 10 \log_{10}\left[1 + (T f_0)\left(\frac{c y_\sigma^{(T)}}{650 \text{ m/s}}\right)\right], \qquad (8.32)$$

for the random hopcode case. It should be remembered that this energy is not

truly lost, since it is merely transferred from the narrow pulse to the central diamond.

Interestingly, if one replaces T by T/N in Eq. (8.32), the formula gives the same result as Eq. (6.84); i.e., it computes the energy lost from the central diamond to the fat diamond. However, significant loss of pulse energy to the fat diamond is not likely (as has already been stated), because of the smallness of the flutter amplitude $y_{\sigma}^{(T/N)}$ over the relatively brief chip interval T/N.

It is also interesting to try the T-value given by Eq. (8.31), which, according to our first informal result, is supposed to cause "substantial" energy to be lost from the narrow pulse. When that T-value is substituted into Eq. (8.32), the resulting energy loss is 5.2 dB, representing a 70% reduction in energy. Thus, our two informal results appear to be compatible.

8.9 PROCESSING GAIN FOR A RANDOM HOPCODE

For the case of a random hopcode transmission, the preceding section made it clear that flutter does not elongate the compressed pulse in a gradual way. Consequently, it makes no sense to compensate for the flutter environment by adjusting the detector's integration window gradually. Instead, one should set the window length, T_{det}, to a fixed width that matches either the central diamond or the narrow pulse.

If one matches the integration window to the narrow pulse, $T_{det} = 1.5/\Delta f$, then the processing gain is computed by subtracting the energy loss term of Eq. (8.32) from $5 \log_{10}(T/T_{det})$, giving the result

$$\textbf{Proc. Gain} \cong 5 \log_{10}(\Delta f T) - 0.88\,\text{dB} - 10 \log_{10}\left[1 + (T f_0)\left(\frac{c\, y_{\sigma}^{(T)}}{650\ \text{m/s}}\right)\right] . \qquad (8.33)$$

This formula shows the good and bad points of matching the integration window to the narrow pulse. The first term guarantees an optimum processing

gain in the absence of flutter. The last term applies the biggest flutter penalty that has been encountered in this report.

Admittedly, the penalty will not amount to very much until a threshold is reached, i.e., until the second term in the square brackets becomes significant. The penalty will not exceed 3 dB until $T > T_{max}$, where T_{max} is the maximum flutter-safe interval that was defined in Section 8.6 (i.e., it is the value of T that satisfies Eq. (8.22)). But beyond that point the processing gain will lose about 10 dB for each decade of increase in flutter amplitude, center frequency, or transmitted pulse duration.

The more "robust" choice is to match the window to the effective duration of the central diamond; i.e., $T_{det} = 1.11T/N$. (One might prefer to use its full duration, $T_{det} = 2T/N$, but that is a minor detail.) Unless the flutter is of such extraordinarily high amplitude that it drains the energy into the fat diamond, this chip-sized window will capture virtually all of the pulse energy. The processing gain will be $5\log_{10}(T/T_{det})$, where $T_{det} = 1.11T/N$. After simplification, using the fact that $N = \sqrt{\Delta f T}$, one gets the following result:

$$\textbf{Proc. Gain} \cong 2.5\log_{10}(\Delta f T) - 0.2\,\text{dB}. \qquad (8.34)$$

(Another minor detail: This equation, which duplicates Eq. (6.77), would need a correction of –1.8 dB to account for a 33% energy loss that was predicted by the theory of Section 6. The need for such a correction is not certain, however. The discrepancy may be due to approximations that were made in the theory.)

There is no flutter penalty, but this longer integration window provides *only half of the feasible gain* in environments where the flutter is below threshold. The robustness has been bought with a sizable sacrifice.

[NOTE: It has been mentioned in Section 6.8 that when random hopcode transmissions are used in radar, communications, and sonar applications it is sometimes wise to abandon the idea of compressing the pulse to less than a chip's duration, for a variety of reasons. Noncoherent detection of the individual frequency components then becomes a possibility, going under the name of

"post-detection pulse compression." That kind of system architecture, using hopcodes as we have defined them, would force the 2:1 gain sacrifice at the outset.]

8.10 GROUND NOT COVERED

It seems appropriate to mention several relevant topics that, for a variety of reasons, have not been pursued adequately.

Looking beyond processing gain: Throughout this report, attention has been focused upon the pulse compression filter's processing gain. Specifically, it has been defined as the filter's insertion gain, measured with a fixed set of specifications for probability of detection and false alarm rate (not false alarm probability!). Moreover, the definition has assumed a sonar echo from an ideal, point target. However, there are many sonar application scenarios in which this performance measure is not the whole story, and there are some applications for which it is entirely irrelevant. The reader is warned to consider this point carefully, and to supply the appropriate adjustments and modifications.

Doppler-spreading and time-spreading: Much has been published on Doppler-spread and time-spread channels (and targets) in the communications, radar, and sonar literature. Some of the results bear a resemblance to our flutter results. Certainly, flutter produces Doppler spreading of a sort. However, flutter does not create a set of parallel, additive channels that contribute simultaneous components of different Doppler. Such behavior is characteristic of many radar and sonar applications, but not of flutter as we have defined it. Nevertheless, connections between the two theories would be worth pursuing.

Target motions, including aspect rotation: Target motions, as a source of flutter, have been given scant attention. Simple vibration or meandering of the target is probably little different from vibration or meandering of the sonar platform. On the other hand, target rotational motions can bring scattering centers into view and eclipse other scattering centers. The effect may be flutter-like, but it might be more appropriate to regard it as a combination of time-spreading and Doppler spreading. Even a stationary target will appear to be

rotating when viewed by a sidescan sonar that is moving at a significant speed, especially if long duration waveforms are being transmitted.

Other hopcode waveforms: Our definition of a hopcode burst is mathematically neat and simple. It gives an efficiently packed spectrum without gaps. Each chip frequency is visited exactly once during the transmission period. Some of the results will have to be altered if one wants to use another type of hopcode transmission with time gaps, frequency gaps, or other alterations. (However, the fact that we require the time-bandwidth product to be a perfect square of an odd integer is not nearly as restrictive as it sounds.)

Noise-like waveforms: Bandlimited noise bursts have also been studied by the author and his colleagues. Bartels (1989), in his earlier computer simulation studies with bandlimited noise bursts, found flutter effects that were similar to those described here for the random hopcode case, with one exception: The narrow pulse's energy drained directly into the fat diamond, without pausing in the central diamond. This is not too surprising, since there were no chips with which to construct a central diamond. Some subsequent theoretical work has been done on this subject (Brudner *et al.*, 1990), and some unpublished computer simulations have been done, but the results were not complete enough for inclusion in this report.

Limits on time-bandwidth product: For a fixed bandwidth system, a very large time-bandwidth product can be attained only by using a waveform of very long duration. For a monostatic active sonar this restricts the inner range limit, due to acoustic (and possibly electronic) feedover from the transmitter to the receiver, and volume backscatter from the region directly in front of the sonar array, unless it is possible to filter out those sources of interference. As far as we know, the only type of waveform that permits the required rejection filter performance (often >100 dB) is the FM waveform, or some modest modification thereof. Success has been achieved with continuous transmission frequency modulation (CTFM) sonars, but apparently not with any other CTxx type of sonar. Thus, if sonar operation is desired at close range, there may be a significant limit upon the waveform duration and attendant processing gain that can be attained even in the absence of flutter.

8.11 GENERAL CONCLUSIONS

In this report, flutter has been defined, scrutinized, characterized, quantified, and parametrized. The effect of flutter upon replica-correlation processing has been examined in detail. Only time-axis perturbations, not amplitude fluctuations, have been considered. The focus of attention has been upon high resolution sonar, using transmissions with very large time-bandwidth products. It has also been assumed that the transmissions had flat spectra within their bandwidths and constant amplitudes within their durations. Two types of waveforms have been considered in detail: linear FM waveforms and random frequency-hopped waveforms.

In both cases it has been found that there is a threshold, below which the flutter has little or no effect. A product of three factors determines whether the threshold is exceeded: transmitted duration, transmission center frequency, and the amplitude of the physical flutter process (appropriately measured). Transmission bandwidth is *not* one of the factors. Once the threshold is exceeded, the degree of effect depends upon the waveform type, the detector parameters, and the transmission bandwidth.

The studies showed that, for a linear FM waveform, the flutter merely elongates the pulse at the output of the pulse compression filter, without diminishing its energy. When a frequency-hopped waveform with a random hopcode frequency sequence was studied, it was found that it has a rather different behavior. As the flutter grows from zero, the compressed pulse remains narrow but diminishes in amplitude, with the missing energy reappearing as "grass" that sprouts up in a triangular pattern, covering an interval that is twice as long as the chip interval. Eventually the central pulse disappears.

It is not as easy to describe the quantitative effects of flutter upon these two waveform types. Simply put, the linear FM transmission seems to be more forgiving of flutter effects; the processing gain merely tops out at whatever value it had when the threshold was exceeded. On the other hand, for the hopcode

burst the processing gain diminishes rapidly after the threshold is crossed—but not if one is willing to make a 2:1 sacrifice in processing gain in order to achieve "robust" performance. These descriptions inevitably oversimplify the results, however. The reader is referred to the appropriate sections of the report for a better summary.

The results of the theoretical developments, as well as the computer simulation examples, were not in conflict with the more heuristic results that had been reported previously (Brudner *et al.*, 1990) and with the computer simulations that had been done by Bartels (1989) in his thesis. (The latter work, done under the supervision of the author, was the original stimulus for many of the theoretical derivations in this report.)

Experimental data on the characteristics of environmental flutter were found to be sadly deficient. Data that were available, from studies of propagational instabilities in the water, had to be extrapolated to be of any use at all. New ways were suggested for performing such studies in the future. There were no real data available from which to quantify the flutter caused by platform motion; nevertheless, it was guessed that it probably has a more significant effect than flutter induced by propagational instabilities in the medium.

REFERENCES

Allan, David W. (1987). "Time and Frequency (Time-Domain) Characterization, Estimation, and Prediction of Precision Clocks and Oscillators," IEEE Trans. Ultrason. Ferroelec. Freq. Contr. UFFC-34(6), 647-654.

Bartels, Keith A. (1989). "Feasibility of Very Large Time-Bandwidth Signals in Active Sonar Systems," Applied Research Laboratories Technical Report No. 89-11 (ARL-TR-89-11), Applied Research Laboratories, The University of Texas at Austin.

Blachman, Nelson M., and George A. McAlpine (1969). "The Spectrum of a High-Index FM Waveform: Woodward's Theorem Revisited," IEEE Trans. Communications Tech. COM-17(2), 201-207.

Blake, William F. (1986). Mechanics of Flow-Induced Sound and Vibration, Volume II (Academic Press, New York), p. 613.

Boileau, E., and B. Picinbono (1976). "Statistical Study of Phase Fluctuations and Oscillator Stability," IEEE Trans. Instrum. Meas. IM-25(1), 66-75.

Bracewell, Ronald N. (1978). The Fourier Transform and its Applications (McGraw-Hill Book Co., Inc., New York), pp. 160-163.

Brudner, T. J., Terry L. Henderson, and Charles M. Loeffler (1990). "Limitations on Large Time-Bandwidth Product Sonar Signals Due to Flutter," IEEE OCEANS '90 Proceedings, pp. 327-332.

Burdic, William S. (1984). Underwater Acoustic System Analysis (Prentice-Hall, Englewood Cliffs, New Jersey), pp. 196-198, 228-235.

Christoff, J. T., C. D. Loggins, and E. L. Pipkin (1982). "Measurement of the Temporal Phase Stability of the Medium," J. Acoust. Soc. Am. 71(6), 1606-1607.

Clifford, Steven F., and David M. Farmer (1983). "Ocean Flow Measurements Using Acoustic Scintillations," J. Acoust. Soc. Am. 74(6), 1826-1832.

de Coulon, Frederic (1986). Signal Processing Theory (Artech House, Inc., Dedham, Massachusetts), pp. 248-250.

Deutsch, Ralph (1969). System Analysis Techniques (Prentice-Hall, Englewood Cliffs, New Jersey), pp. 134-138.

Duda, Timothy F., Stanley Flatté, and Dennis Creamer (1988). "Modelling Meter-Scale Acoustic Intensity Fluctuations from Oceanic Fine Structure and Microstructure," J. Geophys. Res. 93(C5), 5139-5142.

Dixon, Robert C. (1984). Spread Spectrum Systems, 2nd Edition (John Wiley and Sons, New York), pp. 56-91.

Eaves, Jerry L., and Edward K. Reedy (1987). Principles of Modern Radar (Van Nostrand Reinhold Co., New York), pp. 483-486.

Ewart, T. E. (1976). "Acoustic Fluctuations in the Open Ocean—A Measurement Using a Fixed Refracted Path," J. Acoust. Soc. Am. 60(1), 46-59.

Ewart, T. E., C. Makaskill, and B. J. Uscinski (1983). "Intensity Fluctuations. Part II: Comparison with the Cobb Experiment," J. Acoust. Soc. Am. 74(5), 1484-1499.

Farmer, David M., and Steven F. Clifford (1986). "Space-Time Acoustic Scintillation Analysis: A New Technique for Probing Ocean Flows," IEEE J. Ocean. Eng. OE-11(1), 42-50.

Farmer, David M., Steven F. Clifford, and Jane A. Verrall (1987). "Scintillation Structures of a Turbulent Tidal Flow," J. Geophys. Res. 92, 5369-5382.

Gough, Peter T., and Michael P. Hayes (1989). "Measurement of Acoustic Phase Stability in Loch Linnhe, Scotland," J. Acoust. Soc. Am. 86(2), 837-839.

Harris, Cyril M. (1988). Shock and Vibration Handbook, 3rd Edition (McGraw-Hill Book Co., Inc., New York), Part 44, p. 23.

Ishimaru, Akira (1978). Wave Propagation and Scattering in Random Media, Volume 2 (Academic Press, New York), Section 17.

Kennedy, Robert M. (1969). "Phase and Amplitude Fluctuations in Propagating through a Layered Ocean," J. Acoust. Soc. Am. 46(3), Part 2, 736-745.

Lacker, Stephen G., and Terry L. Henderson (1990). "Wideband Monopulse Sonar Performance: Cylindrical Target Simulation Using an Acoustic Scattering Center Model," IEEE J. Ocean. Eng. OE-15(1), 32-43.

Lesage, P., and C. Audoin (1979). "Characterization and Measurement of Time and Frequency Stability," Radio Science 14(4), 521-539.

McGillem, Clare D., and George R. Cooper (1974). Continuous and Discrete Signal and System Analysis (Holt, Rinehart, and Winston, New York), pp. 50-53.

Papoulis, Athanasios (1965). Probability, Random Variables, and Stochastic Processes, First Edition (McGraw-Hill Book Co., Inc., New York), p. 133.

Papoulis, Athanasios (1984). Probability, Random Variables, and Stochastic Processes, Second Edition (McGraw-Hill Book Co., Inc., New York), pp. 491-496.

Papoulis, Athanasios (1977). Signal Analysis (McGraw-Hill Book Co., Inc., New York), pp. 273-275.

Peebles, Peyton Z. (1976). Communication System Principles (Addison-Wesley, Reading, Massachusetts), pp. 68-72, 219-239.

Proakis, John G. (1989). Digital Communications (McGraw-Hill Book Co., Inc., New York), pp. 396-399, 820, and 832.

Rihaczek, August W. (1969). Principles of High-Resolution Radar (McGraw-Hill Book Co., Inc., New York), pp. 55, 94, 170, 232.

Spiegel, Murray R. (1968). Mathematical Handbook of Formulas and Tables (Schaum's Outline Series) (McGraw-Hill Book Co., Inc., New York), p. 109.

Stark, Henry, and Franz B. Tuteur (1979). Modern Electrical Communications: Theory and Systems (Prentice-Hall, New York), p. 326.

Taub, Herbert, and Donald L. Schilling (1971). Principles of Communication Systems (McGraw-Hill Book Co., Inc., New York), pp. 131-135.

Tuma, Jan J. (1979). Engineering Mathematics Handbook, 2nd Edition (McGraw-Hill Book Co., Inc., New York), p. 161.

Urick, Robert J. (1983). Principles of Underwater Sound, 3rd Edition (McGraw-Hill Book Co., Inc., New York), pp. 383-386.

Urkowitz, Harry (1967). "Energy Detection of Unknown Deterministic Signals," Proc. IEEE 55(4), 523-531.

Verrall, Jane (1990). Personal communication (in response to telephone inquiries regarding details of experimental work of Farmer *et al.*)

5 December 1990

DISTRIBUTION LIST FOR
ARL-TR-90-44
Technical Report under Contract N00039-88-C-0043
TD No. 03A007, Special Acoustic Signals
TD No. 03A011, Special Acoustic Signals - Phase II

Copy No.

Commanding Officer
Coastal Systems Station, Dahlgren Division
Naval Surface Warfare Center
Panama City, FL 32407

1 Attn: J. Wood (Code 20C)
2 J. Wilbur (Code 2230)
3 J. Christoff (Code 3110)
4 E. Linsenmeyer (Code 20C)

Commanding Officer
Naval Research Laboratory
Stennis Space Center, MS 39529-5004

5 Attn: R. Farwell (Code 240)
6 D. Ramsdale (Code 210)
7 Library (Code 125L)

Commanding Officer
Naval Oceanographic Office
Stennis Space Center, MS 39522-5001

8 Attn: W. Jobst (Code OA)

Commanding Officer
Office of Naval Technology
Department of the Navy
Arlington, VA 22217-5000

9 Attn: T. Warfield (Code 234)
10 T. Goldsberry (Code 231)
11 W. Ching (Code 235)
12 D. Steiger (Code 23U)
13 K. Lackie (Code 125)
14 D. Houser (Code 232)

Distribution List for ARL-TR-90-44 under Contract N00039-88-C-0043,
TD Nos. 03A007 and 03A011
(Cont'd)

Copy No.	
	Commander Naval Sea Systems Command Department of the Navy Washington, DC 20362-5101
15	Attn: J. Grembi (PMS407B)
16	D. Gaarde (PMS407-2)
17	J. Neely (PMS418W)
18	T. Douglass (PMS402B)
19	H. Grunin (PMS402)
20	A. Knobler (PMS406B)
21	T. Stanford (PMS395R)
	Commander Naval Undersea Warfare Center Division Newport, RI 02841-5047
22	Attn: J. Kelly (Code 3632)
	Commanding Officer Naval Research Laboratory Washington, DC 20375-5000
23	Attn: Library
	Officer in Charge Naval Undersea Warfare Center Division New London, CT 06320-5594
24	Attn: J. Geary (Code 3221)
25	W. Cary (Code 33A)
26	A. Dugas (Code 3221)
	Office of Naval Research Department of the Navy Arlington, VA 22217-5000
27	Attn: R. Obrochta (Code 1125AR)
28	J. Kravitz (Code 1125GG)
29	M. Orr (Code 1125OA)
30	A. Faulstich (Code 23)
31	R. Madan (Code 1114SE)

Distribution List for ARL-TR-90-44 under Contract N00039-88-C-0043,
TD Nos. 03A007 and 03A011
(Cont'd)

Copy No.	
	Commander Naval Command Control and Ocean Surveillance Center San Diego, CA 92152-5000
32	Attn: R. Anderson (Code 54)
33	R. Moore (Code 632)
34	Library
	Commander Dahlgren Division Naval Surface Warfare Center Silver Spring, MD 20903-5000
35	Attn: W. Dence (U23)
36	S. Poulis (U22)
37	S. Martin (U24)
	Commander Dahlgren Division Naval Surface Warfare Center Dahlgren, VA 22448
38	Attn: Library
39 - 50	Commanding Officer and Director Defense Technical Information Center Cameron Station, Building 5 5010 Duke Street Alexandria, VA 22314
	Applied Physics Laboratory The University of Washington 1013 NE 40th Street Seattle, WA 98105
51	Attn: D. Jackson
52	T. Ewart
53	J. Verrall
54	Library
	Applied Research Laboratory The Pennsylvania State University P.O. Box 30 State College, PA 16901
55	Attn: S. McDaniel
56	D. Ricker
57	Library

Distribution List for ARL-TR-90-44 under Contract N00039-88-C-0043,
TD Nos. 03A007 and 03A011
(Cont'd)

Copy No.	
	Department of Electrical and Computer Engineering The University of Texas at Austin Austin, TX 78712
60	Attn: K. Bartels
61	Ricky S. Bailey, ARL:UT
62	Garland R. Barnard, ARL:UT
63	Hollis Boehme, ARL:UT
64	Terry J. Brudner, ARL:UT
65	Nicholas P. Chotiros, ARL:UT
66	Terry L. Henderson, ARL:UT
67	John M. Huckabay, ARL:UT
68	Robert A. Koch, ARL:UT
69	Stephen G. Lacker, ARL:UT
70	Charles M. Loeffler, ARL:UT
71	T. G. Muir, ARL:UT
72	Robert A. Stewart, ARL:UT
73	Library, ARL:UT
74 - 85	Reserve, ARL:UT